SCIENTIFIC MINING JOURNAL

ISSN 2564-7024
e-ISSN 2587-2613
Vol: 63 *No:* 2 *May*
2024

The Publication of the Chamber of Mining Engineers of Türkiye

E. Tugcan Tuzcu
Original Research
COM_TRD_Sim: A Size Reduction Trade-off Software Part 1: Software Capabilities and Infrastructure

Yakup Umucu
Vedat Deniz
Yaşar Hakan Gürsoy
Original Research
Artificial Intelligence In Mineral Processing: Transforming Mining Operations Through Smart Technology

Ahad Harzanak
E. Caner Orhan
Original Research
DEM aided investigation of the effects of screen surface properties on screening performance

Emrah Durguta
Original Research
Investigation of wet ground limestones on porous ceramic body properties
Yaş öğütülmüş kireçtaşlarının gözenekli seramik bünye özelliklerine etkisinin araştırılması

Xueqi Zhang
Hongbin Li
Yongwei Du
Zhongqiu Wang
Original Research
Reasonable width of coal pillar in fully mechanized caving mining face of extra-thick coal seam–A case study

UCTEA CHAMBER OF MINING ENGINEERS

Scientific Mining Journal

Vol: 63, No: 2, May, *2024*

A peer-reviewed quarterly journal of the Chamber of Mining Engineers of Türkiye

AIMS AND SCOPE

Scientific Mining Journal, which is published in open access electronic environment and in printed, is a periodical scientific journal of Union of Chambers of Turkish Engineers and Architects Chamber of Mining Engineers. The name of the journal was "Mining" until June 2016 and it has been changed to "Scientific Mining Journal" since September 2016 because it can be confused with popular journals with similar names and the ISSN number has been updated from 0024-9416 to 2564-7024.

Scientific Mining Journal, published four times a year (March-June-September-December), aims to disseminate original scientific studies which are conducted according to the scientific norms and publication ethics at national and international scale, to scientists, mining engineers, the public; and thus to share scientific knowledge with society. The journal is in English.

The journal covers theoretical, experimental, and applied research articles, which reflects the findings and results of an original research in the field of mining engineering; review articles, which assess, evaluates, and interprets the findings of a comprehensive review of sufficient number of scientific articles and summarize them at present information and technology level; technical notes, which may be defined as a short article that describes a novel methodology or technique; a case studies, which are based on the theoretical or real professional practice and involves systematic data collection and analysis.

The journal gives priority to works that will enable the advancement of current available information necessary to serve humanity with nonrenewable mineral resources with the perspective of sustainable mining principles. In this context, mine exploration, mineral resource modeling, surveying, mine economics and feasibility, geostatistics, rock mechanics and geotechnics, diggability studies, underground and surface mining, mine design, support design in underground mines and tunnels, rock penetration and rock fragmentation, mine production planning and pit optimization, mine health and safety management, mine ventilation, methane emission and drainage in underground coal mines, mineral processing and beneficiation, process mineralogy, analytical techniques, mineral comminution, mineral classification and separation, flotation/flocculation, solid/liquid separation, physical enrichment methods, hydro and biometallurgy, production metallurgy, modeling and simulation, instrumentation and process control, recycling and waste processing, mining law, environmental health and management, transportation, machinery and equipment selection and planning, coal gasification, marble technology, industrial minerals, space mining, submarine mining and mechanization are included in the journal content.

Submitted manuscripts are evaluated by the editorial board and expert referees independently in accordance with the best practices in academic publishing. The publishing rights of the manuscripts, approved for publication at the end of the evaluation process, are transferred to the Chamber of Mining Engineers by the authors.

Scientific Mining Journal

Scientific Mining Journal is indexed or abstracted in:

SCOPUS

Google Scholar

ULAKBİM TR Dizin

GeoRef

OpenAIRE

Author Instructions, Editorial Advisory Board, the Peer Review Process and Reviewer Lists can be accessed from http://www.mining.org.tr

Publication Ethics

Complying with the research and publication ethics is considered an indisputable precondition to be published. Publication Ethics can be accessed from http://www.mining.org.tr

Scientific Mining Journal

Owner on behalf of the Chamber of Mining Engineers of Türkiye: Ayhan Yüksel

Responsible editing manager: Mehmet Erşat Akyazılı

Correspondence address:
Selanik Cad. No: 19/4 06650 Kızılay-Çankaya / Ankara Türkiye

Tel: +90 312 425 10 80 / +90 312 418 36 57 • Fax: +90 312 417 52 90

e-mail: smj@maden.org.tr
web: http://www.mining.org.tr

Publication type: Local periodical, quarterly

Design: Gülendem Gültekin

Printed at: Ziraat Gurup Matbaacılık Ambalaj San. ve Tic. A.Ş.

Printing date: 27.08.2025

Number of printed copy: 1500

SCIENTIFIC MINING JOURNAL

ISSN 2564-7024
e-ISSN 2587-2613
Vol: 63 *No:* 2 *May*
2024

The Publication of the Chamber of Mining Engineers of Türkiye

CONTENTS

E. Tugcan Tuzcu — 57
Research Article
COM_TRD_Sim: A Size Reduction Trade-off Software Part 1: Software Capabilities and Infrastructure

Yakup Umucu, Vedat Deniz, Yaşar Hakan Gürsoy — 67
Review Article
Artificial Intelligence In Mineral Processing: Transforming Mining Operations Through Smart Technology

Ahad Harzanak, E. Caner Orhan — 87
Research Article
DEM aided investigation of the effects of screen surface properties on screening performance

Emrah Durguta — 95
Original Research
Investigation of wet ground limestones on porous ceramic body properties
Yaş öğütülmüş kireçtaşlarının gözenekli seramik bünye özelliklerine etkisinin araştırılması

Xueqi Zhang, Hongbin Li, Yongwei Du, Zhongqiu Wang — 101
Research Article
Reasonable width of coal pillar in fully mechanized caving mining face of extra-thick coal seam–A case study

ISSN 2564-7024
9 772564 702003

Madencilik - Mining, 2024, 63(2), 57-66

BİLİMSEL MADENCİLİK DERGİSİ
SCIENTIFIC MINING JOURNAL

TMMOB Maden Mühendisleri Odası Yayını / The Publication of the Chamber of Mining Engineers of Turkey

www.mining.org.tr

Research Article

COM_TRD_Sim: A Size Reduction Trade-off Software Part 1: Software Capabilities and Infrastructure

E. Tugcan Tuzcu[1,*]

[1] MPES Engineering, Ankara, TURKEY

Received: 1 September 2021 • Accepted: 1 December 2021

A B S T R A C T

In the past five decades, significant advancements in process simulators and calculators have transformed the mineral processing and chemical industries. These software solutions leverage mathematical models to monitor crucial control variables such as recovery rates, concentrate grades for flotation, ore-to-water feed ratios, and power consumption during crushing and grinding operations. The primary objectives of these applications revolve around optimizing design processes, which can be classified into dynamic (real-time) and steady-state simulations (offline analyses), with the latter predominating in contemporary applications. This paper categorizes the existing software solutions into several key types, including individual unit operation models, integrated flowsheet solvers, iterative simulators, and material balance models, while also highlighting their applicability and evolution through the introduction of complex unit equipment and mass/material balance equations. Despite notable progress, few software tools specifically target the simulation of capital expenditure (CAPEX) and operating expenditure (OPEX) for designed flowsheets, thereby highlighting a critical gap in the market, particularly concerning the economic implications of processing materials with varying characteristics (e.g., abrasiveness and grindability). To address these needs, we introduce the COM_TRD_Sim (Comminution Trade-off Simulator), which estimates consumable requirements based on user-defined parameters and ore characteristics, facilitating informed decision-making in size reduction processes.

Keywords: *Process Simulation, Mineral Processing, CAPEX, OPEX, COM_TRD_Sim.*

Nomenclature

$BW_i BW_i$: Bond ball mill work index, kWh/t

$C_{D_1}, C_{D_2}, C_{D_3} C_{D_1}, C_{D_2}, C_{D_3}$: mill diameter cost constant

$C_{L_1}, C_{L_2}, C_{L_3}: C_{L_1}, C_{L_2}, C_{L_3}$: mill length cost constant

$C_1, C_2, C_3, C_4 C_1, C_2, C_3, C_4$: constants used for crusher wear model equation

$C_{11}, C_{12} C_{11}, C_{12}$: constant used for SAG lifter consumption

$C_5, C_6, C_7 C_5, C_6, C_7$: constants used for crusher liner cost equation

$C_8, C_9, C_{10} C_8, C_9, C_{10}$: constant used for crusher equipment cost

$C_P C_P$: mill power cost constant

$CW_i CW_i$: Bond crusher work index, kWh/t

$F_{80} F_{80}$: 80% passing size of the product, $\mu m \mu m$

$F_{ai} F_{ai}$: French abrasion index, gram/ton

$J_B J_B$: ball charge filling, %

$K_1 K_1$: 1.0 for all circuits that do not contain a recycle pebble crusher and 0.95 where circuits do have a pebble crusher

$K_2 K_2$: 1.0 for all crushers operating in closed circuit with a classifying screen. If the crusher is in open circuit, eg. pebble crusher in a AG/SAG circuit, K2 takes the value of 1.19.

$K_3 K_3$: 1.0 for all HPGRs operating in closed circuit with a classifying screen. If the HPGR is in open circuit, K3 takes the value of 1.19.

$L_{MIN} L_{MIN}$: set minimum (closed set), meter

$L_T L_T$: Throw, meter

$M_{ih} M_{ih}$: HPGR ore work index and is provided directly by SMC Test®, kWh/ton

$M_{ia} M_{ia}$: coarse ore work index and is provided directly by SMC Test®, kWh/ton

$M_{ib} M_{ib}$: fine ore work index, kWh/ton

$M_{ic} M_{ic}$: crushing ore work index and is provided directly by SMC Test®, kWh/ton

$M_{lifter\ consumption} M_{lifter\ consumption}$: HPGR lifter consumption amount, tons

$P_{80} P_{80}$: 80% passing size of the feed, $\mu m\ \mu m$

$P_K P_K$: packing characteristics

* Corresponding author: tugcan.tuzcu@gmail.com • https://orcid.org/0000-0001-7985-0195

https://DOI: 10.30797/madencilik.1389795

$Q_m Q_m$: maximum capacity, ton/hour

$RW_i RW_i$: Bond rod mill work index, kWh/t

$S_c S_c$: parameter related to surface characteristic

$W_h W_h$: specific energy for HPGRs, kWh/t

$W_{SDT} W_{SDT}$: AG/SAG pinion energy from F80 152.4 mm to T80 1.7 mm, kWh/ton

$W_a W_a$: specific energy to grind coarser particles in tumbling mills, kWh/ton

$W_b W_b$: specific energy to grind finer particles in tumbling mills, kWh/ton

$W_c W_c$: specific energy for conventional crushing, kWh/ton

$W_i W_i$: work index, kWh/t

$d_{MAX} d_{MAX}$: maximum particle size, $\mu m \mu m$

$d_{MEAN} d_{MEAN}$: mean particle size, $\mu m \mu m$

$d_{MIN} d_{MIN}$: minimum particle size, $\mu m \mu m$

$\dot{m}\dot{m}$: specific throughput, ts/hm3

$m_s m_s$: SAG mill feed sample mass, gram

$w_c w_c$: charge % solids, fraction by weight

$x_1 x_1$: P80 of the circuit feed, $\mu m \mu m$

$x_2 x_2$: 750, $\mu m \mu m$

$x_2 x_2$: P80 of the circuit product, $\mu m \mu m$

$x_3 x_3$: fractional volumetric void space between rocks and balls

$\varepsilon_B \varepsilon_B$:the fractional volumetric void space between rocks and balls use (0.3)

$\rho_C \rho_C$: density of the charge, t/m3

$\rho_b \rho_b$: density of the balls, t/m3

$\rho_s \rho_s$: density of the solids, t/m3

$\phi_C \phi_C$: mill speed as a fraction of critical

D: Mill effective diameter, meter

$ATWIATWI$: ATWAL Wear Index, gram/ton

$AiAi$: Bond abrasion index

EE: specific energy consumption, kWh/ton

GG: gape, meter

$GbpGbp$: last three net grams per revolution, gram/rev

$GprGpr$: weight of the test sieve fresh undersize per mill revolution, gram/rev

JJ: mill charge filling, %

LL: mill effective grinding length, meter

$S.F S.F.$: SAG cost factor with respect to ball mill

TT: throughput rate, ton/hour

WW: width of jaw plates, meter

aa: model constant

dd: model constant

$revsrevs$: cumulative number of SAG test mill revolutions to T80 1.7 mm, measure by SDT

tt: time, hours

uu: circumferential speed of the rolls

Introduction

Over the past 50 years, substantial advancements have been made in the development of process simulators and calculators for the mineral processing and chemical industries. These software solutions employ mathematical models to track critical control variables, which include recovery rates and grades for flotation, as well as the ore-to-water feed rate and power draw for crushing and grinding processes. The primary goals of these software programs are design and optimization, which can be categorized based on the types of equations they employ: either dynamic (for online applications) or steady-state (for offline applications). Most existing software solutions are primarily configured for steady-state operations.

Figure 1 summarizes some of the key software/simulators utilized in the mineral processing industry. The classification presented in Figure 1 can be expanded to include several categories:

Individual unit operations vs. integrated flowsheet solvers (Sastry and Adel, 1984)

The iterative approach differs from simulators based on the simultaneous equations approach (Mular and Richardson, 1986). • This study focuses on direct versus reserve simulators (Guillaneu et al., 1992). • The discussion centers on the differences between offline (Mular and Herbst, 1980) and online optimizers (Bazin et al., 1984).

The literature compares material balance (Wiegel, 1972; Laguitton, 1980) with flowsheet solvers (Richardson et al., 1981; Gupta and Messa, 1980) and simulation software (Rajamani and Herbst, 1980; Adel, 1982; Adel and Sastry, 1983; King, 1983).

Through the evaluation of technology and the application of complex unit equipment models, ore characteristic parameters, and mass and material balance equations, software has become capable of performing mass balances, flowsheet design, and simulations simultaneously using USIMPAC (Brochot et al., 2002), MODSIM (King, 1983), METSIM (Bartlett, 1987), and JKSimMet (McKee and Napier-Munn, 1990).

However, there is a dearth of software specifically designed to produce or simulate the capital expenditure (CAPEX) and operating expenditure (OPEX) of a given flowsheet. It has been noted that the main goals have not focused on assessing the cost of equipment and the unit cost of processing a particular type of material (abrasiveness, grindability, specific gravity, etc.) in terms of energy and consumables. Instead, cost vs. capacity equations for equipment costs have been integrated into simulators (USIMPAC; Brochot et al., 2002). The developed software, COM_TRD_Sim (Comminution Trade-off Simulator), is capable of sizing and estimating consumables as a function of user-specified schedule data and ore test parameters for the size reduction process. This study focuses on the development and capabilities of the COM_TRD_Sim software, aimed at the mineral processing industry. The purpose of this study is to address the critical gap in existing process simulation software by introducing a tool that can estimate both capital and operating expenditures (CAPEX and OPEX) based on user-specified parameters and ore characteristics. COM_TRD_Sim is designed to optimize size reduction processes by assessing power demand, specific energy needs, and consumable consumption for various equipment types and configurations. This software enhances industry capabilities by enabling informed design and operational decisions through comprehensive comparative analyses and simulations of different size reduction strategies and their economic implications.

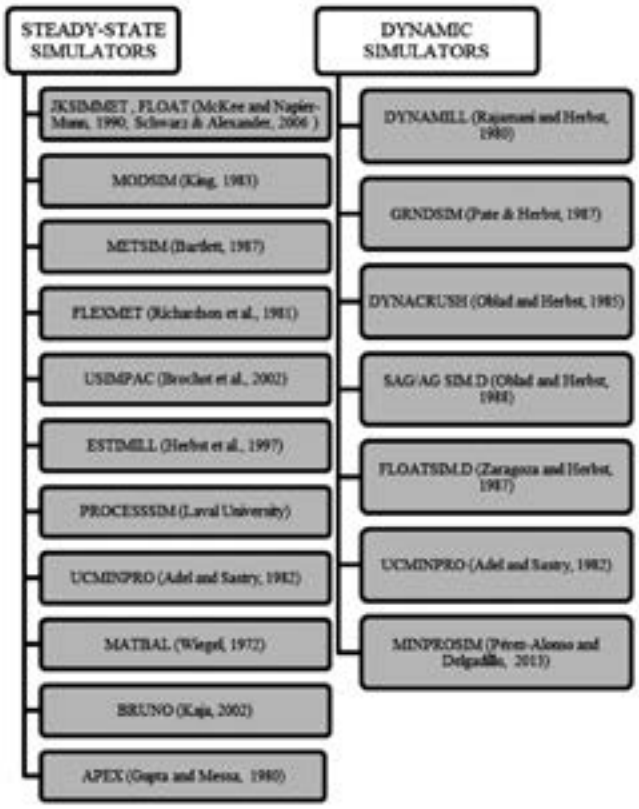

Figure. 1. List of major process software/simulator

1. Materials and Methods

The software accepts the following input parameters (Figure 2a):

- Ore-specific crushing/grinding indices,
- Ore-specific gravity,
- User-defined availability and annual ore processing amounts,
- Consumable unit costs.

The software outputs (Figure 2b):

- Annual liner/lifter consumption and unit operating costs,
- Annual ball/rod consumption and unit operating costs,
- Annual energy consumption and unit operating costs

The following conventional flowsheets are integrated into the software:

Alternative 1: Primary Crushed SABC

o Equipment 1: Jaw/Gyratory Crusher

o Equipment 2: SAG Mill

o Equipment 3: Pebble Crusher

o Equipment 4: Ball Mill

Alternative 2: HPGR/Ball Milling Circuit

o Equipment 1: Jaw/Gyratory Crusher

o Equipment 2: Secondary Crusher

o Equipment 3: HPGR

o Equipment 4: Ball Mill

Alternative 3: Conventional Crushing/Ball Milling Circuit

o Equipment 1: Jaw/Gyratory Crusher

o Equipment 2: Secondary Crusher

o Equipment 3: Tertiary Crusher

o Equipment 4: Ball Mill

Alternative 4: Primary Crushed SS SAG

o Equipment 1: Jaw/Gyratory Crusher

o Equipment 2: SAG Mill

Alternative 5: Conventional 3 Crushing/Rod + Ball Milling

o Equipment 1: Jaw/Gyratory Crusher

o Equipment 2: Secondary Crusher

o Equipment 3: Tertiary Crusher

o Equipment 4: Rod Mill

o Equipment 5: Ball Mill

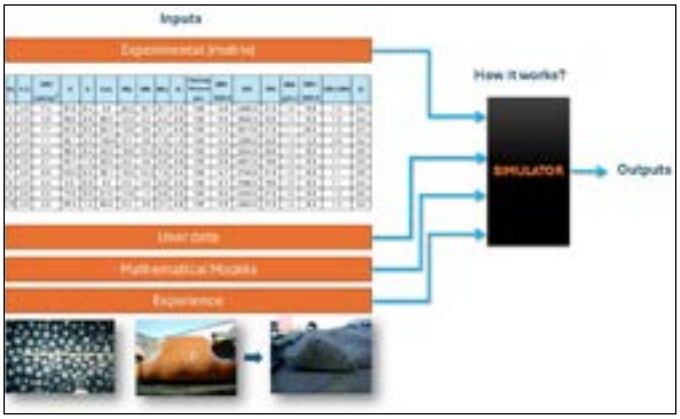

Figure. 2a. Visual representation of software input

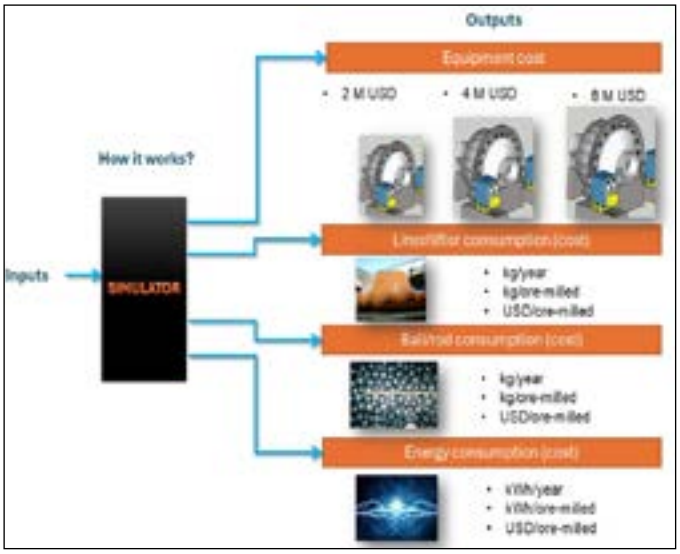

Figure. 2b. Visual representation of software output

1.1. Software by Mineral Processing Wise

The software employs various power and capacity models, experimental indices, equipment cost models, and abrasion tolerances to estimate the sizing of the size reduction system and the consumption of consumables. Once input data is entered into the software, the required hourly capacity is determined, and the calculation sequence proceeds as depicted in Figure 3.

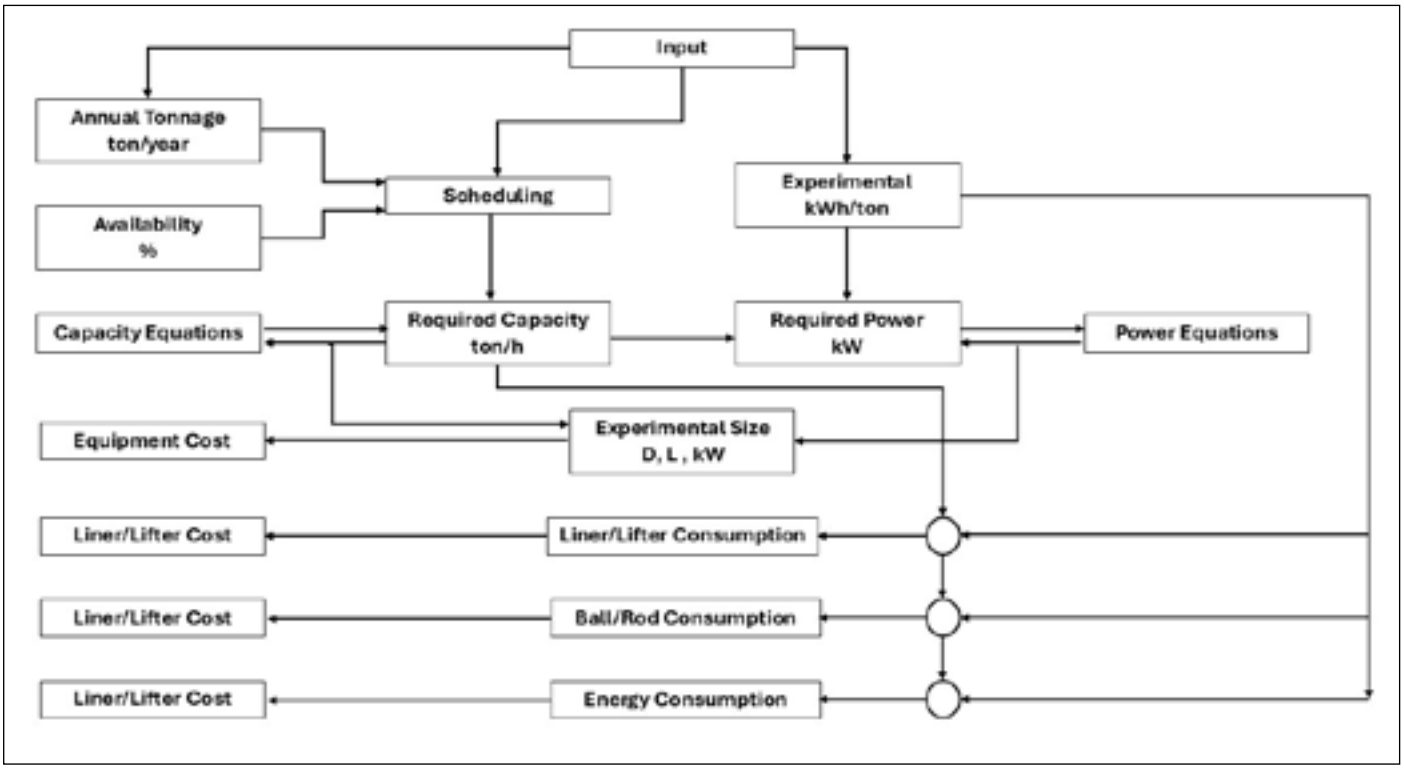

Figure. 3. Software calculation order

The software is not designed for mass and material balance calculations; however, the amount of material entering specified equipment can be manipulated using a coefficient known as the "circulating load ratio." Table 1 presents the model library utilized by the software. Empirical models based on practical experience are categorized as "In-house models," which have been developed over the years through observation and expertise.

1.2. Software Architecture: Backend and Frontend Development

1.2.1. Back-end and Front-end Coding

MPES has developed a web-based software application that offers several advantages, including minimal computational effort required for calculations. Installation is unnecessary; any computer or mobile device equipped with a web browser can access the application. A monolithic architecture has been adopted (as represented in Figure 4), considering the small size of the development team and the expectation that the application will not experience exponential growth in the short term.

Unified Modeling Language (UML) class and use case diagrams have been employed for software design. The front end utilizes the AngularJS 4 framework, a widely used JavaScript API suitable for developing single-page applications. SCSS is implemented for styling. For the back end, Spring Boot—a Java framework for developing web services—is utilized. Deployment involves creating a Docker container from the build to virtualize the application, and Docker Compose is employed to serve the application on a DigitalOcean cloud server.

Table 1. Models utilized by COM_TRD_Sim.

	Model name	Model Equation		Reference
Power and Capacity Models				
Mill	Bond	$E = 10W_i\left(\frac{1}{\sqrt{P_{80}}} - \frac{1}{\sqrt{F_{80}}}\right)$	(1)	(Bond, 1952)
	Hogg_Fuerstenau	$P = 0.238(D\ x\ 3.28)^{3.5}\left(\frac{L}{D}\right)\phi_c\rho_c(J\text{-}1.065J^2)$	(2)	(Hogg and Fuerstenau, 1972)
	Austin	$P = 10{,}6D^{2.5}L(1-1{,}03J)\left[(1-\varepsilon_B)\left(\frac{\rho_s}{w_c}\right)J + 0{,}6J_B\left(\rho_b - \frac{\rho_s}{w_c}\right)\right](\phi_c)\left(1-\frac{0.1}{2^{9-10\phi_c}}\right)$	(3)	(Austin, 1990)

	Model name	Model Equation		Reference
Crusher	Rose and English	$P = W_i Q10\left[\frac{1}{\sqrt{700{,}000(L_{MIN}+L_{T)}}}-\frac{1}{\sqrt{630{,}000G}}\right]$	(4)	(Rose and English, 1967)
		$Q_M = 2820L_T^{0.5}W(2L_{MIN}+L_T)\left(\frac{R}{R-1}\right)^{0.5}\rho_S f(P_K)f(\beta)S_C$	(5)	
		$P_K = (\frac{d_{MAX}-d_{MIN}}{d_{MEAN}})$	(6)	
		$\beta = \frac{set}{mean\ feed\ size}$	(7)	
HPGR		$P_{HPGR} = T\ x\ W_h = \frac{t}{h}x\frac{kWh}{t} = kW$	(8)	(Klymowsky et al., 2006)
		$T = \dot{m}\ x\ D\ x\ L\ x\ u$	(9)	
Experimental Indices Related to Power, Capacity and Abrasion				
Primary Crusher				
	Bond Low Impact	$CW_i = \frac{53.9\ x\ (\frac{J}{mm})}{S.G.}$	(10)	(Bond, 1947)
Secondary / Tertiary Crusher				
	Bond Low Impact	$CW_i = \frac{53.9\ x\ (\frac{J}{mm})}{S.G.}$	(11)	(Bond, 1947)
	SMC	$W_c = K_2 M_{ic} 4(x_2{}^{f(x_2)}\text{-}x_1{}^{f(x_1)})$	(12)	(Morrell, 2009)
		$f(xj) = -(0.295 + \frac{xj}{1{,}000{,}000})$	(13)	(Morrell, 2006)
Ball Mill				
	Bond Ball Mill	$BW_i = \frac{48.95}{P_c{}^{0.23}\ x\ Gpr^{0.82}\ x\ \left(\frac{10}{\sqrt{P_{80}}}-\frac{10}{\sqrt{F_{80}}}\right)}$	(14)	(Bond, 1960)
	SMC	$W_a = K_1 M_{ia} 4(x_2{}^{f(x_2)}\text{-}x_1{}^{f(x_1)})$	(15)	(Morrell, 2009)
		$W_b = M_{ib} 4(x_3{}^{f(x_3)}\text{-}x_2{}^{f(x_2)})$	(16)	
		$M_{ib} = \frac{18.18}{P_1{}^{0.295}(Gbp)(p_{80}{}^{f(p_{80})}\text{-}f_{80}{}^{f(f_{80})})}$	(17)	
Rod Mill				
	Bond Rod Mill	$RW_i = \frac{68.2}{P_1{}^{0.23}\ x\ Gpr^{0.625}\ x\ \left(\frac{10}{\sqrt{P_{80}}}-\frac{10}{\sqrt{F_{80}}}\right)}$	(18)	(Bond, 1960)
	Bond Low Impact	$CW_i = \frac{53.9\ x\ (\frac{J}{mm})}{S.G.}$	(19)	(Bond, 1947
SAG Mill				

	Model name	Model Equation		Reference
	SMC	$W_a = K_1 M_{ia} 4\left(x_2^{f(x_2)} - x_1^{f(x_1)}\right)$	(20)	(Morrell, 2009)
		$W_b = M_{ib} 4\left(x_3^{f(x_3)} - x_2^{f(x_2)}\right)$	(21)	
		$M_{ib} = \frac{18.18}{P_1^{0.295}(Gbp)\left(p_{80}^{f(p_{80})} - f_{80}^{f(f_{80})}\right)}$	(22)	
	MacPherson-W_{MAC} W_{MAC}	$W_{MAC} = kWh/ton$	(23)	(MacPherson and Turner, 1978)
	Starkey-W_{SDT} W_{SDT}	$W_{SDT} = \frac{revs * (16{,}000 + m_s)}{(447.3 * m_s)}$	(24)	(Starkey et al., 2006)
HPGR				
	SMC	$W_h = K_3 M_{ih} 4\left(x_2^{f(x_2)} - x_1^{f(x_1)}\right)$	(25)	(Morrell, 2009)
Abrasion				
Crusher	Experienced based	$Wear\ Model = \frac{\#liner\ pair}{5000\ hours} = 5\ x\ a\ x\ e^{b(C_2 x\ A_i^2 + C_3\ x\ A_i + C_4)}$	(26)	In-house model
		$a = C_1\ x\ P^{-d}$	(27)	
		$F_{ai} = C_2 x\ A_i^2 + C_3\ x\ A_i + C_4$	(28)	
Ball Mill	Bond Ai	$Ball\ Wear = 0.159\ (Ai\text{-}0.015)^{0.34}$	(29)	(Bond, 1963)
		$Liner\ Wear = 0.0118\ (Ai\text{-}0.015)^{0.3}$	(30)	
	French Ai in terms of Bond Ai	$F_{ai} = C_2 x\ A_i^2 + C_3\ x\ A_i + C_4$	(31)	In-house model
HPGR	Atwal	gram/ton	(32)	ATWI
SAG Mill	Experienced Based	$M_{lifter\ consumption} = C_{11}\ x\ P\ x\ t\text{-}C_{12}$	(33)	In-house model
Equipment Cost Model				
Crusher	Data base fitted our model	$Crusher\ Eq.Cost = C_8\ x\ P^2 + C_9\ x\ P + C_{10}$	(34)	In-house model
		$Liner\ Cost = C_5\ x\ P^2 + C_6\ x\ P + C_7$	(35)	
Ball Mill Rod Mill		$Ball\text{-}Rod\ Eq.Cost = \left(C_{D_1}\ x\ D^2 + C_{D_2}\ x\ D + C_{D_3}\right) x\ D + \left(C_{L_1}\ x\ L^2 + C_{L_2}\ x\ L + C_{L_3}\right) x\ L + C_{16}$	(36)	In-house model
SAG Mill		$SAG\ Eq.Cost = S.F.\ x\ Ball\ Eq.Cost$	(37)	In-house model
Abrasion Tolerances				In-house model
Mill	Experienced based	%40 *for mill liners*%40 *for mill liners*, %30 for HPGR liners		In-house model

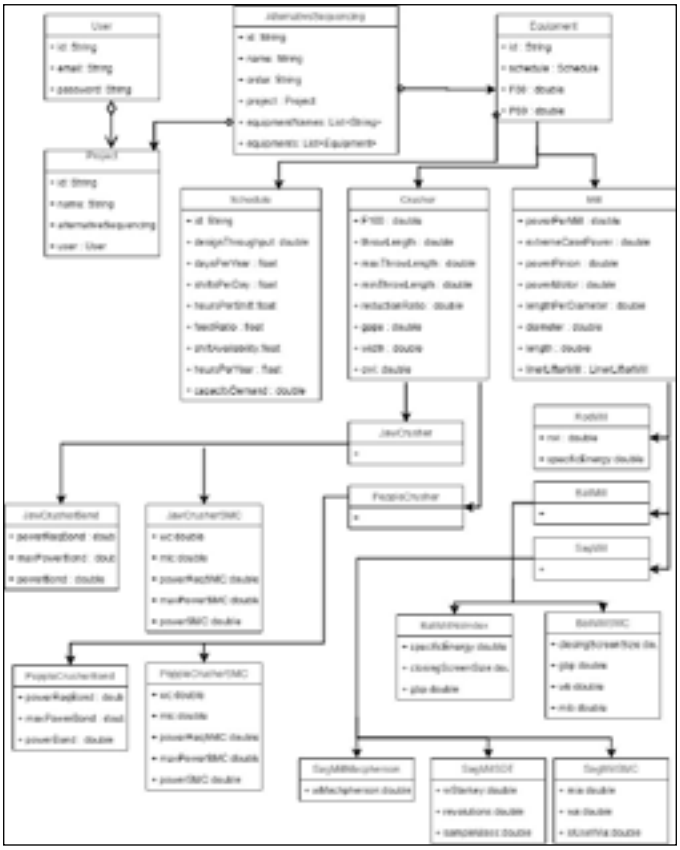

Figure. 4. Software architecture

1.2.2 GUI/UX (Graphical User Interface / User Experience Design)

MPES has employed the Lean UX methodology in the development of its software product. Lean UX is centered around three primary concepts: Think, Make, and Check. The "Think" phase involves generating hypotheses regarding a particular problem and leveraging existing knowledge about the subject area. During this stage, we examined users' mental models and initiated ideation sessions to explore potential solutions.

The "Make" phase is iterative in nature, emphasizing the creation of wireframes and prototypes to test minimum viable functionalities. In the final "Check" phase of our Lean UX loop, we conducted testing of our software product with users to validate our hypotheses. Several usability tests were undertaken to gain insights into how users interact with the product, thereby informing our design decisions and enhancing clarity. The main page of the graphical user interface (GUI) is depicted in Figure 5.

Figure. 5. Software GUI showing selection of alternatives

2. Continuous Development

The COM_TRD_Sim team is committed to continuously enhancing the software by integrating new models and improving overall functionality for industry applications. To this end, new models (outlined in Table 2) will be incorporated to expand the available options. Additionally, the GUI (illustrated in Figure 6) will enable users to select their preferred combinations rather than being limited to predefined conventional models.

Table 2. New models those will be added

	Current Model/ Approach	Coming Model/ Approach
Power and Capacity Models		
Mill	Bond	Loveday and Barratt
	Hogg and Fuerstenau	Morrell C
	Austin	
Crusher	Rose and English	
HPGR		Austin and Trubelja
Experimental Indices		
Primary Crusher		
	Bond Low Impact	Narayanan & Whiten rebound pendulum
		JKMRC-Drop weight
Secondary / Tertiary Crusher		
	Bond Low Impact	Narayanan & Whiten rebound pendulum
	SMC	JKMRC-Drop weight
Ball Mill		
	Bond Ball Mill	Selection and Breakage Functions (S_iS_i and $B_{ij}B_{ij}$)
	SMC	
Rod Mill		
	Bond Rod Mill	
	Bond Low Impact	
SAG Mill		
	SMC	SAG power index-SPI
	MacPherson-W_{MAC} W_{MAC}	JKMRC-Drop weight
	Starkey-$W_{SDT}W_{SDT}$	
HPGR		
	SMC	
Abrasion		
Mill, crusher	Bond A_iA_i, French A_iA_i	JKMRC A_iA_i
HPGR	Atwal	
Lifter material	Steel	Rubber and hybrid materials

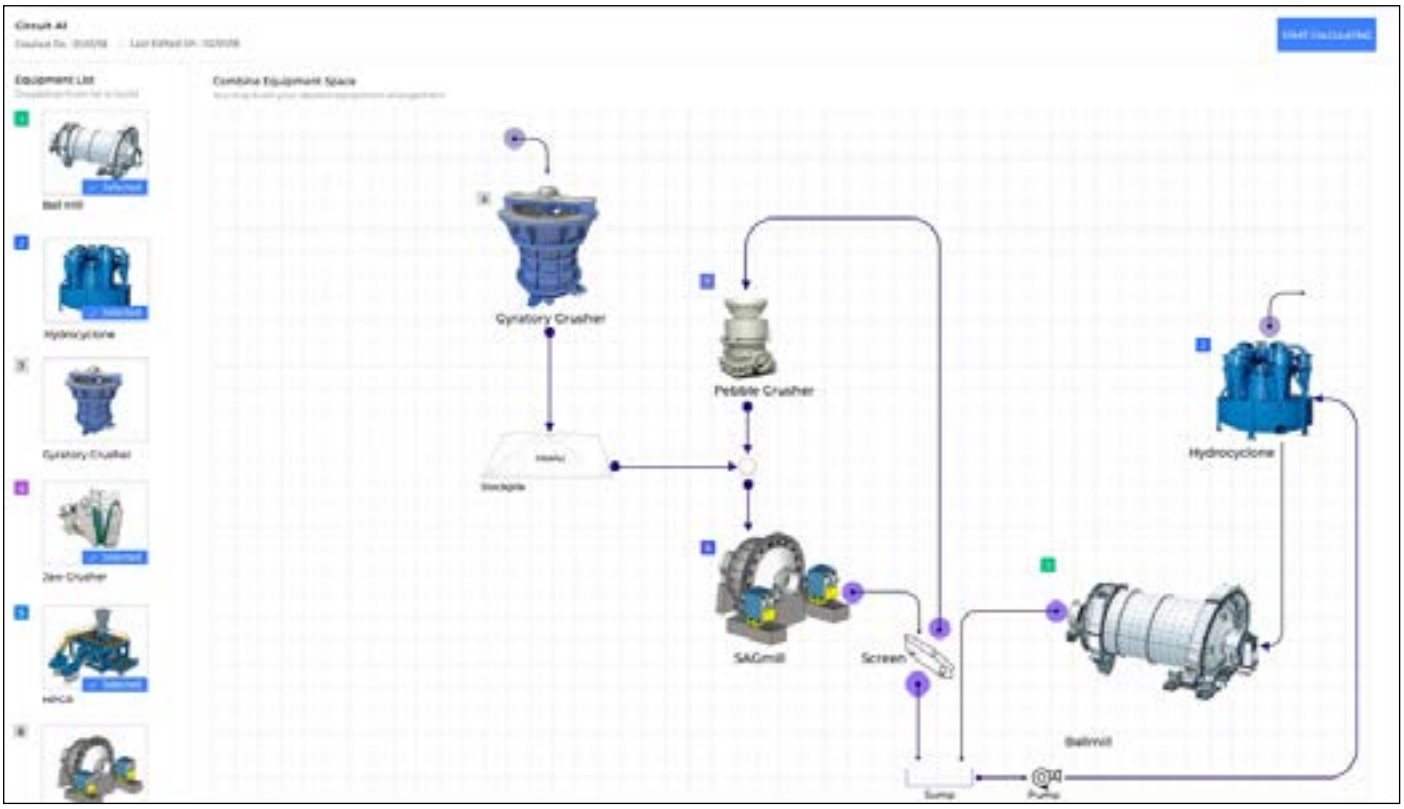

Figure. 6. CAPEX, OPEX vs experimental indices and availability

3. Discussion and Results

In evaluating the performance and utility of COM_TRD_Sim, the following key findings and advantages were highlighted:

Operational Efficiency: COM_TRD_Sim was tested across several mineral processing scenarios, based on real-world data from industry partners. The program demonstrated an ability to reduce the time needed for selecting size reduction alternatives, thanks to its streamlined, integrated approach that consolidates multiple tasks into a single platform.

Accuracy and Consistency: The software's prediction accuracy was assessed using a dataset of historical process simulations. Results showed that COM_TRD_Sim achieved over a 95% consistency rate in predicting energy consumption and mill sizing. The close alignment of the simulation outputs with empirical data underscores the robustness of the underlying models.

Cost-Benefit Analysis: Utilizing COM_TRD_Sim for CAPEX and OPEX estimation proved advantageous, with the software enabling a reduction in projected operational costs by optimizing equipment configurations and avoiding over-specification of machinery. This resulted in tangible savings for industry users, particularly in energy usage and consumable procurement.

User Experience: Feedback from pilot users indicated that the software improved design workflow efficiency, with user-friendly interfaces and intuitive model selection enhancing the decision-making process. The software was rated highly for user satisfaction.

Overall, COM_TRD_Sim demonstrates significant improvements in efficiency and cost savings, offering consistency in outputs and flexibility in its application. The software stands as a valuable tool for enhancing strategic planning and operational efficiency within the mineral processing industry.

4. Conclusions

The findings of this study highlight the capabilities of the COM_TRD_Sim software in quantifying critical factors related to size reduction. The software systematically decomposes and analyzes:

Power demand

Power needed at pinion

Specific energy demand

Operational specific energy demand

These data points are assessed against:

Various experimental indices associated with specific types of equipment (e.g., SMC, Bond, MacPherson)

Different equipment types (e.g., SAG mills, ball mills, rod mills, jaw crushers)

Multiple OPEX components (e.g., energy, ball, and rod consumption)

Diverse CAPEX and OPEX configurations stemming from distinct experimental indices

Various CAPEX and OPEX options resulting from different size reduction methodologies

The current version of the software encapsulates five alternative configurations for comparative analysis:

Alternative 1: Primary Crushed SABC

Alternative 2: HPGR/Ball Milling Circuit

Alternative 3: Conventional Crushing/Ball Milling Circuit

Alternative 4: Primary Crushed SS SAG

Alternative 5: Conventional 3 Crushing/Rod+Ball Milling

Furthermore, the software incorporates a minimum of 36 principal mathematical models, which include:

Nine power and capacity models applicable to mills, crushers, and HPGRs

Twenty-three experimental indices relevant to power, capacity, and abrasion for mills, crushers, and HPGRs

Four equipment cost models for mills, crushers, and HPGRs

The innovative software, COM_TRD_Sim, addresses a significant gap by merging theoretical frameworks with practical industrial requirements. Its operational logic integrates the following critical elements:

Investors as key determinants and contributors to capacity

Laboratories as providers of diverse experimental indices

Design engineers as integrators and compilers of comprehensive data

This collective approach facilitates the identification of the most viable size reduction options and enables comprehensive comparisons of these alternatives from both technical and economic perspectives.

Acknowledgement

We would like to express our gratitude to Emre Esirik (Software Engineer) and Çağatay Çelebioğlu (Lead UX Designer) at Picus Security Inc. for their contributions during the software's development phase. Additionally, we extend our thanks to Zafer Demirtaş (Mineral Process Engineer) at MPES Engineering for his assistance with the formatting of this paper.

Compliance with Ethical Standards

Conflict of interest The author declares no conflict of interest in terms of the publication of the present article.

References

Adel, G. T., 1982. An Interactive Simulation Package for Mineral Processing Systems. D. Eng Thesis, University of California, Berkeley, California.

Adel, G. T., Sastry, K. V. S., 1983. A Computer Simulator for Dynamic Analysis of Mineral Processing Circuits. In: AIME Meeting, SME, Atlanta, Georgia

Adel, G.T., Sastry, K.V.S., 1982. Design aspects of a mineral processing simulation package. Proceedings of the APCOM'82, AIME, New York.

Austin, L.G., 1990. A mill power equation for SAG mills. Mining, Metallurgy & Exploration, 7(1), 57-63.

Bartlett, J. T., 1987. Process Simulation and Optimization Using METSIM. In Mineral Resource Management by Personel Computer, T. M. Li, S.D. Hadelsman and L. Kovisaars (Eds.). SME, Littleton, 105-116.

Bazin, C., Franklin, M.,Perry, R., 1994. On-line Material Balance for flotation plants. In: International Conference on Innovations in Mineral Processing, Sudbury.

Bond F.C., 1947. Crushing Tests by Pressure and Impact. Trans. AIME, Vol. 169, 58-66.

Bond F.C., 1960. Crushing and Grinding Calculations. British Chemical Engineering. Vol.6 (Rev 1961 by A/C Pub. 07R9235B).

Bond, F. C., 1963. Metal Wear in Crushing and Grinding. Allis Chalmers Publication No. 07P1701.

Bond, F.C., 1952. The third theory of comminution. Trans. AIME, Vol. 193, 484–494.

Brochot, S., Villeneuve, J., Guillaneau, J.C., Durance, M.V., and Bourgeois, F., 2002. USIM PAC 3: Design of mineral processing plants from crushing to refining. In: Mineral Processing Plant Design, Practice, and Control, A.L. Mular, D.N. Halbe, and D.J. Barratt (Eds.). Society for Mining, Metallurgy, and Exploration (SME), Vancouver, Canada, 479-494

Grinding Roll Technology, Vancouver, Canada, Paper No 12.

Guillaneau, J.-C., Villeneuve, J., Blot, P., 1992. Advances in the Design and Optimization of Mineral Processing Plants. Proceedings of the APCOM'92, 23rd International Symposium on the Application of Computers and Operations Research in the Mineral Industry, Tucson, Arizona, U.S.A., April 7-11, Chapter 54, 549-566.

Gupta, V.S., Messa, C.J., 1980. AMAX process evaluation executive (APEX): a general purpose simulator for computing steady state material and energy balances of metallurgical process flowsheets. In: 109th AIME Annual. Meeting, Las Vegas, Nevada.

Herbst, J.A., Rajamani, K., and Kinneberg, D.J., 1977. ESTIMILL - A Program for Grinding Simulation and Parameter Estimation with Linear Models. User's Manual, Dept. of Metallurgy, University of Utah, Salt Lake City, Utah.

Hogg, R., Fuerstenau, D.W., 1972. Power Relationship for Tumbling Mills. Transactions of the Society of Mining Engineers-AIME, Vol. 252, 418-432.

KAJA, D.M., 2002. BRUNO: Metso Minerals' Plant Simulator. In: Mineral Processing Plant Design, Practice and Control, A.L. Mular, D.N. Halbe, and D.J. Barratt (Eds.). Society for Mining, Metallurgy, and Exploration (SME), vol. 1, 404–420

King R. P., 1983. MODSIM, Modular Method for Design, Balancing and Simulation· of Ore Dressing Plant Flowsheets. Report No. G9, Department of Metallurgy, University of Witwatersrand, Johannesburg, South Africa.

Klymowsky, R., Patzelt, N., Knecht, J., Burchardt, E., 2006. An overview of HPGR technology. In: Proceeding International Conference on Autogenous and Semiautogenous Grinding Technology, Vancouver, Vol. IV, 11-26.

Laguitton, D., 1980. Material Balance of Mineral Processing Flowsheets: FORTRAN Program MATBAL2 – Users Manuel. Report No. MRP/MSL 80-33 (IR), CAN-MET, Ottawa, Canada.

MacPherson A. R., and Turner R. R., 1978. Autogenous Grinding from Test Work to Purchase of Commercial Unit. In: Mineral Processing Plant Design, A.L. Mular and R.B. Bhappu (Eds.), AIME, New York, 279-305.

McKee, D.J. Napier-Munn, T.J., 1990 The status of comminution simulation in Australia. Minerals Engineering, 3(1-2), 7-21.

Morrell, S., 2009. Predicting the overall specific energy requirement of crushing, high pressure grinding roll and tumbling mill circuits. Mineral Engineering, 22(6), 544-549.

Morrell, S., 2006. Rock characterization for high pressure grinding rolls circuit design. In: Proceedings of the International Autogenous and Semi Autogenous Grinding Technology, Vol. IV, Vancouver, 267–278.

Mular, A. L., Richardson, J. M., 1986. Metallurgical Balance. In: Design and Installation of Concentration and Dewatering Circuits, A. L. Mular and M. A. Anderson (Eds.). SME, New York, 607-632.

Mular, A., Herbst, J., 1980. Digital Simulation: An aid for Mineral Processing Plant Design. In: Mineral Processing Plant Design 2nd ed, A. L. Mular and B. Bhappu (Eds.). SME, New York, 306-338.

Oblad, A.E., Herbst, J. A., 1985. DYNACRUSH - A Program for the Simulation of the Dynamic Behavior of Crusher Circuits, User's Manual, Dept. of Metallurgy, University of Utah, Salt Lake City.

Oblad, A.E., Herbst, J.A., 1988. SAG/AG S1M.D - A Program for the Dynamic Simulation of Autogenous and Semi-autogenous Grinding Circuits, Manuscript in preparation.

Pate, W.T., Herbst, J.A., 1987. GRINSIM.D - A Fortran Simulator for Steady State Grinding Circuits. Manuscript in preparation.

Pérez-Alonso, C. A., Delgadillo, J. A., 2013. DEM-PBM approach to predicting particle size distribution in tumbling mills. Mining, Metallurgy & Exploration, 30(3), 145–150.

Rajamani, K., Herbst, J. A., 1980. A Dynamic Simulator for the Evaluation of Grinding Control Strategies. Proceedings Particle Technology, Frankfurt, West Germany, Vol. 1, pp. 64-81.

Richardson, J. M ., D. R. Coles, and J. W. White., 1981. FLEXMET. A Computer Aided and Flexible Metallurgical Technique for Steady-State Flowsheet Analysis. Eng. And Min. J. 182, 88-95.

Rose, H.E., English J.E., 1967 Transaction of. IMM, 76, C32.

Sastry, K. V. S. & Adel, G. T, 1984. A survey of computer simulation software for mineral processing systems. In: Control '84, J. A. Herbst (Ed.), AIME, New York, 121-130.

Schwarz, S., Alexander, D., 2006. JKSimFloat V6.1PLUS: Improving flotation circuit performance by simulation. In: Proceeding of the Mineral Process Modelling, Simulation and Control Conference, Laurentian University, Mineral Industry (APCOM), Santiago, Chile, 461-466.

Starkey, J., Hindstrom, S., and Nadasdy, G. 2006. SAGDesign Testing-What it is and Why it Works. In: Proceedings of the Conference on International Autogenous and Semi-Autogenous Grinding Technology, Vancouver, 240-254.

Wiegel, R. L., 1972. Advances in Mineral Processing Material Balances. Canadian Metallurgical Quarterly, Vol. 11, No. 2, 417-424.

Zaragoza, R., Herbst. J.A., 1988. Model-based Feedforward Control scheme for Flotation Plants. Minerals and Metallurgical Processing Vol.5, No. 4, 177-185.

Madencilik - Mining, 2024, 63(2), 67-85

BİLİMSEL MADENCİLİK DERGİSİ
SCIENTIFIC MINING JOURNAL

TMMOB Maden Mühendisleri Odası Yayını / The Publication of the Chamber of Mining Engineers of Turkey

www.mining.org.tr

Review Article

Artificial Intelligence In Mineral Processing: Transforming Mining Operations Through Smart Technology

Cevher Hazırlamada Yapay Zeka: Madencilik Operasyonlarını Akıllı Teknolojiyle Dönüştürmek

Yakup Umucu[a,*], Vedat Deniz[b,**], Yaşar Hakan Gürsoy[a,***]

a Eskişehir Osmangazi University, Faculty of Engineering and Architecture, Department of Mining Engineering, Eskişehir, TÜRKİYE
b Hitit University, Faculty of Engineering, Department of Polymer Materials Engineering, Çorum, TÜRKİYE

Received: 20 March 2024 • Accepted: 24 October 2024

A B S T R A C T

Back in the early 1980s, computer technology was actually in an incomparable state compared to today. At that time, could the human brain be replicated? Could a robot be created that could behave like a human? Can computers think? Can they learn things? Answers to questions like these have not yet been found. In fact, such questions have been asked continuously for years. They have continued to be asked, and as a result, some of these questions have been partially answered today.

Numerous artificial neural network models have been developed, and countless applications have emerged. Developments show that these systems will enter more and more people's lives in the future. These studies have actually emerged as a result of curiosity about how the human brain works and how it learns. How is the human brain works not yet known today? However, studies have shown that computers can learn and produce successful results. These systems are used effectively, especially in events that require the evaluation of a large amount of information. Applications are seen in many fields, from industrial life to financial life, from medical science to military systems. The successes obtained in these applications both increase the importance of artificial neural networks and increase interest in these systems.

In the mining industry, there is a need for improved quality control systems in the production of minerals. In addition, the desire to recover minerals of low economic value in a cost-effective way requires a higher level of control and automation. As a result of these demands, the success and necessity of instant messaging mineral classification and the use of this information have led to the use of artificial neural networks in the mining industry. Since the 1990s, the use of artificial neural networks has been increasing day by day. However, artificial neural networks should also be selected appropriately. In this article, information about the use of artificial neural networks in the world is given, and how they are used with mineral processing systems is explained. Multifaceted research results are given on the benefits of its use in mineral processing systems.

Keywords: *Artificial Neural Network, Mineral Processing, Grinding, Flotation.*

Introduction

Mineral processing is a fundamental and indispensable segment of the mining industry, playing a crucial role in the extraction of valuable minerals from ore. This process involves various physical and chemical methods to separate and concentrate valuable minerals from the less valuable gangue materials. The background and significance of mineral processing in the mining industry can be understood through several key points (Telsmith, Inc., 2011. Mineral Processing Handbook 11/11 - 1st printing Printed in U.S.A., 10910 N. Industrial Dr. P.O. Box 539, pages,145. ; Fuerstenau and Han, 2003):

Resource Extraction and Recovery: Mining is the process of extracting natural resources from the earth, including ores containing valuable minerals. However, these minerals are often mixed with other non-valuable materials. Mineral processing is the key step in refining raw ores, ensuring that the valuable minerals are recovered efficiently (Wills, B.A., Finch, J., 2016. Wills' Mineral Processing Technology: An Introduction to the Practical Aspects of Ore Treatment and Mineral Recovery, eighth ed. Elsevier Science and Technology Books Inc, E-book, p. 1. online resources (512 pages). ; Fuerstenau and Han, 2003) Gupta, A., Yan, D. S, 2006. Mineral Processing Design and Operation: An Introduction, Elsevier Science, Pages, 693. USA.

* Corresponding author: yakup.umucu@esogü.edu.tr • https://orcid.org/0000-0002-6317-4070
** vedatdeniz@hitit.edu.tr • https://orcid.org/0000-0003-4098-959X
*** hgursoy@ogu.edu.tr • https://orcid.org/0000-0001-8987-7818

https://DOI: 10.30797/madencilik.1456066

Economic Value: Valuable minerals such as gold, silver, copper, and rare earth elements are critical components of various industries, including electronics, construction, and manufacturing. The economic significance of these minerals makes their extraction and processing essential for modern society (Wills, 2016; Gupta and Yan, 2006; Telsmith, 2011; Fuerstenau and Han, 2003).

Resource Depletion: As easily accessible, high-grade ore deposits become scarcer, mining operations often need to process lower-grade ores. Mineral processing technologies have been evolved to address the challenge of extracting valuable minerals from increasingly complex and lower-grade deposits (Wills, 2016; Gupta and Yan, 2006; Telsmith, 2011; Fuerstenau and Han, 2003).

Environmental Stewardship: Modern mining and mineral processing face growing pressure to operate in an environmentally responsible manner. Sustainable practices aim to minimize the environmental impact of mining and processing, including water and energy consumption, waste generation, and emissions (Wills, 2016; Gupta and Yan, 2006; Telsmith, 2011; Fuerstenau and Han, 2003).

Value Chain Integration: Mineral processing is an integral part of the mining value chain, from exploration to the final product. Efficient mineral processing contributes to the overall competitiveness and profitability of mining operations (Wills, 2016; Gupta and Yan, 2006; Telsmith, 2011; Fuerstenau and Han, 2003).

Metallurgical Testing and Innovation: Mineral processing involves extensive metallurgical testing and innovation. Researchers and engineers continuously develop new techniques, equipment, and approaches to optimize processes and recover valuable minerals more effectively (Wills, 2016; Gupta and Yan, 2006; Telsmith, 2011; Fuerstenau and Han, 2003).

Safety and Occupational Health: Mining and mineral processing are historically associated with challenging working conditions and safety concerns. Advances in technology have led to improved safety measures and automation, enhancing protection (Wills, 2016; Gupta and Yan, 2006; Telsmith, 2011; Fuerstenau and Han, 2003).

Research and Development: Ongoing research and development efforts focus on improving the efficiency of mineral processing, reducing energy and water consumption, and developing environmentally friendly practices. This includes innovations in grinding technologies, flotation processes, and material handling (Wills, 2016; Gupta and Yan, 2006; Telsmith, 2011; Fuerstenau and Han, 2003).

Technological Advancements: Advances in automation, data analytics, and digital transformation are being integrated into mineral processing operations. These technologies enhance process control, reduce variability, and optimize operations (Wills, 2016; Gupta and Yan, 2006; Telsmith, 2011; Fuerstenau and Han, 2003).

Global Significance: Mineral processing is a global industry that contributes significantly to the economies of many countries. Mineral-rich regions often rely on mining and mineral processing for employment, economic growth, and infrastructure development (Wills, 2016; Gupta and Yan, 2006; Telsmith, 2011; Fuerstenau and Han, 2003).

In conclusion, mineral processing plays a vital role in the mining industry by separating and refining valuable minerals from raw ores, contributing to economic growth, environmental sustainability, and technological innovation. As the mining industry faces evolving challenges, the continued development of mineral processing technologies remains essential to meet the demands of the modern world (Wills, 2016; Gupta and Yan, 2006; Telsmith, 2011; Fuerstenau and Han, 2003, Umucu, 2011).

1. Artificial Intelligence Applications

Artificial Intelligence (AI) is rapidly transforming various industrial sectors, ushering in a new era of automation, efficiency, and innovation. Its applications are diverse and continually expanding, leading to significant changes in how businesses and industries operate.

Here's an overview of the evolving role of AI in different industrial sectors:

1.1. Manufacturing and Industry 4.0

AI-powered robots and automation systems are enhancing manufacturing processes, enabling greater precision, speed, and flexibility.

Predictive maintenance uses AI to monitor equipment and anticipate breakdowns, reducing downtime. Quality control and defect detection benefit from AI image and pattern recognition systems (Arrieta et al., 2020).

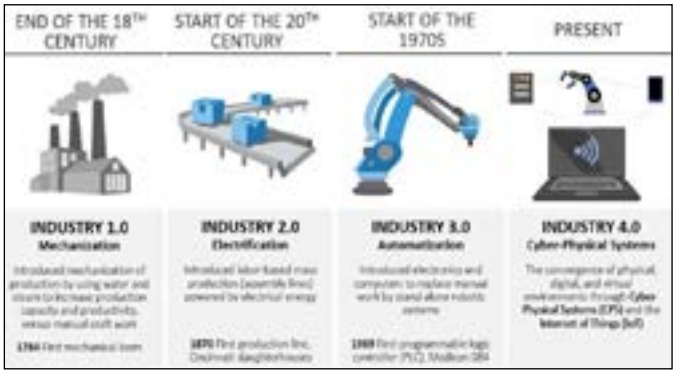

Figure 1. Diagram depicting the four industrial revolutions (Interchange, 2024).

1.2. Healthcare:

AI assists in medical diagnosis and treatment recommendations by analyzing patient data, medical images, and genetic information. Chatbots and virtual nurses provide patient support and healthcare information. Drug discovery and development processes are accelerated using AI for molecular modeling and data analysis (Ahmad, 2018).

1.3. Finance and Banking:

AI-driven algorithms are used for risk assessment, fraud detection, and personalized investment recommendations. Chatbots and virtual assistants handle customer inquiries and transactions. Algorithmic trading relies on AI for market analysis and decision-making (Gurney, 2018).

1.4. Retail and E-Commerce:

AI algorithms are what power customized shopping recommendations and targeted advertising. Inventory management and demand forecasting benefit from predictive analytics. Chatbots and virtual shopping assistants provide customer support (Mehmet and Doğansoy, 2022; Mokhtari et al., 2019).

1.5. Agriculture:

Precision agriculture uses AI to optimize crop management, irrigation, and resource allocation. Drones and sensors collect data for monitoring crop health and yield prediction. AI enhances pest and disease identification in plants (Arrieta et al., 2020).

1.6. Transportation and Logistics:

Autonomous vehicles, such as self-driving cars and drones, rely on AI for navigation and obstacle avoidance. AI optimizes routing, scheduling, and supply chain management, reducing costs and improving efficiency. Public transportation systems use AI for predictive maintenance and passenger information (Tsamados et al., 2022).

1.7. Energy and Utilities:

AI enhances energy grid management, optimizing power generation and distribution. Predictive maintenance minimizes downtime in the energy sector. Smart meters and sensors collect data for real-time energy monitoring (Liu et al., 2021).

Figure 2. Smart grid AI control schemes (Zulu et al.,2023).

1.8. Education:

AI-based educational platforms offer personalized learning experiences and assessments. Chatbots provide support for student inquiries. Learning analytics analyze student performance data to improve teaching methods (Aydın, 2021; Çavaş et al., 2004; Öztemel, 2003).

1.9. Entertainment and Media:

AI-driven content recommendation systems personalize streaming services and news feeds. AI is used in content creation, including music and video generation. Facial recognition technology assists in film and TV production (Haykin, 2009; Bahtiyar, 2021).

1.10. Legal and Compliance:

AI assists in legal research and contract analysis, reducing the time and effort required.

Regulatory compliance monitoring is automated, helping organizations adhere to complex legal requirements (Batal, 2016; Boden, 2018).

1.11. Construction and Real Estate:

AI supports project management, progress monitoring, and cost estimation. Smart building technologies use AI for energy efficiency and security. Virtual reality and augmented reality technologies enhance real estate tours and design visualization (Ramujee, 2013).

1.12. Environmental Monitoring:

AI is used in climate modeling, disaster prediction, and natural resource management. Sensor networks collect and analyze environmental data, aiding in conservation efforts.

Machine learning, natural language processing, computer vision, and data analytics advancements are the driving forces behind AI's evolving role in these industries. The integration of AI technologies allows businesses and industries to make data-driven decisions, automate routine tasks, and provide enhanced products and services. As AI continues to evolve, it is poised to further reshape the landscape of various industrial sectors (Çetin, 2016).

2. The Fundamentals of Mineral Processing

Mineral processing, also known as ore dressing or mineral beneficiation, is the process of separating valuable minerals from their ores. It involves various techniques, including crushing, grinding, screening, classification, gravity separation, flotation, magnetic separation, and leaching, to extract and concentrate valuable minerals while discarding the gangue (waste) materials. The primary objective of mineral processing is to produce a marketable product from a mineral deposit, meeting the desired specifications for purity and quality ((Wills, 2016; Gupta and Yan, 2006; Telsmith, 2011; Fuerstenau and Han, 2003).

The importance of mineral processing can be understood through the following points:

- Resource Utilization: Mineral processing plays a pivotal role in efficiently utilizing natural resources, ensuring that valuable minerals are extracted from ore deposits. This is especially crucial for finite and depleting resources, such as precious metals, rare earth elements, and critical minerals.
- Economic Significance: Valuable minerals, including gold, silver, copper, and other metals, are essential commodities used in various industries, from electronics to construction. Mineral processing adds significant value to these raw materials, making them economically viable.
- Environmental Stewardship: Effective mineral processing minimizes the environmental impact of mining activities. Sustainable practices reduce the waste generated, mitigate habitat disruption, and manage water and chemical usage, contributing to environmentally responsible mining.
- Energy Efficiency: Mineral processing strives to optimize energy consumption in comminution (grinding and crushing) and other processing steps. This is vital in a world concerned with energy conservation and climate change.
- Product Quality: Mineral processing ensures that the final product meets the desired quality and purity standards. It removes impurities and tailors the product to specific industry requirements, enhancing its marketability.
- Waste Reduction: By separating and discarding gangue materials, mineral processing minimizes the amount of waste that needs to be managed, reducing the environmental burden.
- Downstream Processing: Processed minerals serve as feedstock for various downstream industries, such as metallurgy, chemicals, and construction. Efficient mineral processing ensures a consistent and high-quality supply of raw materials for these industries.
- Product Diversification: Mineral processing enables the production of a wide range of marketable products, from metals to industrial minerals, addressing the needs of diverse industries.

Safety and Health: Mineral processing focuses on safe and

efficient methods of extracting and handling minerals, reducing risks to workers, and minimizing accidents (Wills, 2016; Gupta and Yan, 2006; Telsmith, 2011; Fuerstenau and Han, 2003; Drelich, 2012; Malhotra et al., 2009).

Research and Innovation: Ongoing research and innovation in mineral processing technology enhance efficiency, reduce environmental impacts, and enable the recovery of minerals from lower-grade and more complex ore deposits (Wills, 2016; Gupta and Yan, 2006; Telsmith, 2011; Fuerstenau and Han, 2003; Drelich, 2012; Malhotra et al., 2009).

In summary, mineral processing is of paramount importance in the mining industry as it transforms raw ore into valuable, marketable products. It ensures the responsible utilization of natural resources, contributes to economic growth, and addresses environmental and sustainability concerns. The field continues to evolve with advancements in technology, making mineral processing more efficient, sustainable, and integral to a variety of industrial sectors (Wills, 2016; Gupta and Yan, 2006; Telsmith, 2011; Fuerstenau and Han, 2003; Drelich, 2012; Malhotra et al., 2009).

2.1. Key stages of mineral processing: comminution, separation, concentration, and dewatering

Mineral processing involves a series of key stages, each aimed at extracting valuable minerals from raw ore and preparing them for marketable products. The four primary stages in mineral processing are comminution, separation, concentration, and dewatering (Umucu, 2011; Umucu et al., 2016).

2.1.1. Comminution:

- Crushing: The first stage of mineral processing typically involves the crushing of mined ore to reduce its size. Crushing can be done with various types of crushers, such as jaw crushers and cone crushers, which break down the ore into smaller pieces (Wills, 2016; Gupta and Yan, 2006; Telsmith, 2011; Fuerstenau and Han, 2003; Drelich, 20122; Malhotra et al., 2009).
- Grinding: After crushing, the ore is further reduced in size through grinding. Grinding is usually performed in ball mills or rod mills, and it transforms the ore into fine particles, making it ready for subsequent separation processes (Wills, 2016; Gupta and Yan, 2006; Telsmith, 2011; Fuerstenau and Han, 2003; Drelich, 2012; Malhotra et al., 2009).
- Sizing: Sizing, or screening, is a process that classifies particles by size. Screens are used to separate the ground ore into different size fractions, ensuring that the particle size is suitable for downstream processing steps Casali et al., 2001; Wills, 2016; Gupta and Yan, 2006; Telsmith, 2011; Fuerstenau and Han, 2003; Drelich, 2012; Malhotra et al., 2009).

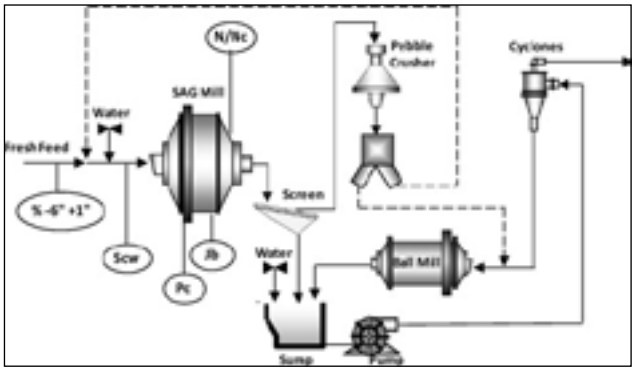

Figure 3. Control circuit of the grinding system with artificial intelligence (Umucu,2011).

2.1.2. Separation:

- Gravity Separation: Gravity separation techniques, such as jigging, spirals, and shaking tables, exploit the differences in density between valuable minerals and gangue to separate them. This is particularly effective for dense minerals like gold and heavy minerals (Wills, 2016; Gupta and Yan, 2006; Telsmith, 2011; Fuerstenau and Han, 2003; Drelich, 2012; Malhotra et al., 2009).
- Magnetic Separation: Magnetic properties are used to separate minerals. Magnetic separators are employed to separate ferromagnetic and paramagnetic minerals from non-magnetic gangue (Malhotra, D., Taylor, P.R., Spiller, E. and LeVier, M., 2009. Recent Advances in Mineral Processing Plant Design, Pages, 587, Society for Mining, Metallurgy, and Exploration, Inc. (SME), Shaffer Parkway Littleton, Colorado, USA.).
- Electrostatic Separation: Electrostatic separators utilize the different electrical conductivity of minerals to separate them. This is often used for separating conductive minerals like rutile and ilmenite from non-conductive minerals (Wills, 2016; Gupta and Yan, 2006; Telsmith, 2011; Fuerstenau and Han, 2003; Drelich, 2012; Malhotra et al., 2009).
- Froth Flotation: In froth flotation, minerals are separated based on their surface properties. Reagents are added to create a froth layer, and air bubbles selectively attach to valuable minerals, allowing them to be separated from the gangue (Conradie and Aldrich, 2001; Cutmore et al., 1997; (Wills, 2016; Gupta and Yan, 2006; Telsmith, 2011; Fuerstenau and Han, 2003; Drelich, 2012; Malhotra et al., 2009).

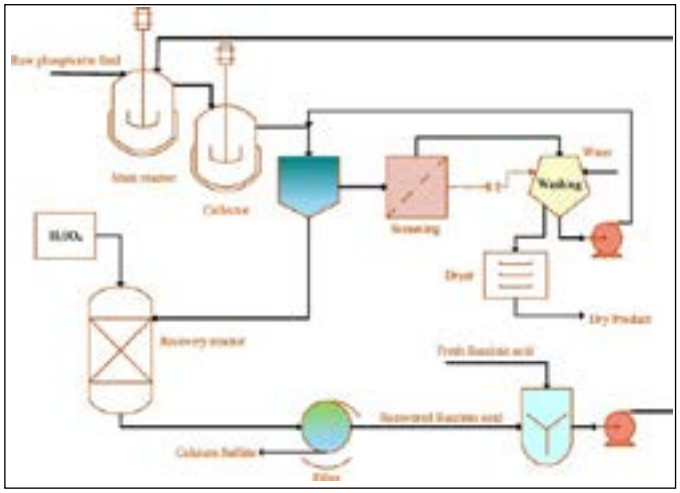

Figure 4. Control of the flotation circuit with artificial intelligence (Rhosonics, 2024)

2.1.3. Concentration:

- Flotation: After separation, the valuable minerals are concentrated through froth flotation. The froth is skimmed off, and the minerals are collected as a concentrate. This step is essential for improving the grade of the final product (Wills, 2016; Gupta and Yan, 2006; Telsmith, 2011; Fuerstenau and Han, 2003; Drelich, 2012; Malhotra et al., 2009).
- Hydrometallurgical Processes: In some cases, minerals are concentrated through chemical leaching processes. For example, in the case of uranium ore, acid leaching is used to extract uranium from the ore (Wills, 2016; Gupta and Yan, 2006; Telsmith, 2011; Fuerstenau and Han, 2003; Drelich, 2012; Malhotra et al., 2009).
- Gravity Concentration: Gravity concentrators like centrifugal concentrators and spirals are used to further concentrate

valuable minerals (Guyot et al., 2004; Conradie et al., 2001; Cutmore et al., 1997; (Wills, 2016; Gupta and Yan, 2006; Telsmith, 2011; Fuerstenau and Han, 2003; Drelich, 2012; Malhotra et al., 2009).

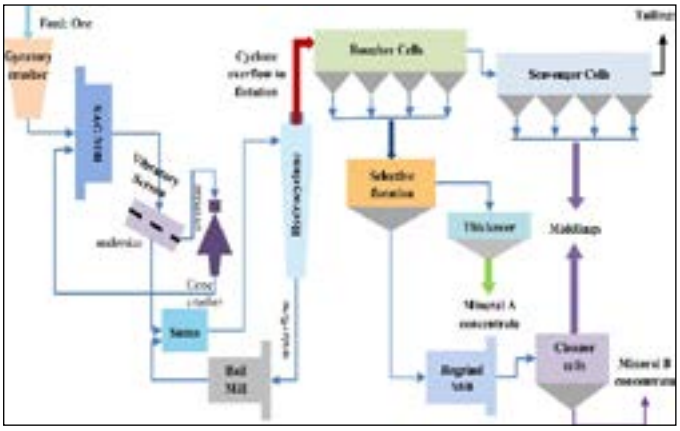

Figure 5. Control of the crushing and enrichment plant together with artificial intelligence (Masampally et al., 2023).

2.1.4. Dewatering:

- Thickening: Thickening is the process of removing excess water from the mineral concentrate. It involves settling particles to increase the solid content and decrease the water content of the concentrate.
- Filtration: Filtration methods, such as vacuum and pressure filtration, are used to further remove water from the concentrate, resulting in a solid cake and a liquid.
- Drying: The final step in dewatering involves drying the concentrate, typically through methods like rotary dryers or flash dryers. This reduces the moisture content to meet product specifications.

The combination of these stages in mineral processing is tailored to the specific characteristics of the ore and the desired final product. These stages are integral to the extraction and concentration of valuable minerals, ensuring the production of high-quality, marketable materials while minimizing waste and environmental impact (Wills, 2016; Gupta and Yan, 2006; Telsmith, 2011; Fuerstenau and Han, 2003; Drelich, 2012; Malhotra et al., 2009).

2.2. Challenges and complexities in mineral processing operations

Mineral processing operations face several challenges and complexities that can impact efficiency, sustainability, and profitability. These challenges are often linked to the characteristics of the ore, environmental concerns, and the need to meet stringent product quality standards. Some of the key challenges and complexities in mineral processing operations include (Wills, 2016; Gupta and Yan, 2006; Telsmith, 2011; Fuerstenau and Han, 2003; Drelich, 2012; Malhotra et al., 2009;).

- Ore Variability: Ores vary in terms of composition, mineralogy, and physical properties. Processing ore with high variability can be challenging as the processing plant needs to adapt to changing conditions.
- Low-Grade Ores: The depletion of high-grade ore deposits means that mining companies are increasingly processing lower-grade ores. This requires more extensive processing and energy input to extract valuable minerals, affecting both cost and environmental impact.
- Complex Ores: Some ores are complex and contain a combination of different minerals. Separating and concentrating these minerals can be complex and may require multiple processing steps.
- Energy Consumption: Comminution (crushing and grinding) is an energy-intensive process in mineral processing. Reducing energy consumption while maintaining efficient processing is a significant challenge.
- Water Usage and Management: Mineral processing operations consume substantial amounts of water for various purposes, including slurry transport and froth flotation. Managing water resources efficiently and sustainably is crucial.
- Environmental Regulations: Meeting environmental standards and regulations is a growing concern for the mining industry. This includes addressing issues like tailings management, dust and emissions control, and water treatment.
- Tailings Management: The handling and disposal of tailings (waste materials from mineral processing) can be a significant challenge. Preventing environmental contamination and ensuring tailings stability are essential.
- Mineral Liberation: Achieving optimal mineral liberation (the separation of valuable minerals from gangue) is essential for maximizing recovery. Achieving this without overgrinding or creating excessive fines can be complex.
- Equipment Maintenance: Mineral processing equipment, such as crushers, mills, and flotation cells, requires regular maintenance to prevent downtime and ensure efficient operations. Maintenance challenges can impact production schedules.
- Operator Skills: Skilled operators are crucial for the efficient operation of mineral processing plants. Recruiting and retaining a skilled workforce can be a challenge, especially in remote mining locations.
- Market Fluctuations: The global market for minerals can be subject to fluctuations in demand and prices. Mineral processors must adapt to market dynamics and changing customer requirements.
- Metallurgical Challenges: Some minerals, like refractory gold ores, have metallurgical challenges due to their unique properties. Specialized processing techniques may be required.
- Regulatory Approval and Permitting: Establishing and operating a mineral processing facility often requires approvals and permits from regulatory authorities, which can be time-consuming and complex.
- Technological Advancements: Staying current with technological advancements and integrating them into operations can be a challenge, but it is essential for maintaining competitiveness and efficiency.
- Sustainability and Social Responsibility: Increasingly, mineral processing operations are expected to adhere to sustainable and socially responsible practices. This includes community engagement, ethical sourcing, and minimizing the environmental footprint (Wills, 2016; Gupta and Yan, 2006; Telsmith, 2011; Fuerstenau and Han, 2003; Drelich, 2012; Malhotra et al., 2009;)

Addressing these challenges and complexities in mineral processing operations requires ongoing research, innovation, and a commitment to responsible and sustainable practices. Collaboration between the mining industry, researchers, and regulatory bodies is essential to finding solutions that balance economic, environmental, and social considerations (Glen et al., 2022; (Wills, 2016; Gupta and Yan, 2006; Telsmith, 2011; Fuerstenau and Han, 2003; Drelich, 2012; Malhotra et al., 2009;).

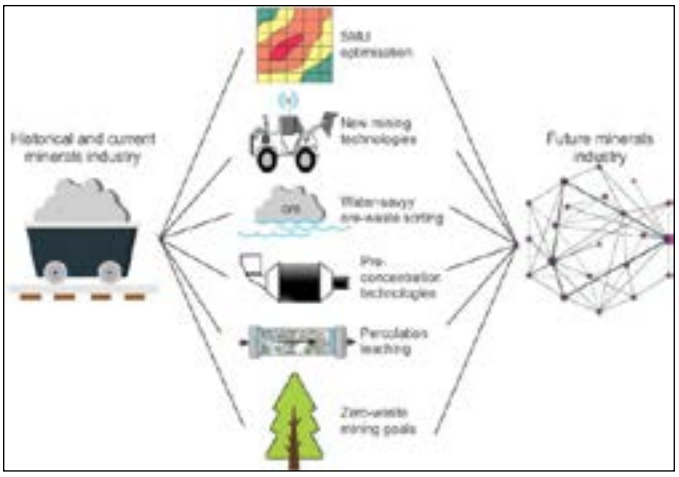

Figure 6. The impact of transforming mining processes into artificial intelligence (Nwaila et al. 2022).

3. Artificial Intelligence

Artificial Intelligence (AI) is a multidisciplinary field of computer science that focuses on the creation of intelligent machines capable of performing tasks that typically require human intelligence. AI encompasses a wide range of techniques, methods, and technologies that aim to enable computers and software systems to simulate and replicate human cognitive functions, such as problem-solving, learning, reasoning, perception, and language understanding (Bahtiyar, 2021; Batal, 2016; Bishop, 2005; Çetin, 2016; Demuth et al., 2008; Haykin, 2009; Jackson, 2019; Kecman, 2001; Öztemel, 2003; Sağıroğlu et al., 2003).

3.1. Scope of artificial intelligence

The scope of artificial intelligence is broad and continually evolving, covering various subfields and applications, including (Bahtiyar, 2021; Batal, 2016; Bishop, 2005; Çetin, 2016; Demuth et al., 2008; Haykin, 2009; Jackson, 2019; Kecman, 2001; Öztemel, 2003; Sağıroğlu et al., 2003; Wong, 2023):

- Machine Learning: Machine learning is a subset of AI that involves training algorithms and models to learn from data, make predictions, and improve their performance over time. It is widely used in applications like image and speech recognition, recommendation systems, and in predictive statistics.
- Deep Learning: Deep learning is a subfield of machine learning that uses neural networks with many layers (deep neural networks) to model and solve complex problems. Deep learning has revolutionized areas such as natural language processing and computer vision.
- Natural Language Processing (NLP): NLP focuses on enabling computers to understand, interpret, and generate human language. It is used in chatbots, language translation, sentiment analysis, and text summarization.
- Computer Vision: Computer vision involves enabling machines to interpret and understand visual information from the world, including images and videos. Applications range from facial recognition and object detection to autonomous vehicles.
- Robotics: AI is applied to control and coordinate robots and autonomous systems. This includes industrial robots, drones, and even humanoid robots capable of performing tasks in unstructured environments.
- Expert Systems: Expert systems are AI programs designed to emulate the decision-making capabilities of a human expert in a particular domain. They are used in fields like medicine, finance, and engineering for diagnosis and decision support.
- Autonomous Systems: AI powers autonomous systems, including self-driving cars, drones, and unmanned aerial vehicles (UAVs), enabling them to navigate and make decisions independently.
- Reinforcement Learning: Reinforcement learning involves training agents to make sequences of decisions in an environment, with the aim of maximizing cumulative rewards. It is commonly used in game-playing AI and robotics.
- AI in Healthcare: AI is applied in the healthcare industry for medical imaging analysis, disease diagnosis, drug discovery, and personalized medicine.
- AI in Finance: In finance, AI is used for algorithmic trading, fraud detection, risk assessment, and financial advisory services.
- AI in Education: AI is employed in educational technology for personalized learning, intelligent tutoring systems, and educational analytics.
- AI in Customer Service: Chatbots and virtual assistants use AI to provide automated customer support, handle inquiries, and streamline customer interactions.
- AI in Entertainment: AI is used in the entertainment industry for content recommendation, video game design, and special effects in movies and animations.
- AI in Environmental Monitoring: AI technologies are employed for environmental monitoring, including climate modeling, wildlife tracking, and conservation efforts.
- Ethical AI: Ensuring the ethical and responsible use of AI is an emerging area, focusing on fairness, accountability, transparency, and the avoidance of bias in AI systems.

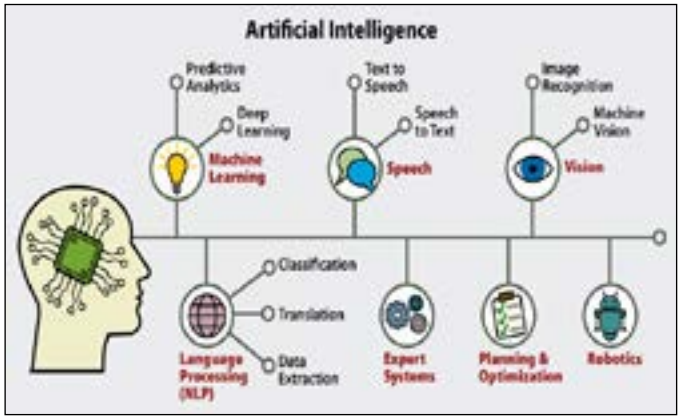

Figure 7. Working stages of artificial intelligence (Swiss Cognitive, 2024).

The scope of artificial intelligence is vast and continues to expand as new technologies and applications emerge. AI has the potential to transform numerous industries and enhance various aspects of daily life. Researchers and practitioners are continually pushing the boundaries of AI, developing innovative solutions to complex problems, and shaping the future of intelligent systems (Bahtiyar, 2021; Batal, 2016; Bishop, 2005; Çetin, 2016; Demuth et al., 2008; Haykin, 2009; Jackson, 2019; Kecman, 2001; Öztemel, 2003; Sağıroğlu et al., 2003; Wong, 2023; Data-science, 2024).

3.2. Machine learning, deep learning, and neural networks

Machine learning, deep learning, and neural networks are interconnected concepts within the broader field of artificial intelligence (AI). Here's an explanation of each and how they relate to one another:

3.2.1. Machine Learning (ML)

Machine learning is a subset of artificial intelligence that focuses on developing algorithms and models that enable computers to learn and make predictions or decisions based on data. In traditional programming, humans write explicit instructions to solve a problem, while in machine learning, the system learns patterns from data and uses these patterns to make predictions.

Machine learning encompasses various techniques, including supervised learning, unsupervised learning, and reinforcement learning. It involves the use of algorithms to train models on data, with the primary goal of generalizing from that data to make accurate predictions or decisions on new, unseen data (Bahtiyar, 2021; Batal, 2016; Bishop, 2005; Çetin, 2016; Demuth et al., 2008; Haykin, 2009; Jackson, 2019; Kecman, 2001; Öztemel, 2003; Sağıroğlu et al., 2003; Wong, 2023; Faster Capital, 2024).

3.2.2. Deep Learning

Deep learning is a subfield of machine learning that deals specifically with artificial neural networks, which are modeled after the structure and function of the human brain. Deep learning focuses on deep neural networks, which have multiple layers of interconnected neurons (nodes). These neural networks are designed to automatically learn hierarchical features from data, allowing them to solve complex problems.

Deep learning has gained popularity and success in various AI applications, including computer vision, natural language processing, speech recognition, and autonomous systems. Convolutional neural networks (CNNs) are commonly used in image analysis, while recurrent neural networks (RNNs) and transformer models excel in natural language understanding tasks (Bahtiyar, 2021; Batal, 2016; Bishop, 2005; Çetin, 2016; Demuth et al., 2008; Haykin, 2009; Jackson, 2019; Kecman, 2001; Öztemel, 2003; Sağıroğlu et al., 2003; Wong, 2023; Faster Capital, 2024).

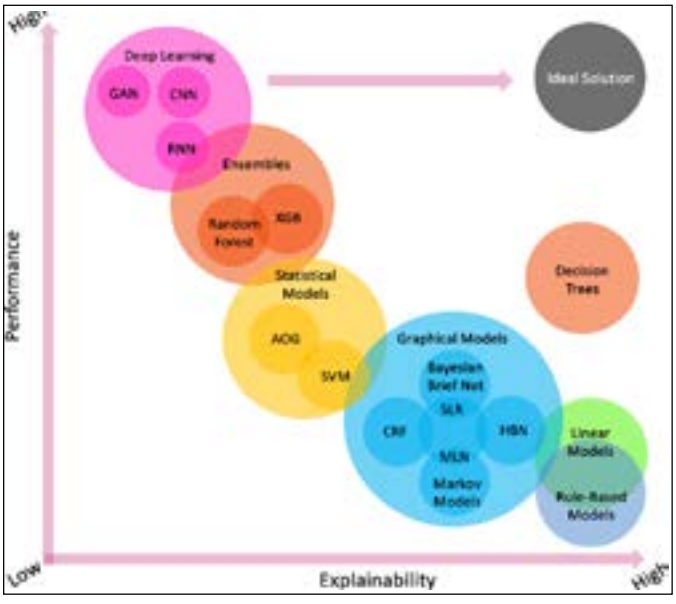

Figure 8. Machine learning skills and performance (Wordstream, 2024).

3.2.3. Neural Networks

Neural networks are computational models that draw inspiration from the biological neural networks in the human brain. They consist of layers of interconnected nodes, which are also known as neurons or artificial neurons. Each connection between nodes has a weight associated with it, and nodes apply mathematical operations, such as weighted sums and activation functions, to transform input data.

Neural networks can be shallow, with just a few layers (as in traditional machine learning models), or deep, with many hidden layers. Deep neural networks, often referred to as deep learning models, are capable of learning complex, hierarchical representations of data.

In summary, deep learning is a specific subfield of machine learning that focuses on deep neural networks. Neural networks are the fundamental building blocks for both machine learning and deep learning, and they play a critical role in pattern recognition, feature extraction, and decision-making in these systems. Deep learning has demonstrated remarkable success in various AI applications, largely due to the ability of deep neural networks to learn and represent complex features from data (Bahtiyar, 2021; Batal, 2016; Bishop, 2005; Çetin, 2016; Demuth et al., 2008; Haykin, 2009; Jackson, 2019; Kecman, 2001; Öztemel, 2003; Sağıroğlu et al., 2003; Wong, 2023; Data-science, 2024).

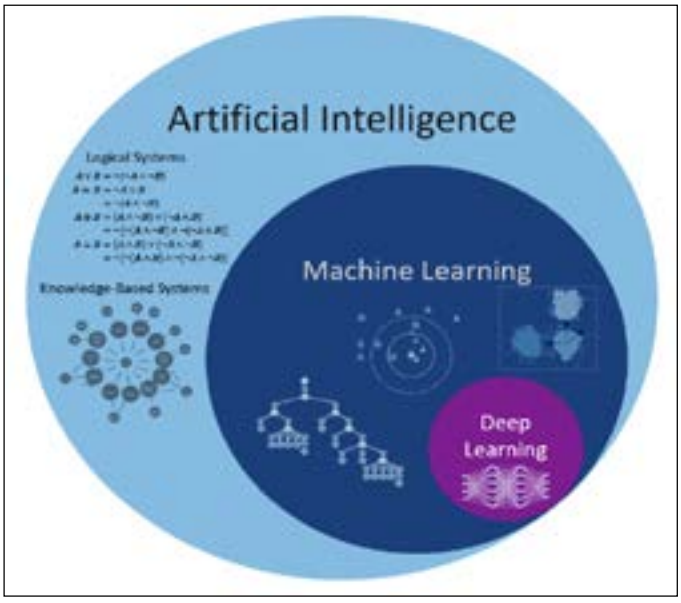

Figure 9. Fields of artificial intelligence and automatic control (Knifexns, 2024).

3.3. How AI algorithms work and their applications

AI algorithms work by leveraging mathematical and computational techniques to process data, recognize patterns, make predictions, and optimize decision-making. These algorithms are designed to simulate human cognitive functions, such as learning, reasoning, and problem-solving. Here is an overview of how AI algorithms work and their diverse applications (Bahtiyar, 2021; Batal, 2016; Bishop, 2005; Çetin, 2016; Demuth et al., 2008; Haykin, 2009; Jackson, 2019; Kecman, 2001; Öztemel, 2003; Sağıroğlu et al., 2003; Wong, 2023):

3.3.1. How AI Algorithms Work

- Data Collection: AI algorithms require data to operate effectively. This data can come in various forms, including text, images, audio, and structured data.

- Data Preprocessing: Raw data is often noisy and unstructured. Preprocessing involves cleaning, transforming, and normalizing the data to make it suitable for analysis. This step can also include data reduction and feature engineering to extract relevant information.
- Feature Extraction: For structured data, feature extraction involves selecting and transforming specific attributes or variables that are relevant to the problem being solved. In the case of unstructured data (e.g., images or text), feature extraction may involve techniques like image convolution or natural language processing (NLP) to identify meaningful patterns.
- Algorithm Selection: Different AI algorithms are chosen based on the nature of the problem. Common algorithms include linear regression, decision trees, support vector machines, k-means clustering, and deep neural networks, among others.
- Training: AI algorithms, particularly machine learning algorithms, learn from historical data. During the training phase, the algorithm uses labeled data to adjust its internal parameters to make accurate predictions or classifications.
- Testing and Validation: The algorithm's performance is evaluated on a separate dataset to ensure it can generalize its learning to new, unseen data. This process helps assess the algorithm's accuracy and generalization capabilities.
- Model Deployment**:** Once trained and validated, the AI model is deployed in a real-world application where it processes new data and makes predictions or decisions.

3.3.2. Applications of AI Algorithms

AI algorithms are applied across a wide range of industries and domains, offering solutions to numerous problems. Some common applications include (Bahtiyar, 2021; Batal, 2016; Bishop, 2005; Çetin, 2016; Demuth et al., 2008; Haykin, 2009; Jackson, 2019; Kecman, 2001; Öztemel, 2003; Sağıroğlu et al., 2003; Wong, 2023):

• Natural Language Processing (NLP)

Sentiment Analysis: Determining the sentiment (positive, negative, or neutral) of text data, often used in social media monitoring and customer feedback analysis.

Language Translation: Translating text from one language to another.

Chatbots: Building virtual conversational agents for customer support and information retrieval.

• Computer Vision

Image Classification: Categorizing images into predefined classes, used in facial recognition, object detection, and medical image analysis.

Optical Character Recognition (OCR): Extracting text from images or scanned documents.

Autonomous Vehicles: Enabling self-driving cars to interpret and navigate their surroundings.

• Recommendation Systems

Content Recommendations: Suggesting movies, products, or articles based on a user's preferences and behavior.

Personalized Marketing: Targeting users with customized ads and promotions.

• Healthcare

Medical Image Analysis: Assisting radiologists in diagnosing diseases from X-rays, MRIs, and CT scans.

Drug Discovery: Identifying potential drug candidates and optimizing drug development processes.

• Finance

Fraud Detection: Identifying fraudulent financial transactions.

Algorithmic Trading: Automating trading decisions based on market analysis.

Credit Scoring: Assessing an individual's creditworthiness.

• Industry and Manufacturing

Predictive Maintenance: Using sensor data to forecast equipment failures and optimize maintenance schedules.

Quality Control: Ensuring product quality through visual inspection and anomaly detection.

• Environmental Monitoring

Climate Modeling: Predicting and monitoring climate changes.

Wildlife Conservation: Tracking and analyzing animal behavior and population dynamics.

• Robotics

Industrial Automation: Programming robots for manufacturing tasks.

Humanoid Robots: Developing robots capable of human-like movements and interaction.

• Education

Adaptive Learning: Personalizing educational content and assessments for students.

• Agriculture

Precision Agriculture: Optimizing crop management, irrigation, and resource allocation.

These examples illustrate the versatility of AI algorithms and their potential to enhance productivity, efficiency, and decision-making across various fields. AI continues to evolve, leading to the development of increasingly sophisticated algorithms and expanding its applications to new and diverse areas ((Bahtiyar, 2021; Batal, 2016; Bishop, 2005; Çetin, 2016; Demuth et al., 2008; Haykin, 2009; Jackson, 2019; Kecman, 2001; Öztemel, 2003; Sağıroğlu et al., 2003; Wong, 2023; Data-science, 2024).

3.4. Applications of AI in Mineral Processing

3.4.1. Ore Prospecting and Targeting

AI has various applications in mineral processing, including ore prospecting and targeting. Here's how AI is used in this specific aspect of the mining industry (Aldrich et al., 2010; Bartolacci et al., 2006; Benardos and Kaliampakos, 2004; Chen et al., 2018; Cutmore et al., 1997; Davila-Santiago et al., 2022; De Lima et al., 2020; Folorunso et al., 2012; López et al., 2017; Lobo et al., 2021; Perez et al., 2015; Prabhavathy et al., 2019):

Geological Data Analysis: AI can analyze geological and geospatial data to identify potential areas for ore prospecting. This includes the analysis of geological maps, satellite imagery, and geological surveys. AI algorithms can identify geological formations, structures, and anomalies that may indicate the presence of valuable minerals.

Exploration Targeting: AI can assist geologists and mining companies in targeting specific areas for mineral exploration. Machine learning models can process historical exploration data, identifying patterns and correlations that suggest where valuable ore deposits are more likely to be found. This predictive capability can save time and resources in the exploration process.

Remote Sensing and Imaging: AI is used to analyze remote

sensing data, such as hyperspectral imaging and airborne surveys, to detect mineral signatures. These technologies can identify the spectral signatures associated with various minerals, helping geologists locate potential deposits from a distance.

Drilling and Core Sample Analysis: AI can analyze drilling data and core samples to determine mineral composition and quality. This information guides further exploration and helps geologists make informed decisions about whether to continue drilling in a particular area.

Mineralogical Characterization: AI-powered microscopy and imaging systems are used to identify and characterize minerals within samples. This information is crucial for understanding the mineral composition and quality of ore bodies.

Pattern Recognition and Anomaly Detection: AI algorithms can detect patterns and anomalies in geological data that may indicate the presence of valuable minerals. For example, the presence of certain minerals in proximity to others can be a strong indicator of a deposit.

Data Fusion: AI techniques are used to integrate and analyze data from multiple sources, such as geophysical surveys, geochemical data, and geospatial information. By combining various data types, AI can provide a more comprehensive view of the subsurface geology.

Predictive Modeling: Machine learning models can predict the likelihood of discovering valuable minerals in a specific area based on historical data, geospatial features, and geological knowledge.

Resource Estimation: AI is used to estimate the size and grade of mineral deposits based on geological and drilling data. This information is essential for resource assessment and mine planning.

Efficiency and Cost Reduction: AI applications in ore prospecting can lead to cost savings by optimizing drilling and exploration efforts. By targeting high-potential areas with greater accuracy, companies can reduce the costs associated with unsuccessful exploration.

AI's ability to analyze vast datasets and recognize patterns makes it a valuable tool in ore prospecting and targeting, enhancing the efficiency and success rate of mineral exploration efforts. By improving the accuracy and precision of exploration, AI contributes to more sustainable and responsible mining practices ((Aldrich et al., 2010; Bartolacci et al., 2006; Benardos and Kaliampakos, 2004; Chen et al., 2018; Cutmore et al., 1997; Davila-Santiago et al., 2022; De Lima et al., 2020; Folorunso et al., 2012; López et al., 2017; Lobo et al., 2021; Perez et al., 2015; Prabhavathy et al., 2019; Tyagi and Tiwari, 2024; Tabassum et al., 2024; Emeritus, 2024).

3.4.2. Automated Drilling and Blasting

AI is increasingly being utilized in mineral processing, including automated drilling and blasting operations, to enhance safety, precision, and efficiency in the mining industry. Here are some key applications and benefits of AI in this context Ambrozic and Turk, 2003; Benardos, and Kaliampakos, 2004; Feng and Seto 1999; Huang, 1999; Kahraman et al., 2006; Perez et al., 2015; Ojha and Jaiswal, 2023; Benardos and Kaliampakos, 2004; Bishop, 2005; Canakcı and Pala, 2007; Demuth et al., 2008; Eberhart and Shi, 2007):

Drill Hole Optimization: AI algorithms analyze geological data and historical drilling patterns to optimize the placement and depth of drill holes. This results in more precise drilling and reduces the need for over-drilling, minimizing waste and energy consumption

Real-Time Geological Data Analysis: AI systems can process real-time geological data from sensors and drilling equipment, adjusting drilling parameters to adapt to changing subsurface conditions. This ensures that drill holes are accurately placed in mineral-rich areas.

Blast Pattern Design: AI algorithms consider factors such as ore body shape, rock type, and desired fragmentation size to design efficient blast patterns. This leads to improved ore recovery rates and minimized rock oversize.

Sequenced Blasting: AI-driven systems can sequence the blasting of drill holes to achieve optimal fragmentation and minimize vibrations and fly-rock. This helps in preventing damage to equipment and structures in the vicinity of the blasting site.

Energy Efficiency: AI helps optimize drilling and blasting parameters, reducing energy consumption and the environmental impact associated with these operations.

Remote Operation: Some AI-powered drilling and blasting systems can be operated remotely, enhancing safety by keeping workers out of hazardous areas.

Data Collection and Analysis: AI systems collect and analyze vast amounts of data from drilling and blasting operations. This data can be used for performance analysis, predictive maintenance, and process improvement.

Safety Enhancement: Automated systems reduce the need for manual labor in drilling and blasting operations, leading to a safer work environment. Workers are less exposed to hazardous conditions.

Environmental Impact Reduction: AI-driven precision in drilling and blasting minimizes the environmental impact by reducing overbreak and the generation of flyrock. Controlled blasting also lowers the risk of ground vibrations and air overpressure.

Cost Savings: The precision and efficiency achieved with AI automation lead to cost savings through reduced rework, secondary blasting, and excessive use of explosives.

Scheduling and Planning: AI can assist in scheduling drilling and blasting operations based on production targets, equipment availability, and environmental considerations.

Regulatory Compliance: AI systems can be programmed to comply with environmental regulations, helping mining companies meet their legal and environmental responsibilities.

AI-driven automation in drilling and blasting not only enhances the efficiency and safety of mineral processing operations but also contributes to a more sustainable and environmentally responsible mining industry. As AI technologies continue to advance, their applications in drilling and blasting will further improve productivity and reduce the environmental footprint of mining activities. (Ojha and Jaiswal, 2023; Ambrozic and Turk, 2003; Benardos and Kaliampakos, 2004; Bishop, 2005; Canakcı and Pala, 2007; Demuth et al., 2008; Eberhart and Shi, 2007; Feng and Seto, 1999; Kahraman et al., 2006; Huang 1999).

3.4.3. Mineral Identification

AI plays a significant role in mineral identification and characterization within the field of mineral processing. Here are some of the applications and benefits of AI in mineral identification (Ramil et al., 2018; López et al., 2017; DeTore, 1989; Folorunso et al., 2012; Okada et al., 2020; Mishra, 2021; Izadi et al., 2017; Prabhavathy et al., 2019; Chen et al., 2018; Lobo et al., 2021; De Lima et al., 2020; Tang et al., 2020; Wang et al., 2021).:

Automated Mineral Classification: AI systems, especially

machine learning and computer vision techniques, can classify minerals based on their physical and chemical properties. This is particularly valuable in geological exploration and mining operations, as it helps in identifying the composition of ore and gangue minerals.

Spectral Analysis: AI is used to analyze spectral data, such as hyperspectral or multispectral imaging, to identify minerals. Different minerals have distinctive spectral signatures that can be recognized by AI algorithms. This is valuable for remote sensing and geological surveys.

Mineral Liberation Analysis: AI can be applied to determine the liberation of valuable minerals from gangue materials in ore samples. It can analyze the mineral grain sizes, shapes, and associations, aiding in process optimization and mineral recovery.

Image Analysis: AI-driven image analysis techniques are used to identify minerals within ore samples. This includes identifying and segmenting mineral grains in images, allowing for quantitative mineralogy.

X-ray Diffraction (XRD) Analysis: AI can assist in interpreting XRD data, which provides information about the crystallography and mineral phases present in a sample.

Mineral Mapping: AI and remote sensing technologies are employed to map the distribution of minerals across large areas. This is valuable for identifying potential ore bodies during exploration.

Mineralogical Characterization: AI can help characterize the mineral composition of samples by interpreting data from tools like X-ray fluorescence (XRF) spectrometers.

Mineral Quantification: AI algorithms can quantify the amount or concentration of specific minerals in a sample, helping to determine the ore grade.

Mineralogical Data Integration: AI can integrate and analyze data from various sources, such as geophysical surveys, drilling data, and geospatial information, to build a comprehensive picture of the mineralogy of a deposit.

Real-Time Analysis: AI systems can provide real-time mineral identification and characterization, allowing for immediate decision-making in mineral processing operations.

Predictive Modeling: Machine learning models can predict the presence of specific minerals in an ore sample based on historical data and geological context.

Quality Control: AI is used for quality control in mineral processing plants to ensure that the mineral product meets specified quality and purity standards.

Sustainability and Efficiency: Accurate mineral identification helps in optimizing the mineral processing process, reducing waste, and improving energy efficiency.

AI-driven mineral identification provides the mining industry with valuable tools to optimize mineral processing operations, reduce costs, enhance productivity, and make more informed decisions about the extraction and processing of valuable minerals. It contributes to more efficient and sustainable mining practices (Ramil et al., 2018; López et al., 2017; DeTore, 1989; Folorunso et al., 2012; Okada et al., 2020; Mishra, 2021; Izadi et al., 2017; Prabhavathy et al., 2019; Chen et al., 2018; Lobo et al., 2021; De Lima et al., 2020; Tang et al., 2020; Wang et al., 2021).

3.4.4. Crushing and Grinding Optimization

AI plays a crucial role in optimizing crushing and grinding operations in the mineral processing industry. These processes are energy-intensive and directly impact the efficiency and cost-effectiveness of mineral extraction. Here are some key applications and benefits of AI in crushing and grinding optimization (Casali et al., 2001; Conradie and Aldrich, 2001; Elmas, 2003; Fuerstenau et al., 2004; Guyot et al., 2004; Kecman, 2001; Nabiyev, 2003; Sağıroğlu et al., 2003):

Process Control: AI systems monitor and control various parameters in crushing and grinding circuits, such as feed rates, particle size, and equipment settings. They make real-time adjustments to optimize the process and ensure consistent product quality.

Predictive Maintenance: AI can predict equipment failures and maintenance needs by analyzing sensor data from crushers, mills, and other machinery. This prevents unexpected downtime and reduces maintenance costs.

Energy Efficiency: AI algorithms help minimize energy consumption during crushing and grinding by adjusting equipment settings and process parameters based on real-time conditions. This leads to significant energy savings.

Particle Size Control: AI systems can maintain tight control over the particle size distribution in the grinding process. This is essential for ensuring that the final product meets the desired specifications and is ready for downstream processing.

Automatic Process Adjustment: AI continuously adjusts the crushing and grinding process to maximize throughput while maintaining product quality. This results in higher production rates and cost savings.

Optimal Feed Control: AI systems analyze the properties of the ore feed, such as hardness and composition, and adjust the feed rate to maintain efficient processing. This helps prevent overloading and equipment wear.

Wear and Liner Monitoring: AI monitors the wear and tear of crushers and mills by analyzing sensor data. This information is used to optimize the replacement of wear parts, reducing downtime and maintenance costs.

Closed-Loop Control: AI provides closed-loop control of grinding circuits, ensuring that the system is operating at maximum efficiency and maintaining consistent product quality.

Data Analysis and Modeling: AI algorithms process vast amounts of historical data to build predictive models for crushing and grinding operations. These models help in process optimization, allowing for better decision-making.

Operational Insights: AI systems provide operators and engineers with insights into the performance of crushing and grinding processes. This helps in identifying areas for improvement and making informed decisions.

Environmental Impact Reduction: By optimizing crushing and grinding operations, AI contributes to reduced energy consumption and fewer emissions, leading to a more environmentally sustainable mineral processing process.

Reduced Overgrinding: AI helps prevent overgrinding, which can result in excessive energy usage and the production of fine particles that are difficult to recover. Maintaining optimal particle size distribution improves recovery rates.

Optimizing crushing and grinding operations through AI not only improves productivity and energy efficiency but also reduces equipment wear and tear, leading to longer equipment lifespans. This contributes to more cost-effective and sustainable mineral processing practices (Casali et al., 2001; Conradie and Aldrich, 2001; Elmas, 2003; Fuerstenau et al., 2004; Guyot et al., 2004; Kecman, 2001; Nabiyev, 2003; Sağıroğlu et al., 2003)

3.4.5. Process Control

AI-driven process control in mineral processing offers several applications and benefits, contributing to enhanced efficiency, productivity, and sustainability. Here are specific applications of AI in process control within the mineral processing industry (Zhou et al., 2020; Ahl et al., 2019; Dupont et al., 2012; Mahmud et al., 2020; Thomas et al., 2019; Cheng and Yu, 2019; Babacan et al., 2020; Zhao et al., 2012; Kang et al., 2012; Thomson et al., 2017; Siler-Evans et al., 2012; Hawkes, 2010; Li and Yao, 2020):

Automated Equipment Control: AI systems can autonomously control and adjust the settings of processing equipment, such as crushers, mills, flotation cells, and separators. These adjustments optimize the processing parameters, such as rotation speed and feed rates, for maximum efficiency and resource utilization.

Predictive Process Optimization: AI algorithms continuously analyze process data and use predictive modeling to optimize operations. They can anticipate fluctuations in ore quality or feed composition and adjust the process accordingly to maintain high product quality and efficiency.

Quality Control and Real-Time Adjustments: AI systems monitor product quality and make real-time adjustments to process parameters to ensure that the final product meets specified quality standards. This includes monitoring particle size distribution, chemical composition, and other quality metrics.

Energy Efficiency: AI-driven process control aims to minimize energy consumption by optimizing the operation of energy-intensive equipment. It can adjust equipment settings to reduce energy usage and, in turn, operational costs.

Closed-Loop Control: AI systems provide closed-loop control of various processes, ensuring that the system operates efficiently and maintains product quality consistently. They can automatically adjust process parameters to achieve desired outcomes.

Environmental Impact Reduction: AI-driven precision in process control minimizes the environmental impact of mineral processing. Reduced energy consumption and optimized operations lead to lower emissions and resource usage, contributing to sustainability.

Resource Optimization: AI optimizes the use of resources such as water and reagents. It can monitor resource consumption, adjust usage as needed, and reduce waste, improving resource efficiency.

Waste Management: AI systems can optimize waste handling and disposal by predicting waste volumes and minimizing environmental impact.

Operational Insights: AI systems provide valuable insights into the performance of mineral processing operations. Operators and engineers can use these insights to make informed decisions, improve process efficiency, and address operational challenges.

Minimization of Overprocessing: AI helps prevent overprocessing, overgrinding, and overuse of reagents, reducing energy consumption and operational costs. Maintaining an optimal particle size distribution and process efficiency leads to better recovery rates.

Scheduling and Planning: AI assists in scheduling and planning mineral processing operations based on production targets, equipment availability, and environmental considerations.

Environmental Compliance: AI systems can be programmed to ensure that mineral processing operations comply with environmental regulations and standards. They make real-time adjustments to control emissions, water usage, and other environmental impact factors.

AI-driven process control optimizes mineral processing operations, leading to increased efficiency, cost savings, improved product quality, and reduced environmental impact. These applications are integral to the sustainability and profitability of the mining industry (Zhou et al., 2020; Ahl et al., 2019; Dupont et al., 2012; Mahmud et al., 2020; Thomas et al., 2019; Cheng and Yu, 2019; Babacan et al., 2020; Zhao et al., 2012; Kang et al., 2012; Thomson et al., 2017; Siler-Evans et al., 2012; Hawkes, 2010; Li and Yao, 2020).

3.4.6. Froth Flotation Optimization

Froth flotation is a critical process in mineral processing for separating valuable minerals from gangue. AI is increasingly applied to optimize and enhance froth flotation operations, leading to improved efficiency and resource utilization. Here are the applications and benefits of AI in froth flotation optimization (Ahmad et al., 2017; Goldberg et al., 2015; Gomez-Flores et al., 2020; Hogarth et al., 2015; Hu et al., 2013; Jahedsaravani et al., 2014; Massinaei and Doostmohammadi, 2010; Moolman et al., 1995; Nakhaei and Irannajad, 2013; Nakhaei et al., 2012; Nakhaeie et al., 2013; Pirouzan et al., 2014; Ren et al., 2015; Semwayo and Ajoodha, 2021; Wang and Han, 2015):

Real-Time Process Monitoring: AI systems continuously monitor the froth flotation process by collecting data from various sensors and instruments. These systems provide real-time insights into variables such as froth depth, air and slurry flow rates, and chemical dosages.

Predictive Modeling: AI leverages historical data to build predictive models for froth flotation. These models can predict the response of the process to changes in input variables, helping operators make informed decisions.

Reagent Dosage Optimization: AI algorithms optimize the dosage of chemical reagents used in froth flotation. By analyzing ore properties and real-time process data, AI can precisely control reagent addition to maximize mineral recovery while minimizing costs.

Particle Size Analysis: AI can analyze particle size distribution data in the ore feed and in the froth product. This information is used to make adjustments to the process to optimize the desired mineral recovery.

Froth Quality Control: AI systems monitor the quality of the froth, assessing its stability and characteristics. Real-time adjustments can be made to maintain optimal froth quality, leading to enhanced mineral recovery.

Air Distribution Control: AI can optimize the distribution of air within the flotation cells to ensure the formation of a stable and well-structured froth. This is essential for efficient mineral separation.

Bubble Size and Velocity Analysis: AI systems can assess the size and velocity of bubbles within the flotation cells. Controlling bubble characteristics can improve the selectivity of the process.

pH Control: AI systems can maintain optimal pH levels within the flotation cells by adjusting chemical dosages. This helps in achieving the desired mineral separation and recovery rates.

Optimal Flotation Circuit Configuration: AI can recommend the most suitable configuration of flotation cells and circuits based on

the ore type and mineralogy, ensuring that the processis tailored for maximum efficiency.

Reduced Environmental Impact: By optimizing the froth flotation process, AI helps reduce the usage of chemicals and water, leading to lower environmental impact and operational costs.

Product Quality Assurance: AI ensures that the final product meets specified quality standards by maintaining consistent froth quality and mineral recovery rates.

Waste Minimization: AI can minimize waste production and the generation of tailings by optimizing the separation process, reducing resource waste and environmental impact.

AI-driven froth flotation optimization is crucial for mineral processing operations, particularly in achieving higher mineral recovery rates and reducing operational costs. By automating and fine-tuning the process, AI contributes to improved resource utilization and more sustainable mining practices (Ahmad et al., 2017; Goldberg et al., 2015; Gomez-Flores et al., 2020; Hogarth et al., 2015; Hosseini et al., 2015; Hu et al., 2013; Jahedsaravani et al., 2014; Massinaei and Doostmohammadi, 2010; Moolman et al., 1995; Nakhaei and Irannajad, 2013; Nakhaei et al., 2012; Nakhaeie et al., 2013; Pirouzan et al., 2014; Ren et al., 2015; Semwayo and Ajoodha, 2021; Wang and Han, 2015).

3.4.7. Predictive Maintenance

Predictive maintenance is a crucial application of AI in mineral processing. It involves the use of artificial intelligence to monitor the condition of mining and processing equipment, predict when maintenance is needed, and schedule maintenance activities before a breakdown occurs. Here are the applications and benefits of AI in predictive maintenance in the mining and mineral processing industry (Joshi, 2020; Hassanien, 2020; Jackson, 2019; Kamel, 2012; Thomas, 2018; Mathworks, 2020; Killeen et al., 2019; Pampel, 2000):

Real-Time Equipment Monitoring: AI systems continuously collect and analyze real-time data from various sensors and instruments installed on mining and processing equipment. This data includes information on temperature, vibration, pressure, and other critical parameters.

Anomaly Detection: AI algorithms use machine learning techniques to identify anomalies and deviations from normal equipment behavior. When unusual patterns or abnormal data are detected, the system generates alerts for further investigation.

Predictive Modeling: AI builds predictive models based on historical equipment data and operational conditions. These models can forecast equipment failures and performance degradation, taking into account factors like usage patterns and environmental conditions.

Remaining Useful Life Prediction: AI systems estimate the remaining useful life of equipment components and systems. This information helps in planning maintenance activities and minimizing unplanned downtime.

Maintenance Recommendations: AI provides maintenance recommendations based on the analysis of equipment condition data. These recommendations include scheduling preventative maintenance, identifying the components that need attention, and suggesting the optimal maintenance approach.

Downtime Reduction: By predicting maintenance needs and scheduling maintenance activities proactively, predictive maintenance minimizes unscheduled downtime. This leads to increased operational efficiency and productivity.

Cost Savings: Predictive maintenance reduces maintenance costs by avoiding unnecessary repairs and component replacements. It also optimizes the use of resources, such as spare parts and maintenance personnel.

Safety Enhancement: Predictive maintenance helps maintain a safer work environment by preventing sudden equipment failures that can pose risks to workers. It minimizes the need for emergency repairs in potentially hazardous situations.

Environmental Impact Reduction: By minimizing equipment failures and the associated emissions and waste, predictive maintenance contributes to environmental sustainability and regulatory compliance.

Data Integration: AI integrates data from various sources, including equipment sensors, historical maintenance records, and process data. This comprehensive dataset enables more accurate predictions and recommendations.

Remote Monitoring: AI-driven predictive maintenance systems often support remote monitoring, allowing maintenance teams to assess equipment conditions and make decisions from a safe location.

Process Optimization: By maintaining equipment in optimal condition, predictive maintenance contributes to overall process optimization in mineral processing operations.

Predictive maintenance powered by AI is instrumental in minimizing unplanned downtime, optimizing maintenance practices, and ensuring the reliability of mining and processing equipment. It enhances safety, reduces costs, and contributes to more efficient and sustainable mineral processing operations (Joshi, 2020; Hassanien, 2020; Jackson, 2019; Kamel, 2012; Thomas, 2018; Mathworks, 2020; Killeen et al., 2019; Pampel, 2000).

3.4.8. Supply Chain Optimization

AI-driven supply chain optimization has become increasingly important in the mineral processing industry. By applying artificial intelligence, companies can improve the efficiency, reliability, and sustainability of their supply chains. Here are the applications and benefits of AI in supply chain optimization for mineral processing (Pournader et al., 2021; Nazeri and Keshavarzi, 2019; Min, 2010; Baryannis et al., 2019a; Pandian, 2019; Misra et al., 2020; Baryannis et al., 2019b; Dwivediet al., 2021; Eskandari-Khanghahi et al., 2018; Araldo et al., 2019; Gholamrezaei et al., 2023; Maleki, 2023; Karami, 2022; Ssempijja et al., 2021; Hellingrath and Lechtenberg, 2019; Lotfi et al., 2021a; Lotfi et al., 2021b; Nikookar et al., 2021):

• Demand Forecasting:

Data-Driven Forecasting: AI uses historical data, market trends, and external factors to generate accurate demand forecasts for minerals and mineral products. These forecasts are essential for planning production and logistics.

Dynamic Forecasting: AI systems can adjust forecasts in real-time based on changing market conditions, enabling companies to respond quickly to fluctuations in demand.

Inventory Optimization: AI-driven demand forecasting helps in managing inventory levels efficiently, reducing excess inventory and carrying costs while ensuring that demand is met.

Lead Time Prediction: AI can predict lead times for mineral shipments, considering factors like supplier reliability, transportation options, and potential delays. This helps in planning and reducing supply chain disruptions.

Demand Variation Analysis: AI identifies patterns and variations in demand, allowing companies to adjust their supply chain strategies accordingly and avoid under or overstocking.

• Inventory Management:

Just-in-Time Inventory: AI supports the implementation of just-in-time (JIT) inventory strategies, reducing carrying costs and the need for large storage facilities.

Safety Stock Management: AI optimizes safety stock levels to ensure that enough inventory is on hand to meet demand while minimizing excess stock.

Demand-Driven Replenishment: AI systems initiate replenishment orders based on actual demand, reducing the risk of stockouts and improving operational efficiency.

Supplier Performance Monitoring: AI monitors supplier performance and can trigger alerts or actions when suppliers fail to meet delivery commitments, ensuring a reliable supply chain.

• Logistics Optimization:

Route Optimization: AI optimizes transportation routes for minerals, taking into account factors such as distance, transportation costs, fuel efficiency, and delivery deadlines.

Load Optimization: AI helps determine the most efficient way to load minerals onto transport vehicles to maximize capacity while ensuring safe transport.

Carrier Selection: AI evaluates carrier performance and selects the most suitable carriers based on factors like reliability, cost, and past performance.

Risk Mitigation: AI assesses various risks in logistics, including weather-related delays, port congestion, and geopolitical factors, and recommends strategies to mitigate these risks.

Environmental Impact Reduction: AI can optimize logistics to reduce the environmental impact of mineral transport, such as minimizing emissions and fuel consumption.

Real-Time Visibility: AI provides real-time visibility into the supply chain, allowing companies to track the location and condition of minerals and monitor the progress of shipments.

Cost Reduction: AI-driven logistics optimization reduces transportation costs, including fuel expenses and maintenance costs, while also enhancing overall efficiency.

AI applications in supply chain optimization contribute to the efficient, cost-effective, and environmentally responsible transportation of minerals and mineral products in the mineral processing industry. These applications enhance supply chain visibility, reliability, and sustainability, ultimately benefiting the entire mineral processing ecosystem (Pournader et al., 2021; Nazeri and Keshavarzi, 2019; Min, 2010; Baryannis et al., 2019a; Pandian, 2019; Misra et al., 2020; Baryannis et al., 2019b; Dwivediet al., 2021; Eskandari-Khanghahi et al., 2018; Araldo et al., 2019; Gholamrezaei et al., 2023; Maleki, 2023; Karami, 2022; Ssempijja et al., 2021; Hellingrath and Lechtenberg, 2019; Lotfi et al., 2021a; Lotfi et al., 2021b; Nikookar et al., 2021).

3.4.9. Safety and Environmental Monitoring:

AI has valuable applications in safety and environmental monitoring in the mineral processing industry. These applications enhance worker safety and help manage and minimize the environmental impact of mining and processing operations. Here are the applications and benefits of AI in safety and environmental monitoring (Aires et al., 2001; Ankley et al., 2010; Bariotakis et al., 2019; Borba et al., 2022; C´ aceres, E.L. et al., 2020; Chen et al., 2021; Choi and Park, 2001; Davila-Santiago et al., 2022; Dobbelaere et al., 2022; Hale et al., 2020; Jeong and Choi, 2022; Lei et al., 2023; Li et al., 2018; Oliker and Ostfeld, 2014; Chai et al., 2009; Di Noia and Hasekamp, 2018; Freeman et al., 2018; LeCun et al.,2015; Lipton et al., 2015; Liu and Wu, 2016).:

• Worker Safety and Hazard Detection:

Real-Time Safety Monitoring: AI systems use sensors, cameras, and wearable devices to monitor the safety of workers in mining and processing environments. They can detect unsafe conditions or behaviors in real-time.

Hazard Identification: AI can identify potential safety hazards, such as equipment malfunctions, unstable ground conditions, or the presence of toxic gases. It can issue alerts or shut down operations when hazards are detected.

Fatigue and Distraction Detection: AI can analyze worker behavior and biometric data to identify signs of fatigue or distraction. This helps in preventing accidents caused by tired or inattentive workers.

Emergency Response: AI can trigger automatic emergency responses, such as alarms, evacuation procedures, or equipment shutdown, in the event of accidents or dangerous situations.

Access Control: AI systems can control access to hazardous areas, ensuring that only authorized personnel with the necessary training and safety equipment can enter restricted zones.

Health Monitoring: AI can monitor worker health, detecting early signs of illness or injury. This allows for timely medical interventions to prevent more serious health issues.

Training and Education: AI can be used for virtual reality (VR) and augmented reality (AR) training simulations to prepare workers for potential hazards and emergencies.

• Environmental Impact Management:

Emissions Monitoring: AI helps monitor emissions of pollutants and greenhouse gases, ensuring compliance with environmental regulations and identifying areas for improvement.

Water Quality Monitoring: AI can assess water quality in mining operations, detecting contamination and facilitating timely responses to prevent environmental damage.

Waste Management: AI optimizes waste handling and disposal by predicting waste volumes and minimizing environmental impact. It can suggest strategies for waste reduction and recycling.

Ecological Impact Assessment: AI analyzes data to assess the ecological impact of mining operations on local flora and fauna. It helps identify mitigation strategies and sustainable practices.

Real-Time Environmental Monitoring: AI provides real-time data on environmental conditions, such as air quality, water levels, and soil composition, to detect any deviations from acceptable standards.

Resource Efficiency: AI can recommend measures to optimize resource usage, such as water and energy, reducing waste and environmental impact.

Compliance Reporting: AI simplifies the process of reporting environmental data to regulatory authorities, ensuring that companies meet their legal and environmental responsibilities.

AI applications in safety and environmental monitoring enhance worker safety, reduce accidents, and contribute to a more sustainable and environmentally responsible approach to mineral processing. These applications are crucial for ensuring the well-being of workers and the long-term viability of mining operations. Certainly, here are some real-world examples of AI applications in mineral processing along with the outcomes and benefits (Aires et al., 2001; Ankley et al., 2010; Bariotakis et al., 2019; Borba et al., 2022; C´ aceres, E.L. et al., 2020; Chen et al., 2021; Choi and Park, 2001; Davila-Santiago et al., 2022; Dobbelaere et al., 2022; Hale et al., 2020; Jeong and Choi, 2022; Lei et al., 2023; Li et al., 2018; Oliker and Ostfeld, 2014; Chai et al., 2009; Di Noia and Hasekamp, 2018; Freeman et al., 2018; LeCun et al.,2015; Lipton et al., 2015; Liu and Wu, 2016).

3.5. Highlight real-world examples of AI applications in mineral processing

3.5.1. Rio Tinto's Mine of the Future

AI Application: Rio Tinto, one of the world's largest mining companies, has implemented autonomous drilling and hauling systems. These systems use AI to operate mining equipment remotely (Marshall et al., 2016).

Outcomes and Benefits: Increased safety as fewer workers are exposed to hazardous environments, enhanced equipment utilization, reduced fuel consumption, and higher productivity.

3.5.2. Teck Resources' Digital Operations Center

AI Application: Teck Resources established a Digital Operations Center that uses AI and data analytics to monitor and optimize their mining operations. AI algorithms analyze vast amounts of data to improve decision-making (Tessier et al., 2007).

Outcomes and Benefits: Improved operational efficiency, reduced energy consumption, optimized maintenance, and a significant decrease in operating costs.

3.5.3. Newcrest Mining's Cave Management System

AI Application: Newcrest Mining, an Australian mining company, implemented a cave management system that utilizes AI to monitor underground mining operations. The system optimizes the extraction of ore from underground mines (Ambrozic and Turk, 2003).

Outcomes and Benefits: Increased ore recovery, reduced waste, minimized environmental impact, and enhanced safety in underground mining.

3.5.4. Anglo American's P101 Project

AI Application: Anglo American launched the P101 Project to implement process optimization and automation across their mining operations. AI is used for predictive maintenance, equipment monitoring, and energy optimization (https://www.angloamerican.com/futuresmart/futuresmart-mining; https://www.miningweekly.com/).

Outcomes and Benefits: Decreased downtime, reduced maintenance costs, enhanced energy efficiency, and a more sustainable approach to mining.

3.5.5. Goldcorp's Gold Production Enhancement

AI Application: Goldcorp, a gold mining company, implemented AI-powered algorithms to optimize their milling and flotation processes. This helped in achieving finer particle sizes and better gold recovery rates (https://ir.usgoldcorp.gold/annual-reports-2023; https://www.northernminer.com/).

Outcomes and Benefits: Increased gold recovery by approximately 3%, reduced energy consumption, and improved overall production efficiency.

3.5.6. BHP's Maintenance Optimization

AI Application: BHP, a major mining company, utilizes AI for predictive maintenance on their mining equipment. The AI system monitors equipment condition and predicts maintenance needs (https://www.bhp.com/news/bhp-insights/2024/08/artificial-intelligence-is-unearthing-a-smarter-future).

Outcomes and Benefits: Reduced downtime, lower maintenance costs, and extended equipment lifespan.

3.5.7. Cleveland-Cliffs' Process Control

AI Application: Cleveland-Cliffs, an iron ore mining company, uses AI for process control in their grinding and flotation circuits. The AI system optimizes grinding parameters and froth flotation for improved iron ore recovery (https://www.aist.org/conferences-expositions/technology-training/digital-transformation-forum/digital-transformation-forum-for-the-steel-industry-881767b52e153d8380d1f6d1933a4836; https://www.aist.org/local-member-chapters/find-a-chapter/southeast/annual-meeting-f651bd79de304665813e70907d471296)

Outcomes and Benefits: Enhanced iron ore recovery, reduced energy consumption, and improved product quality.

These real-world examples demonstrate how AI is transforming mineral processing by improving safety, operational efficiency, energy consumption, and environmental sustainability. The applications of AI in mining continue to evolve, contributing to a more advanced and responsible mining industry (Aldrich et al., 2010; Andersson et al., 2012; Bartolacci et al., 2006; Dorfling et al., 2013; Gonzalez et al., 2008; Groenewald et al., 2006; Horrocks et al., 2015; Jahedsaravani et al., 2014; Kistner et al., 2013; le Roux et al., 2013; Perez et al., 2015; Qin, 2018; Tessier et al., 2007; Thurley, 2009; Zhou et al., 2009).

4. Conclusion

AI applications in mineral processing must take ethical and environmental considerations into account. Mining activities have the potential to impact local communities and ecosystems. AI should be leveraged to minimize these impacts, prevent resource over-exploitation, and ensure responsible mining practices. Ethical issues, such as the fair treatment of workers and local communities, also need to be addressed when implementing AI solutions.

The use of AI in mining generates vast amounts of data, including sensitive information about operations, geological surveys, and resource reserves. Protecting this data from cyber threats and ensuring compliance with data privacy regulations are significant challenges. Robust data security measures, encryption, and access controls must be in place to safeguard sensitive information.

Integrating AI systems into existing mining operations can be complex and costly. Companies must invest in infrastructure, hardware, and software to support AI applications. Ensuring compatibility with legacy systems and training personnel to use AI tools can pose challenges. There is a need for careful planning and management to maximize the benefits of AI while minimizing disruptions and additional costs.

The future of AI in mineral processing holds several exciting possibilities:

- Advanced Automation: AI-driven autonomous mining operations are likely to become more prevalent, further enhancing safety and efficiency.
- Quantum Computing: Quantum computing can revolutionize data analysis and optimization, enabling more complex and real-time decision-making in mining.
- Explainable AI: Developing AI models that are more transparent and interpretable will be crucial for gaining trust in AI solutions and ensuring regulatory compliance.
- Integration with IoT and Blockchain: Integration with the Internet of Things (IoT) and blockchain technologies will enhance transparency, traceability, and accountability in the supply chain.

- Sustainable Mining: AI will play a central role in making mining operations more environmentally sustainable, with a focus on reducing waste, energy consumption, and emissions.

AI has already had a transformative impact on mining operations by improving safety, efficiency, and sustainability. It has led to optimized exploration, better ore processing, reduced maintenance costs, and increased energy efficiency. The real-time data analysis capabilities of AI have made it possible to make quicker and more informed decisions. The mining industry has seen improvements in worker safety and reduced environmental impact due to AI applications.

In conclusion, AI has the potential to revolutionize the mining industry by addressing many of its traditional challenges. It enhances productivity, safety, and sustainability while reducing operational costs. However, it is essential for mining companies, researchers, and regulators to continue working together to overcome the challenges and ensure responsible and ethical AI adoption in mineral processing. Continued research and investment in AI technologies are critical to unlock their full potential and shape the future of mining. This journey towards smarter and more responsible mining practices is one that must be pursued with diligence and dedication.

References

Ahl A., Yarime M., Tanaka K., Sagawa D., 2019. Review of blockchain-based distributed energy: Implications for institutional development, Renew Sust Energy Rev 107, 200–211.

Ahmad, M.A., Eckert, C., Teredesai, A. 2018. Interpretable machine learning in healthcare. In Proceedings of the 2018 ACM International Conference on Bioinformatics, Computational Biology, and Health Informatics, Washington, DC, USA, 29 August–1 September 2018, 559–560.

Ahmad, M.W., Mourshed, M., Rezgui, Y. 2017. Trees vs Neurons: Comparison between random forest and ANN for high-resolution prediction of building energy consumption. Energy Buildings 147, 77–89.

Aires, F., Prigent, C., Rothstein, M. 2001. A new neural network approach including first guess for retrieval of atmospheric water vapor, cloud liquid water path, surface temperature, and emissivities over land. J. Geophys. Res. 106, 14887–14907.

Aldrich, C., Marais, C., Shean, B.J., Cilliers, J.J., 2010. Online monitoring and control of froth flotation systems with machine vision: a review. Int. J. Miner. Process. 96, 1–13. https://doi.org/10.1016/j.minpro.2010.04.005.

Ambrozic, T.,Turk, G. 2003. Prediction of subsidence due to underground mining by artificial neural networks. Computers & Geosciences, 29, 627–637.

Andersson, T., Thurley, M.J., Carlson, J.E. 2012. A machine vision system for estimation of size distributions by weight of limestone particles. Miner. Eng. 25, 38–46. https:// doi.org/10.1016/j.mineng.2011.10.001.

Ankley, G.T., Bennett, R.S., Erickson, R.J., Hoff, D.J., Hornung, M.W., Johnson, R.D. et al. 2010. Adverse outcome pathways: a conceptual framework to support ecotoxicology research and risk assessment. Environ. Toxicol. Chem. 29, 730–741. https://doi.org/10.1002/etc.34

Arrieta, A.B., Díaz-Rodríguez, N., Del Ser, J., Bennetot, A., Tabik, S., Barbado, A., García, S., Gil-López, S., Molina, D., Benjamins, R., Chatila, R., Herrera, F. 2020. Explainable Artificial Intelligence (XAI): Concepts, taxonomies, opportunities and challenges toward responsible AI. Inf. Fusion, 58, 82–115.

Araldo, A., Gao, S., Seshadri, R., Azevedo, C. L., Ghafourian, H., Sui, Y., Ben - Akiva,M., 2019. System level optimization of multi-modal transportation networks for energy efficiency using personalized incentives: formulation, implementation, and performance. Transportation Research Record, 2673(12), 425-438.

Aydın, F. 2021. Sınıf öğretmeni adaylarının eğitimde sanal gerçeklik kullanımına ilişkin görüşleri. Çanakkale Onsekiz Mart Üniversitesi Lisansüstü Eğitim Enstitüsü, Yüksek Lisans Tezi.

Babacan O., De Causmaecker S., Gambhir A., Fajardy M., Rutherford A. W., Fantuzzi A., Nelson J. 2020. Assessing the feasibility of carbon dioxide mitigation options in terms of energy usage. Nat Energy, 5 (9), 720–728.

Bahtiyar, K. (2021). Türkiye'de farklı sektörlerdeki yapay zeka uygulamalarına ilişkin müşteri algılarının değerlendirilmesi. Kütahya Dumlupınar Üniversitesi Lisansüstü Eğitim Enstitüsü, Yüksek Lisans Tezi.

Bariotakis, M., Luciana Georgescu, L., Laina, D., Oikonomou, I., Ntagounakis, G., Koufaki, M.I., Souma, M., Choreftakis, M., Zormpa, O.G., Smykal, P., Sourvinos, G., Lionis, C., Castanas, E., Karousou, R., Pirintsos, S.A. 2019. From wild harvest towards precision agriculture: use of ecological niche modelling to direct potential cultivation of wild medicinal plants in crete. Sci. Total Environ. 694, 133681 https://doi.org/10.1016/j.scitotenv.2019.133681.

Bartolacci, G., Pelletier, P., Tessier, J., Duchesne, C., Bossé, P.-A., Fournier, J. 2006. Application of numerical image analysis to process diagnosis and physical parameter measurement in mineral processes—Part I: flotation control based on froth textural characteristics. Miner. Eng. 19, 734–747. https://doi.org/10.1016/j.mineng.2005. 09.041.

Baryannis, G., Dani, S., Antoniou, G. 2019a. Predicting supply chain risks using machine learning: The trade -off between performance and interpretability. Future Generation Computer Systems, 101, 993-1004.

Baryannis, G., Validi, S., Dani, S., Antoniou, G. 2019b. Supply chain risk management and artificial intelligence: state of the art and future research directions. International Journal of Production Research, 57(7), 2179-2202.

Batal, M. S. 2016. Yapay zeka uygulamaları ve yapay zekanın geleceği. Uluslararası Sunhill Üniversitesi, Yüksek Lisans Tezi.

Benardos, A.G., Kaliampakos, D.C. 2004. Modelling TBM performance with artificial neural networks. Tunnelling and Underground Space Technology, 19, 597–605.

Bishop, C.M. 2005. Neural networks for pattern recognition. Oxford University Press, 482.

Boden, M. A. 2018. Artificial intelligence: A very short introduction. Oxford University Press.

Borba, J.V.B., Alves, V.M., Braga, R.C., Korn, D.R., Overdahl, K., Silva, A.C., Hall, S.U.S., Overdahl, E., Kleinstreuer, N., Strickland, J., Allen, D., Andrade, C.H., Muratov, E.N., Tropsha, A. 2022. STopTox: an in silico alternative to animal testing for acute systemic and topical toxicity. Environ. Health Perspect. 130. https://doi.org/10.1289/EHP9341.

Casali, A., Gonzalez, G., Vallebuona, G., Perez, C., Vargas, R. 2001. Grindability Soft-Sensors Based On Lithological Composition and On-line Measurements, Minerals Engineering. Vol.14, No. 7, 689–700.

Caceres, E.L., Mew, N.C., Keiser, M.J. 2020. Adding stochastic negative examples into machine learning improves molecular bioactivity prediction. J. Chem. Inf. Model. 60, 5957–5970. https://doi.org/10.1021/acs.jcim.0c00565.

Chai, S.S., Walker, J.P., Makarynskyy, O., Kuhn, M., Veenendaal, B., West, G. 2009. Use of soil moisture variability in artificial neural network retrieval of soil moisture Remote Sens., 2, 166-190.

Chen, Z., Liu, X., Yang, J., Little, E., Zhou, Y. 2018. Deep learning-based method for SEM image segmentation in mineral characterization, an example from Duvernay Shale samples in Western Canada Sedimentary. Basin. Comput. Geosci., 138, 104450.

Chen, K., Peng, Y., Lu, S., Lin, B., Li, X. 2021. Bagging based ensemble learning approaches for modeling the emission of PCDD/Fs from municipal solid waste incinerators. Chemosphere 274, 129802. https://doi.org/10.1016/j.chemosphere.2021.129802.

Cheng L., Yu T. 2019. A new generation of ai: A review and perspective on machine learning technologies applied to smart energy and electric power systems, Int J Energy Res 43 (6), 1928–1973.

Choi, D.J., Park, H. 2001. A hybrid artificial neural network as a software sensor for optimal control of a wastewater treatment process. Water Res. 35, 3959–3967. https://doi.org/10.1016/S0043-1354(01)00134-8.

Conradie, A.V.E., Aldrich, C. 2001. Neurocontrol of A Ball Mill Grinding Circuit Using Evolutionary Reinforcement Learning. Minerals Engineering, Vol.14, No. 10, 1277–1294.

Cutmore, N.G., Liu, Y., Middleton, A.G. 1997. Ore Characterisation and Sorting. Minerals Engineering, Vol. 10, No. 4, 421–426.

Canakcı, H., Pala, M. 2007. Tensile strength of basalt from a neural network. Engineering Geology, 94, 10–18.

Çavaş, B., Çavaş, P., Can, B. 2004. Eğitimde sanal gerçeklik. The Turkish Online Journal of Educational Technology, 3(4), 110-117.

Çetin, E. 2016. Yapay zeka uygulamaları (3. Basım). Seçkin Yayınevi.

Data-Science. 2024. An Intuitive Explanation of Data Science Concepts. Part I: DS, AI, ML, and DL in Simple Words. https://data-science-ua.com/blog/an-intuitive-explanation-of-data-science-concepts-part-l-ds-ai-ml-and-dl-in-simple-words/ [Accessed March 15, 2024].

Davila-Santiago, E., Cheng Shi, C., Mahadwar, G., Medeghini, B., Insinga, L., Hutchinson, R., Good, S., Jones, G.D. 2022. Machine learning applications for chemical fingerprinting and environmental source tracking using non-target chemical data. Environ. Sci. Technol. 56, 4080–4090. https://doi.org/10.1021/acs.est.1c06655.

Demuth, H., Beale, M., Hagan, M. 2008. Neural network. The MathWorks, Inc., 906s.

De Lima, R.P., Duarte, D., Nicholson, C., Slatt, R., Marfurt, K.J. 2020. Petrographic microfacies classification with deep convolutional neural networks. Comput. Geosci., 142, 104481.

DeTore, A.W. 1989. An introduction to expert systems. J. Insur. Med., 21, 233–236.

Di Noia A., Hasekamp O.P. 2018. Neural networks and support vector machines and their application to aerosol and cloud remote sensing: a review. Springer Series in Light Scattering, Springer, 279-329.

Dobbelaere, M.R., Ureel, Y., Vermeire, F.H., Tomme, L., Stevens, C.V., Van Geem, K.M. 2022. Machine learning for physicochemical property prediction of complex hydrocarbon mixtures. Ind. Eng. Chem. Res. 61, 8581–8594. https://doi.org/10.1021/acs.iecr.2c00442.

Dorfling, C., Akdogan, G., Bradshaw, S.M., Eksteen, J.J., 2013. Modelling of an autoclave used for high pressure sulphuric acid/oxygen leaching of first stage leach residue, Part 2: model application. Miner. Eng. 53, 213–219. https://doi.org/10.1016/ J.MINENG.2013.03.011.

Dupont B., Vingerhoets P., Tant P., Vanthournout K., Cardinaels W., De Rybel T., Peeters E., Belmans R. 2012. Linear breakthrough project: Large-scale implementation of smart grid technologies in distribution grids. in: Proc 3rd IEEE PES Innov Smart Grid Technol (ISGT Europe), IEEE, 1–8.

Drelich, J., (Ed.)., 2012. Water in Mineral Processing, Society for Mining, Metallurgy, and Exploration, (SME) Inc., Pages. 416, ProQuest Ebook Central.

Dwivedi, Y.K., Hughes, L., Ismagilova, E., Aarts, G., Coombs, C., Crick, T., Williams, M.D. 2021. Artificial Intelligence (AI): Multidisciplinary perspectives on emerging challenges, opportunities, and agenda for research, practice and policy. International Journal of Information Management, 57, 101994.

Eberhart, R.C., Shi, Y. 2007. Computational intelligence concepts to implementations, Morgan Kaufmann, 467.

Elmas, C. 2003. Yapay Sinir Ağları. Seckin Yayıncılık, Ankara.

Emeritus. 2024. Financial Digital Transformation: What is It, Its Benefits and Challenges. https://emeritus.org/in/learn/financial-digital-transformation/ [Accessed March 15, 2024].

Eskandari - Khanghahi, M., Tavakkoli - Moghaddam, R., Taleizadeh, A. A., Amin, S. H. 2018. Designing and optimizing a sustainable supply chain network for a blood platelet bank under uncertainty. Engineering Applications of Artificial Intelligence, 71, 236-250.

Faster Capital. 2024. Deep Learning. https://fastercapital.com/keyword/deep-learning.html [Accessed March 15, 2024].

Freeman B.S., Taylor G., Gharabaghi B., J. 2018. The Forecasting air quality time series using deep learning, J. Air Waste Manage. Assoc., 68, 866-886.

Feng, X.T., Seto, M. 1999. A new method of modelling the rock microfracturing process in double-torsion experiments using neural networks. International Journal for Numerical and Analytical Methods in Geomechanics, 23, 905-923.

Folorunso, I., Abikoye, O., Jimoh, R., Raji, K. 2012. A rule-based expert system for mineral identification. J. Emerg. Trends Comput. Inf. Sci., 3, 205–210.

Fuerstenau, M.C., Han, K.N. 2003. Principles of Mineral Processing. Society for Mining, Metallurgy, and Exploration.

Fuerstenau, D.W., De, A., Kapur, P.C. 2004. Linear and nonlinear particle breakage process in comminution systems. International Journal of Mineral Processing, 74, 317-327.

Glen, T., Nwailab, H.E., Frimmele, F., Steven, E., Zhangb, C.D, Julie, E., Bourdeauc, Leon C.K. Tolmayg, R.J., Durrheima, Y.G. 2022. The minerals industry in the era of digital transition: An energy-efficient and environmentally conscious approach, ResourcesPolicy, V78, 102851.

Gholamrezaei, A., Shabbooei, A. R., Ghaferin, S. A. 2023. Application of novel and green technology in industry. International journal of industrial engineering and operational research, 5(1), 1-7.

Goldberg, E., Scheringer, M., Bucheli, T.D., Hungerbuhler, K. 2015. Prediction of nanoparticle transport behavior from physicochemical properties: machine learning provides insights to guide the next generation of transport models. Environ. Sci-Nano 2 (4), 352–360.

Gomez-Flores, A., Solongo, S.K., Heyes, G.W., Ilyas, S., Kim, H. 2020. Bubble – particle interactions with hydrodynamics, XDLVO theory and surface roughness for flotation in an agitated tank using CFD simulations. Miner. Eng 152, 106368.

Gonzalez, G.D., Miranda, D., Casali, A., Vallebuona, G. 2008. Detection and identification of ore grindability in a semiautogenous grinding circuit model using wavelet transform variances of measured variables. Int. J. Miner. Process. 89, 53–59. https:// doi.org/10.1016/j.minpro.2008.09.002.

Groenewald, J.W.de V., Coetzer, L.P., Aldrich, C. 2006. Statistical monitoring of a grinding circuit: an industrial case study. Miner. Eng. 19, 1138–1148. https://doi. org/10.1016/j.mineng.2006.05.009.

Guyot, O., Monredon, T., LaRosa, D., Broussaud, A. 2004. VisioRock, an integrated vision technology for advanced control of comminution circuits, Minerals Engineering, vol.17, 1227–1235.

Gurney, K. 2018. An Introduction to Neural Networks. CRC Press: Boca Raton, FL, USA.

Gupta, A., Yan, D. S, 2006. Mineral Processing Design and Operation: An Introduction, Elsevier Science, Pages, 693. USA.

Hale, S.E., Arp, H.P.H., Schliebner, I., Neumann, M. 2020. Persistent, mobile and toxic (PMT) and very persistent and very mobile (vPvM) substances pose an equivalent level of concern to persistent, bioaccumulative and toxic (PBT) and very persistent and very bioaccumulative (vPvB) substances under REACH. Environ. Sci. Eur. 32, 155. https://doi.org/10.1186/s12302-020-00440-4.

Hassanien, A.E. 2020. Advances in Intelligent Systems and Computing, The International Conference on Advanced Machine Learning Technologies and Applications (AMLTA2018), Volume 921, AMLTA, EGYPT, DOI:10.1007/978-3-319-74690-6.

Haykin, S. 2009. Neural Networks and Learning Machines. Pearson Education Ltd, New Jersey, USA. 906.

Hawkes, A. D. 2010. Estimating marginal CO2 emissions rates for national electricity systems. Energy Policy, 38 (10), 5977–5987.

Hellingrath, B., Lechtenberg, S. 2019. Applications of artificial intelligence in supply chain management and logistics: focusing onto recognition for supply chain execution. The Art of Structuring: Bridging the Gap Between Information Systems Research and Practice, 283-296.

Hogarth, R.M., Lejarraga, T., Soyer, E. 2015. The Two Settings of Kind and Wicked Learning Environments. Curr. Dir. Psychol. Sci. 24 (5), 379–385.

Horrocks, T., Wedge, D., Holden, E.J., Kovesi, P., Clarke, N., Vann, J. 2015. Classification of gold-bearing particles using visual cues and cost-sensitive machine learning. Math. Geosci. 47, 521–545. https://doi.org/10.1007/s11004-015-9597-7.

Hosseini, M.R., Shirazi, H.H.A., Massinaei, M., Mehrshad, N. 2015. Modeling the Relationship between Froth Bubble Size and Flotation Performance Using Image Analysis and Neural Networks. Chem. Eng. Commun. 202 (7), 911–919.

Hu, W., Hadler, K., Neethling, S.J., Cilliers, J.J. 2013. Determining flotation circuit layout using genetic algorithms with pulp and froth models. Chem. Eng. Sci. 102, 32–41.

Huang, Y. 1999. Application of artificial neural networks to predictions of aggregate quality parameters. International Journal of Rock Mechanics and Mining Sciences, 36, 551-561.

Interchange. 2024. What is industry 4.0. https://blog.isa.org/what-is-industry-40. [Accessed March 15, 2024].

Izadi, H., Sadri, J., Bayati, M. 2017. An intelligent system for mineral identification in thin sections based on a cascade approach. Comput. Geosci., 99, 37–49.

Jahedsaravani, A., Marhaban, M.H., Massinaei, M. 2014. Prediction of the metallurgical performances of a batch flotation system by image analysis and neural networks. Miner. Eng. 69, 137–145. https://doi.org/10.1016/j.mineng.2014.08.003.

Jackson, P.C. 2019. Introduction to artificial intelligence, Mineola New York: Dover Publications Inc., 458, ISBN 0-486-24864-X.

Jeong, J., Choi, J. 2022. Artificial intelligence-based toxicity prediction of environmental chemicals: future directions for chemical management applications. Environ. Sci. Technol. 56, 7532–7543. https://doi.org/10.1021/acs.est.1c07413.

Joshi, A.V. 2020. Machine learning and artificial intelligence, Springer International Publishing, 10, 978-3, ISBN-13:978-3030266219

Kang, C., Zhou, T., Chen, Q., Xu, Q., Xia, Q., Ji, Z. 2012. Carbon emission flow in networks, Sci Rep-UK. 2, 479.

Kahraman, S., Altun, H., Tezekici, B.S., Fener, M. 2006. Sawability prediction of carbonate rocks from shear strength parameters using artificial neural networks. International Journal of Rock Mechanics and Mining Sciences, 43, 157-164.

Kamel, H. 2011. Neural Network Application for Structure Design Optimization of Thin-Wall Structures. International Mechanical Engineering Congress and Exposition, ASME 2011, IMECE 2011, vol 9 (American Society of Mechanical Engineers Digital Collection). 41–50.

Knifexns. 2024. https://knifexns.bodegalostoneles.com/enx/machine-learning-ai/ [Accessed March 15, 2024].

Karami, D., 2022. Supply Chain Network Design Using Particle Swarm Optimization (PSO) Algorithm. International journal of industrial engineering and operational research, 4(1), 1-8.

Kecman, V. 2001. Learning and Soft Computing: Support Vector Machines, Neural Networks and Fuzzy Logic Models, A Bradford Book, The MIT Pres, Cambridge, Massachusetts, London, England.

Killeen, P., Ding, B,, Kiringa, I., Yeap T. 2019. IoT-based predictive maintenance for fleet management Procedia Comput. Sci. 151, 607–13.

Kistner, M., Jemwa, G.T., Aldrich, C. 2013. Monitoring of mineral processing systems by using textural image analysis. Miner. Eng. 52, 169–177. https://doi.org/10.1016/j. mineng.2013.05.022.

LeCun, Y., Bengio, Y., Hinton, G. 2015. Deep learning, Nature, 521, 436.

Lei, L., Pang, R., Han, Z., Wu, D. 2023. Current applications and future impact of machine learning in emerging contaminants: a review. Crit. Rev. Environ. Sci. Technol. 1–19. https://doi. org/10.1080/10643389.2023.2190313.

le Roux, J.D., Craig, I.K., Hulbert, D.G., Hinde, A.L. 2013. Analysis and validation of a run-of-mine ore grinding mill circuit model for process control. Miner. Eng. 43, 121–134. https://doi.org/10.1016/j.mineng.2012.10.009.

Li X., Yao X. 2020. Can energy supply-side and demand-side policies for energy saving and emission reduction be synergistic? —a simulated study on china's coal capacity cut and carbon tax, Energy Policy 138. 111232.

Li, Y.G., Jiang, P., She, Q., Lin, G. 2018. Research on air pollutant concentration prediction method based on self-adaptive neuro-fuzzy weighted extreme learning machine. Environ. Pollut. 241, 1115–1127. https://doi.org/10.1016/j.envpol.2018.05.072.

Lipton, Z.C., Berkowitz, J., Elkan, C. 2015. A critical review of recurrent neural networks for sequence learning. arXiv preprint arXiv:1506.00019v1, https://doi.org/10.48550/arXiv.1506.00019.

Liu Y., Wu L. 2016. Geological disaster recognition on optical remote sensing images using deep learning. Procedia Computer Science, 91, 566-575.

Liu, H., Zhong, C., Alnusair, A., Islam, S.R.2021. FAIXID: A framework for enhancingai explainability of intrusion detection results using data cleaning techniques. J.Netw. Syst. Manag., 29, 1–30.

López, A., Ramil, A., Pozo-Antonio, J., Fiorucci, M., Rivas, T. 2017. Automatic Identification of Rock-Forming Minerals in Granite Using Laboratory Scale Hyperspectral Reflectance Imaging and Artificial Neural Networks. J. Nondestruct. Eval., 36, 52.

Lobo, A., Garcia, E., Barroso, G., Martí, D., Fernandez-Turiel, J.L., Ibáñez-Insa, J. 2021. Machine-learning for mineral identification and ore estimation from hyperspectral imagery in tin-tungsten deposits. Remote Sens., 13, 3258.

Lotfi, R., Mehrjerdi, Y. Z., Pishvaee, M. S., Sadeghieh, A., Weber, G. W. 2021. A robust optimization model for sustainable and resilient closed-loop supply chain network design considering conditional value at risk. Numerical Algebra, Control & Optimization, 11(2), 221.

Lotfi, R., Sheikhi, Z., Amra, M., AliBakhshi, M., Weber, G.W. 2021. Robust optimization of risk-aware, resilient and sustainable closed-loop supply chain network design with Lagrange relaxation and fix-and-optimize. International Journal of Logistics Research and Applications, 1-41.

Mahmud, K., Khan, B., Ravishankar, J., Ahmadi, A., Siano, P. 2020. An internet of energy framework with distributed energy resources, prosumers and small-scale virtual power plants: An overview, Renew Sustain Energy Rev. 127, 109840.

Malhotra, D., Taylor, P.R., Spiller, E. and LeVier, M., 2009. Recent Advances in Mineral Processing Plant Design, Pages, 587, Society for Mining, Metallurgy, and Exploration, Inc. (SME), Shaffer Parkway Littleton, Colorado, USA.

Maleki, E. 2023. Resiliency in supply chain. International Journal of Industrial Engineering and Operational Research, 5(1), 8-18.

Marshall, J.A., Bonchis, A., Nebot, E., Scheding, S. 2016. Robotics in Mining. In: Siciliano, B., Khatib, O. (eds) Springer Handbook of Robotics. Springer Handbooks. Springer, Cham., 1549-1576. https://doi.org/10.1007/978-3-319-32552-1_59.

Masampally, V.S., Pareek, A., Nadimpalli, N.R.V., Runkana, V. 2023. Artificial

Intelligence for Monitoring and Optimization of an Integrated Mineral Processing Plant. Trans Indian Inst Met. https://doi.org/10.1007/s12666-023-03093-y.

Massinaei, M., Doostmohammadi, R. 2010. Modeling of bubble surface area flux in an industrial rougher column using artificial neural network and statistical techniques. Miner. Eng. 23 (2), 83–90.

Mathworks, C. 2020. Predictive Maintenance Toolbox TM User's Guide.

Mehmet, A.C.I., Doğansoy, G. A. 2022. Makine Öğrenmesi ve Derin Öğrenme Yöntemleri Kullanılarak E-Perakende Sektörüne Yönelik Talep Tahmini. Gazi Üniversitesi Mühendislik Mimarlık Fakültesi Dergisi, 37(3), 1325-1340.

Min, H. 2010. Artificial intelligence in supply chain management: theory and applications. International Journal of Logistics: Research and Applications, 13(1), 13-39.

Mishra, K.A., 2021. AI4R2R (AI for Rock to Revenue): A Review of the Applications of AI in Mineral Processing. Minerals, 11, 1118.

Misra, N.N., Dixit, Y., Al -Mallahi, A., Bhullar, M.S., Upadhyay, R., Martynenko, A. 2020. IoT, big data, and artificial intelligence in agriculture and food industry. IEEE Internet of things Journal, 9(9), 6305-6324.

Mokhtari, K.E., Higdon, B.P., Basar, A. 2019. Interpreting financial time series with SHAP values. In Proceedings of the 29th Annual International Conference on Computer Science and Software Engineering, Markham, ON, Canada, 4–6 November 2019.166–172.

Moolman, D.W., Aldrich, C., Vandeventer, J.S.J., Bradshaw, D.J. 1995. The interpretation of flotation froth surfaces by using digital image-analysis and neural networks. Chem. Eng. Sci. 50 (22), 3501–3513.

Nabiyev, V.V. 2003. Yapay Zeka, Seckin Yayıncılık, Ankara.

Nakhaei, F., Irannajad, M. 2013. Comparison between neural networks and multiple regression methods in metallurgical performance modeling of flotation column. Physicochem. Probl. Mi 49 (1), 255–266.

Nakhaei, F., Mosavi, M.R., Sam, A., Vaghei, Y. 2012. Recovery and grade accurate prediction of pilot plant flotation column concentrate: Neural network and statistical techniques. Int. J. Miner. Process. 110, 140–154.

Nakhaeie, F., Sam, A., Mosavi, M.R. 2013. Concentrate grade prediction in an industrial flotation column using artificial neural network. Arab. J. Sci. Eng. 38 (5), 1011–1023. https://doi.org/10.1007/s13369-012-0350-y.

Nazeri, A., Keshavarzi, M. 2019. Assessing the Performance of Branches of Refah Bank in Tehran Province by Combining Analytic Hierarchy Process (AHP) and Data Envelopment Analysis (DEA) Algorithms in Fuzzy Conditions. International journal of industrial engineering and operational research, 1(1), 11.

Nikookar, E., Varsei, M., Wieland, A. 2021. Gaining from disorder: Making the case for antifragility in purchasing and supply chain management. Journal of Purchasing and Supply Management, 27(3), 100699.

Nwaila, G., Frimmel, H., Zhang, S.E., Bourdeau, J.E., Tolmay, L.C.K., Durrheim, R.J., Ghorbani, Y. 2022. The minerals industry in the era of digital transition: An energy-efficient and environmentally conscious approach, Resources Policy, Volume 78, 1-18, 102851.

Ojha, R., Jaiswal, C. M. 2023. SAP S/4HANA Asset Management Configure, Equip, and Manage your Enterprise, APRESS Berkeley, CA.

Okada, N., Maekawa, Y., Owada, N., Haga, K., Shibayama, A., Kawamura, Y. 2020. Automated identification of mineral types and grain size using hyperspectral imaging and deep learning for mineral processing. Minerals, 10, 809.

Oliker, N., Ostfeld, A. 2014. A coupled classification – evolutionary optimization model for contamination event detection in water distribution systems. Water Res. 51, 234–245. https://doi.org/10.1016/j.watres.2013.10.060.

Qin, S.J. 2018. Special issue on big data: data science for process control and operations. J. Process Control 67, iii. https://doi.org/10.1016/S0959-1524(18)30086-6.

Öztemel, E. 2003. Yapay Sinir Ağları. Papatya Yayıncılık, İstanbul.

Pampel, F.C. 2000. Logistic Regression: A Primer Sage Univ. Press132, 98.

Pandian, D.A.P. 2019. Artificial intelligence application in smart warehousing environment for automated logistics. Journal of Artificial Intelligence and Capsule Networks, 1(2), 63-72.

Perez, C.A., Saravia, J.A., Navarro, C.F., Schulz, D.A., Aravena, C.M., Galdames, F.J. 2015. Rock lithological classification using multi-scale Gabor features from subimages, and voting with rock contour information. International Journal of Mineral Processing, 144, 56–64.

Pirouzan, D., Yahyaei, M., Banisi, S. 2014. Pareto based optimization of flotation cells configuration using an oriented genetic algorithm. Int. J. Miner. Process., 126, 107–116.

Pournader, M., Ghaderi, H., Hassanzadegan, A., Fahimnia, B. 2021. Artificial intelligence applications in supply chain management. International Journal of Production Economics, 241, 108250.

Prabhavathy, P., Tripathy, B., Venkatesan, M. 2019. Unsupervised learning method for mineral identification from hyperspectral data., In Proceedings of the International Conference on Innovations in Bio-Inspired Computing and Applications, Gunupur, India, Springer: Cham, Switzerland, 148–160.

Ramil, A., López, A., Pozo-Antonio, J., Rivas, T. 2018. A computer vision system for identification of granite-forming minerals based on RGB data and artificial neural networks. Measurement, 117, 90–95.

Ramujee K. 2013. Strength Properties of Polypropylene Fiber reinforced Concrete. International Journal of Innovative Reaserch in Science, Engineering and Technology, 2 (8), 3409-3413.

Ren, C.C., Yang, J.G., Liang, C. 2015. Estimation of Copper Concentrate Grade Based on Color Features and Least-Squares Support Vector Regression. Physicochem. Probl. Mi. 51 (1), 163–172.

Rhosonics. 2024. Control strategies for flotation. https://rhosonics.com/insight/blog/control-strategies-for-flotation/ [Accessed March 15, 2024].

Sağıroğlu, S., Besdok, E., Erler, M. 2003. Muhendislikte Yapay Zekâ Uygulamaları- I, Ufuk Yayıncılık, Kayseri.

Semwayo, D.T., Ajoodha, R. 2021. A Causal Bayesian Network Model for Resolving Complex Wicked Problems. In: 2021 IEEE International IOT Electronics. and. Mechatronics. Conference. (IEMTRONICS), 1–8.

Siler-Evans K., Azevedo I. L., Morgan M. G. 2012. Marginal emissions factors for the us electricity system, Environ Sci Technol 46 (9), 4742–4748.

Ssempijja, M.N., Namango, S., Ochola, J., Mubiru, P.K. 2021. Application of Markov chains in manufacturing systems: A review. International journal of industrial engineering and operational research, 3(1), 1-13.

Swiss Cognitive. 2024. What is Artificial Intelligence? https://swisscognitive.ch/2020/11/24/artificial-intelligence-2/ [Accessed March 15, 2024].

Tabassum Z, Samantaray R, R., Mohammadi S, H., Fathima A. 2024. Artificial Intelligence and Blockchain Technology for Secure Smart Grid and Power Distribution Automation, AI and Blockchain Applications in Industrial Robotics, IGI GLOBAL Chapter 9, 27.

Tang, D.G., Milliken, K.L., Spikes, K.T. 2020. Machine learning for point counting and segmentation of arenite in thin section. Mar. Pet. Geol., 120, 104518.

Telsmith, Inc., 2011. Mineral Processing Handbook 11/11 - 1st printing Printed in U.S.A., 10910 N. Industrial Dr. P.O. Box 539, pages,145.

Tessier, J., Duchesne, C., Bartolacci, G. 2007. A machine vision approach to on-line estimation of run-of-mine ore composition on conveyor belts. Miner. Eng. 20, 1129–1144. https://doi.org/10.1016/j.mineng.2007.04.009.

Thomas, D. S. 2018. The Costs and Benefits of Advanced Maintenance in Manufacturing (Gaithersburg, MD)

Thomas, L., Zhou, Y., Long, C., Wu, J., Jenkins, N. 2019. A general form of smart contract for decentralized energy systems management, Nat Energy 4 (2), 140–149.

Thomson, R.C., Harrison, G.P., Chick, J.P. 2017. Marginal greenhouse gas emissions displacement of wind power in Great Britain, Energy Policy, 101, 201–210.

Thurley, M.J. 2009. Automated online measurement of particle size distribution using 3D range data. IFAC Proc. 42, 134–139. https://doi.org/10.3182/20091014-3-CL-4011. 00025.

Tsamados, A., Aggarwal, N., Cowls, J., Morley, J., Roberts, H., Taddeo, M., Floridi, L. 2022. The ethics of algorithms: Key problems and solutions. AI Soc., 37, 215–230.

Tyagi, A,K, Tiwari, S. 2024. The Future of Artificial Intelligence in Blockchain Applications, e-Book**:** Machine Learning Algorithms Using Scikit and TensorFlow Environments, Mendeley, 28.

Umucu, Y. 2011. Kireçtaşı örneğinin yapay sinir ağları ile öğütme işlemlerinin modellenmesi ve kinetik modelle kıyaslanması, SDÜ Fen Bilimleri Enstitüsü, Maden Mühendisliği Anabilim Dalı, PhD, 457, Isparta, Türkiye.

Umucu, Y., Deniz, V., Bozkurt, V., Çağlar, M.F. 2016. The evaluation of grinding process using artificial neural network, International Journal of Mineral Processing, 146, 46-53.

Wang, J.S., Han, S. 2015. Feed-Forward Neural Network Soft-Sensor Modeling of Flotation Process Based on Particle Swarm Optimization and Gravitational Search Algorithm. Comput. Intel. Neurosc., 1-10.

Wang, Q., Zhang, X., Tang, B., Ma, Y., Xing, J., Liu, L. 2021. Lithology identification technology using BP neural network based on XRF. Acta Geophys., 69, 2231–2240.

Wordstream. 2024. 10 Companies Using Machine Learning in Cool Ways https://www.wordstream.com /blog/ws/2017/07/28/machine-learning-applications [Accessed March 15, 2024].

Wong, K.K.L. 2023. Cybernetical Intelligence: Engineering Cybernetics with Machine Intelligence, e-Book, Wiley-IEEE Press, 432.

Zhao, R., Deutz, P., Neighbour, G., McGuire, M. 2012. Carbon emissions intensity ratio: an indicator for an improved carbon labelling scheme, Environ Res Lett 7 (1), 014014.

Zhou, P., Chai, T., Wang, H. 2009. Intelligent optimal-setting control for grinding circuits of mineral processing process. IEEE Trans. Auto. Sci. Eng. 6, 730–743. https://doi. org/10.1109/TASE. 2008.2011562.

Zhou, Y,J. Wu, G.S., Long, C. 2020. Framework design and optimal bidding strategy for ancillary service provision from a peer-to-peer energy trading community, Appl. Energy, 278, 115671.

Zulu, M.L.T., Carpanen, R.P., Tiako, R. A. Comprehensive Review: Study of Artificial Intelligence Optimization Technique Applications in a Hybrid Microgrid at Times of Fault Outbreaks. Energies 2023, 16, 1786. https://doi.org/10.3390/en16041786.

Wills, B.A., Finch, J., 2016. Wills' Mineral Processing Technology: An Introduction to the Practical Aspects of Ore Treatment and Mineral Recovery, eighth ed. Elsevier Science and Technology Books Inc, E-book, p. 1. online resources (512 pages).

Madencilik - Mining, 2024, 63(2), 86-94

BİLİMSEL MADENCİLİK DERGİSİ
SCIENTIFIC MINING JOURNAL

TMMOB Maden Mühendisleri Odası Yayını / The Publication of the Chamber of Mining Engineers of Turkey

www.mining.org.tr

Research Article

DEM aided investigation of the effects of screen surface properties on screening performance

Ahad Harzanak[a,*], E. Caner Orhan[b,**]

a Demir Export Inc., Research and Development Center, Ankara, TÜRKİYE
b Hacettepe University, Department of Mining Engineering, 06800, Beytepe, Ankara, TÜRKİYE

Received: 17 April 2024 • Accepted: 29 November 2024

A B S T R A C T

Under diverse conditions, multiple empirical models are employed to forecast screen performance. Although they provide good insight for the sizing and selection of screens, they generally are insufficient for the precise quantification of the effects of parameters such as surface dimensions, aperture shape/orientation, and surface open area. Discrete element modelling (DEM) has proved in many instances that it provides close-up examination of particle motion under various conditions for a variety of mineral processing operations and generates data that is not possible to obtain with conventional experimentation or sampling.

This study investigates the influence of screen surface parameters (i.e., surface dimensions, aperture orientation/shape and surface open area) on screening performance using the DEM method for the simulation of vibrating screens. To achieve realistic simulations, "multi-spheres" were used to represent particles with irregular shapes. The simulation results showed that particle motions were accurately predicted. Key findings include that longer screen surfaces increased screening efficiency and mass recovery in the undersize stream and screens with perpendicular apertures to the flow direction achieved higher screening efficiency. Additionally, increased surface open area improved screening efficiency by increasing the recovery of finer particles. These findings were evaluated using conventional screen efficiency criteria, and the separation of particles was also investigated in terms of size distribution of products and residence time of particles along the screen.

Keywords: *Discrete Element Method, Simulation, Vibrating Screen, LIGGGHTS Solver, Spherical Particles, Irregularly Shaped Particles.*

Introduction

Screening finds extensive application in various fields, including ore preparation and industries such as textiles, food, and recycling (Jeanger et al., 2022; Beas et al., 2021). In mineral processing applications, the dimensions, design, and performance of screens determine the efficiency and utilization of subsequent operations/processes. As a critical stage in these industries, optimizing screening operations can yield significant benefits and impact overall productivity and profitability (Wills and Napier-Munn, 2006).

Continuous advancements in computer processing capacity have facilitated the adoption of more accurate simulation methods, such as the discrete element method (DEM). Over the years, DEM has become highly useful in representing realistic screening operations, helping to overcome the limitations of phenomenological and empirical models. DEM, first introduced by Cundall (1971) and further detailed by Cundall and Strack (1979), precisely represents dynamic processes such as segregation, passage, and transport, making it highly suited for the simulation of screening operations.

Recent studies have demonstrated the effectiveness of DEM in optimizing screening performance. For instance, Jiang et al. (2021) and Polanía et al. (2023) investigated the impact of particle shape and size on screening efficiency, revealing significant effects on the screening process. Similarly, Wang et al. (2023) and Liu et al. (2023) optimized vibration parameters like frequency, amplitude, and direction, showing enhancements in vibrating screen performance. Additionally, the optimization of banana screens using DEM has proven to improve unit-time screening efficiency (Extrica, 2023).

Earlier attempts at DEM modeling of screening, as described by Shimosaka et al. (2000), Li et al. (2002; 2003), Hilden (2007), Cleary et al. (2009a, 2009b), Dong and Brake (2009), Chen and Tong (2010), Zhao et al. (2011), Delaney et al. (2012), Elskamp

* Corresponding author: first.author@e-mail.address.com • https://orcid.org/0000-0000-0000-0000
** second.author@e-mail.address.com • https://orcid.org/0000-0000-0000-0000
*** third.author@e-mail.address.com • https://orcid.org/0000-0000-0000-0000

https://DOI: 10.30797/madencilik.1469819

and Kruggel-Emden (2015), Jahani et al. (2015), Zhao et al. (2017), Elskamp et al. (2017), Cleary et al. (2018), and Aghlmandi Harzanagh et al. (2018), explored various parameters using DEM. However, few studies have addressed the validation of created models (Hilden 2007; Delaney et al. 2012; Zhao et al. 2016; Aghlmandi Harzanagh et al. 2018).

After successful validation of the DEM model developed using a pilot-scale vibrating screen and studying the effects of some design and operational parameters (such as feed flow rate, vibration amplitude, screen deck inclination, vibration direction, and vibration frequency) in the previous study (Aghlmandi Harzanagh et al., 2018), this current study addresses the influence of screen surface parameters (i.e., screen surface dimensions, aperture shape, and surface open area) on the screening performance of a vibrating pilot-scale screen. This study focuses on surface parameters with a perspective meaningful for mineral processing experts and evaluates these parameters using classic evaluation approaches.

The researchers utilized the open-source LIGGGHTS software (Kloss et al., 2012) to conduct DEM simulations. Within these simulations, multi-spheres (sphere clumps) were employed to model irregularly shaped particles. The effects of various parameters on screening performance were investigated based on partition curve, cut-size, imperfection, screening efficiency, mean residence time of particles, and more.

1. Geometry and Simulation Setup of the Pilot-Scale Vibrating Screen

Similar to the validation of DEM simulations performed in the previous study (Aghlmandi Harzanagh et al. 2018), this study focuses on the investigation of additional screen surface parameters on a pilot-scale vibrating inclined screen. The present study employed the Hertz-Mindlin particle contact model, with a comprehensive description available in Jahani et al. (2015). For conducting DEM simulations, the researchers utilized the open-source LIGGGHTS solver. To facilitate the simulations, they prepared various 3D models of the screen. Fig. 1, shows the pilot scale vibrating screen and its CAD model alongside the available feeding system. The polyurethane screen surface is comprised of six square panels in length and two in width, resulting in overall dimension of 90×30cm. The screen surface was inclined at an angle of 10 degrees to facilitate the study. Table 1 provides the size distribution of the feed material and DEM model parameters that were used in DEM simulations. This table compiles the essential parameters and variables used as inputs in the simulations to accurately model the screening process.

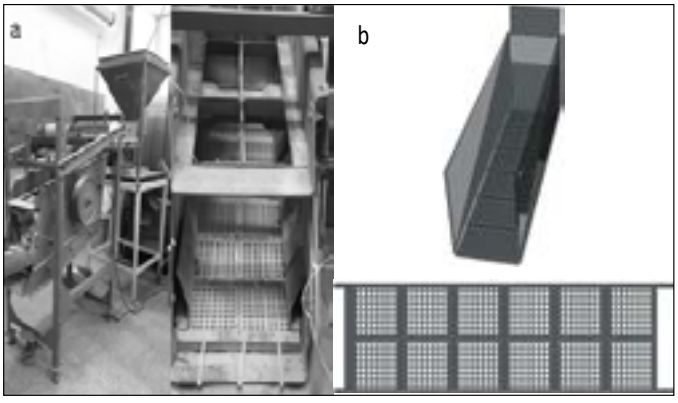

Fig. 1. (a) Real version of the vibrating screen and feeder system. (b) CAD version of the vibrating screen

Table 1. The data used in DEM simulations.

Feed size distribution	
Size (mm)	Weight (%)
26.6	10
20.6	10
15.7	20
12.1	8
9.5	14
6.7	14
4.7	14
2.8	10

Parameter	Value
Type of vibration	Linear oscillatory motion Amplitude: 4mm Frequency: 25Hz Direction: 95° according to horizontal axis
Particle density (kg/m^3)	2700
Modulus of elasticity (N/m^2)	5×10^7
Poisson's ratio	0.45
Restitution coefficient	0.3
Sliding friction coefficient	0.5
Rolling friction coefficient	0.01
Time Step (s)	5×10^{-6}
Simulation timeframe (s)	In the range of 25-35

The model parameters, such as Young's modulus (modulus of elasticity), time-step, Poisson's ratio, etc., were thoroughly tested through several simulations in alignment with previous studies in the literature. This rigorous testing aimed to ensure the accuracy and reliability of the DEM model in accurately representing the screening process. Multiple simulations were conducted to achieve a suitable time-step based on the concept of "Rayleigh time," ensuring practical and efficient simulation durations. This approach aimed to strike a balance between computational efficiency and maintaining accurate representation of the screening process.

Numerous simulations were performed at various screen surface dimensions, aperture shapes and open area values while holding all other parameters constant to examine how different parameters affect screening performance. Non-spherical particles were utilized in the simulations. While modelling irregular particle shapes, multi-spheres (sphere clumps) method of LIGGGHTS' multi-sphere module was used. This method uses sphere clumps for the creation of a new non-spherical particle. To implement this method, coordinates of the centers and radii of the spheres need to be imported into the solver through a text file. The simulation supports the utilization of several particle templates, providing the flexibility to incorporate diverse particle shapes and properties within a single study. To create a new non-spherical particle with an optimal number of spheres, the authors developed an in-house program which takes the CAD model of a high-resolution particle, reduces the number of vertices to the desired resolution, and then fills the volume with spheres. This innovative approach allows for efficient and accurate representation of particles in the DEM simulations while maintaining computational feasibility. Using this methodology, a sphere is created at each vertex and expanded until it touches any other vertex. After iterating this process for every vertex, a simplified sphere clump representation of the particle is obtained (Fig. 2). The resulting sphere clump serves as an efficient and effective model for the irregularly shaped particles in the DEM simulations. Table 2 shows the values of parameters used in the simulations.

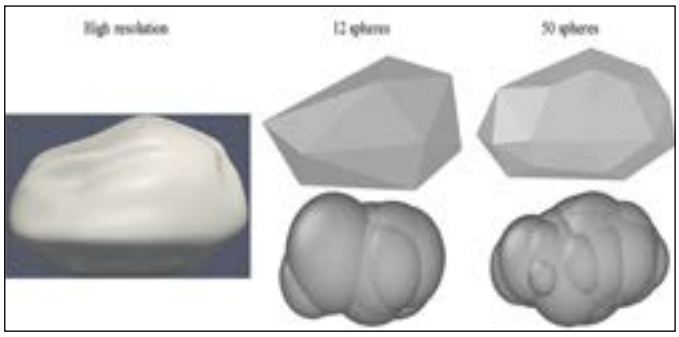

Fig. 2. The stages of creating a non-spherical particle template

Table 2. List of values of parameters used in simulations

Parameter	Values
Surface length (cm)	60, 75, 90
Aspect ratio of the aperture	2H*, 2V*, 3H, 3V, 4H, 4V
Surface open area	21.78, 16, 11.11

* relative to the horizontal / vertical

The simulation starts by creating and letting particles fall from the virtual feeder under gravity. As these particles reach and move along the screen surface, they either pass through the surface or flow along it towards the discharge, replicating real-world screening behavior in the DEM simulations. In order for a proper evaluation, the screen operation needs to achieve the steady-state (namely, the inlet flow rate equals the combined flow rates of the oversize and undersize streams for each size fraction). Therefore, the data in the first few seconds until the steady-state is maintained are disregarded. A typical illustration of the simulations is given in Fig. 3, which shows a visual representation of the particle motion during screening.

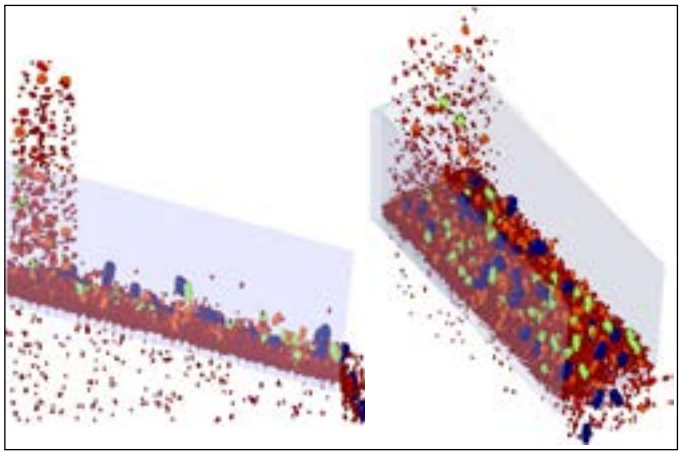

Fig. 3. Typical illustration of simulations

At the end of the simulations, the data files were obtained which includes the coordinates, velocity, acceleration and force of each particle at each time step. These data were then used to calculate the residence time of individual particles or particle size classes on the screen surface and to determine whether the screen has reached a steady state. These precise data points provide critical insights into the screening process and aid in analyzing the behavior and performance of particles throughout the simulation duration.

2. Results and Discussion

Depending on the simulation parameters, substantial amount of data is generated in each simulation which includes the location, velocity, angular velocity, and torque of each particle at every time step. This data can be visualized using suitable post-processing software to gain insights from the simulation results. OVITO (Open Visualization Tool) was used for the visualization of DEM data. Researchers designed and implemented an in-house program to extract essential information from the extensive dataset. This custom program was developed to efficiently process and analyze the simulation data, enabling the extraction of the required results. The custom program reads and analyzes the data files obtained in the simulations, extracts crucial information such as the system's state (steady or unsteady), final fractionation of particles to products (undersize or oversize stream), the size distributions of both (coarse and fine) products, as well as the residence time of each particle on screen.

Equation 1 was utilized to determine the overall screening efficiency (Wills and Napier-Munn, 2006).

$$E = \frac{c\text{-}f}{c(1-f)} E = \frac{c\text{-}f}{c(1-f)} \qquad \text{Equation 1}$$

The fractions f and c in Equation 1 correspond to the material within a size range in the feed and oversize streams, respectively. The study also involved calculating and plotting partition curves for each size fraction, representing the percentage of the feed reporting to the oversize product. This analysis provided valuable insights into the distribution of material across different size ranges during the screening process. Partition curves were then used to determine the separation size of the screen and the sharpness of separation which is an indication of the efficiency of separation. The efficiency and sharpness of the screening is a measure of the slope of the middle section of the partition curve. The inefficiency of separation, or the so-called imperfection, *I*, is then given by:

$$I = \frac{d_{75}\text{-}d_{25}}{2d_{50}} I = \frac{d_{75}\text{-}d_{25}}{2d_{50}} \qquad \text{Equation 2}$$

the sharpness and therefore efficiency of the screening decreases by increasing of the imperfection value (Wills and Napier-Munn, 2006).

Moreover, the study encompassed the calculation of mean residence times of particles for each size fraction, which served as an additional indicator of separation efficiency. This analysis provided valuable information about how long particles of different sizes remained within the system during the screening process, contributing to a better understanding of the overall performance. Discrete element modeling provides a unique opportunity to evaluate particle behavior under various conditions, including the reliable calculation of mean residence times for different size fractions. This capability is difficult to achieve through traditional experimental methods in actual screening operations.

2.1 Effects of screen surface dimension

The dimensions of the screen surface, especially the length of the screen (stream direction), affects the screening performance by controlling the particles' residence time and the bed depth, whereas the width of the screen determines the capacity of the screen. As the length of the screen increases, particles spend more time on the screen surface which increases the possibility of fine particles passing through the apertures. To examine these effects, three different screen surfaces with various lengths were designed. Designed screen surfaces have 4, 5 and 6 longitude panels, the dimension of each panel being 15×15cm (Fig. 4). During the simulations, 10.5mm square apertures were used.

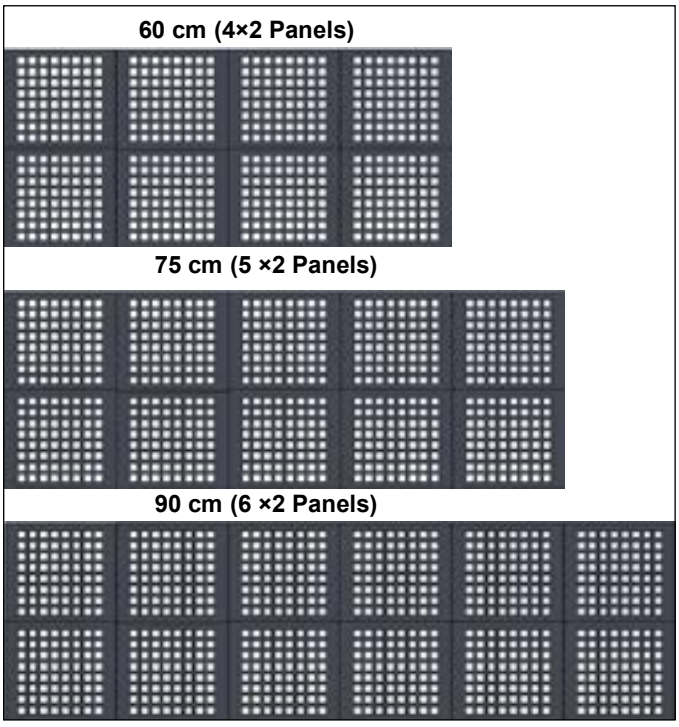

Fig. 4. Screen surfaces with different lengths

In order to be able to isolate the effects of the length of the screen surface, the other parameters like feed flowrate (25 t/h), feed size distribution, vibration parameters (amplitude, frequency and direction), etc. were kept constant in these simulations (Table 1).

As expected, the results of simulations show that the longer screen surface provides higher efficiency and higher mass recovery in the undersize stream (Fig. 5).

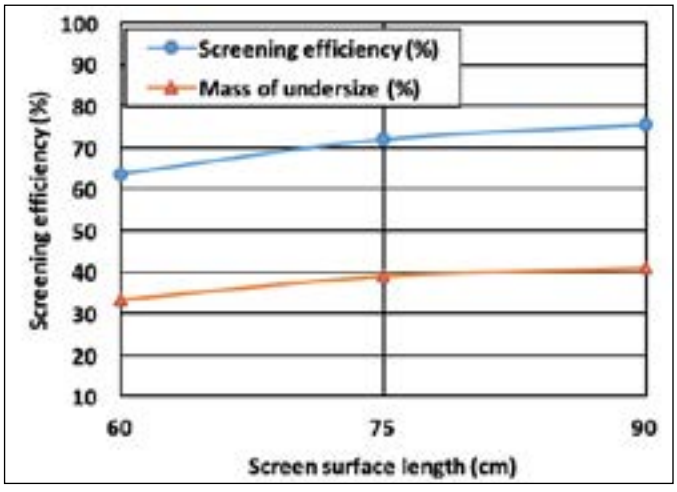

Fig. 5. Effects of length of screen surface on screening efficiency and mass of undersize stream

Fig. 6 shows the partition curves of the separation performed at various surface lengths. The d_{25}, d_{50}, d_{75} values and the calculated imperfections of the separations at different screen surfaces lengths are given in Table 3.

Partition curves and imperfection values indicate that longer sieves work more efficiently and also cut-size is higher in longer surfaces as expected. According to Fig. 6, the differences in the partition coefficients are more pronounced in finer particles (2.8, 4.7 and 6.7mm) rather than the near mesh particles (9.5mm) which shows that efficiency-oriented effects of surface length is observed as an improvement of the passing of fine particles.

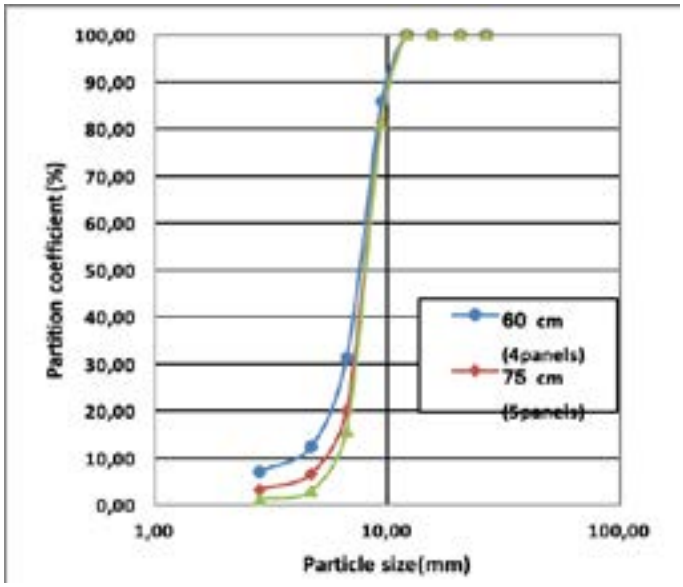

Fig. 6. Partition curves at different screen surface lengths

Table 3. Performance parameters for different screen surface lengths

Screen Length	d_{25}	d_{50}	d_{75}	Imperfection
60 cm	6.25	7.60	8.80	0.17
75 cm	6.95	8.00	9.10	0.13
90 cm	7.15	8.10	9.10	0.12

Fig. 7 illustrates the mean residence time (MRT) of particles reporting to oversize and undersize streams across different screen surface lengths. In the case of particles reporting to undersize stream, the MRT is increasing with increasing particle size in all cases which indicates that fine particles pass through apertures in the initial parts of the screen whereas larger particles pass mainly in the latter parts, spending more time on the screen surface and the bed. On the other hand, increasing the surface length causes an increase in the mean residence time of particles, however this increase is more pronounced for near mesh and middle-sized particles (9.5 and 6.7mm). The larger particles need more time to pass and longer screen surfaces provide extra time to these particles and therefore improve the overall screening efficiency.

In the case of particles reporting to oversize stream, the mean residence time of the finest particles is the minimum in all of the simulations, but MRT increase with increasing particle size and reaches a maximum value for near mesh particles and follows a decreasing trend with increasing particle size. This is an important observation because the time the particle spends on the screen surface would be an indication of the bed depth. The existence of fine particles (2.83 mm) in the oversize stream are due to their misplacement and not finding a chance to contact to screen surface. It is observed in the simulation animations that very fine and very coarse particles leave the screen surface placing in top layers of material bed with minimum interaction with screen surface but other particles with sizes towards near mesh size (9.5mm) locate in lower positions of the material bed and therefore have higher interaction with screen surface. This finding agrees well with the mean residence time of particles reporting to oversize stream (Fig. 7)

As can be seen in Fig. 7, increasing in surface length causes an upward shift in MRT curves as higher lengths mean larger residence times on the screen surface.

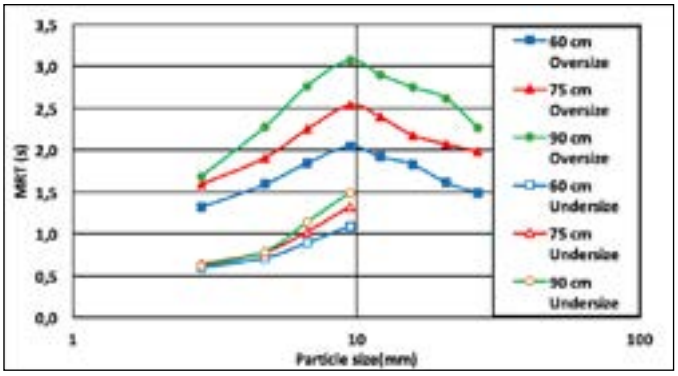

Fig. 7. Mean residence time of particles at various screen surface lengths

2.2 Effects of aperture shapes

It is well-known that in the screens with rectangular apertures, the flow-oriented apertures serve the purpose of capacity while apertures perpendicular to the flow direction are useful to maintain high screening efficiencies (Dong et al. 2016). In order to have a deep insight on how aperture orientation affects the screening process, six different screen surfaces with various aperture aspect ratios and orientations were designed. Simulations were performed using these 3D models keeping other parameters constant (Table 1). Fig. 8, shows the single panel of each designed screen surface. Complete screen surface models consist of 12 panels (2×6).

As per the simulation results, the screening efficiency demonstrated an upward trend with an increase in the aspect ratio of the aperture. Additionally, at the same aspect ratio, the screen with apertures perpendicular to the flow direction have higher screening efficiency in the case of screen surfaces with rectangular apertures (Fig. 9).

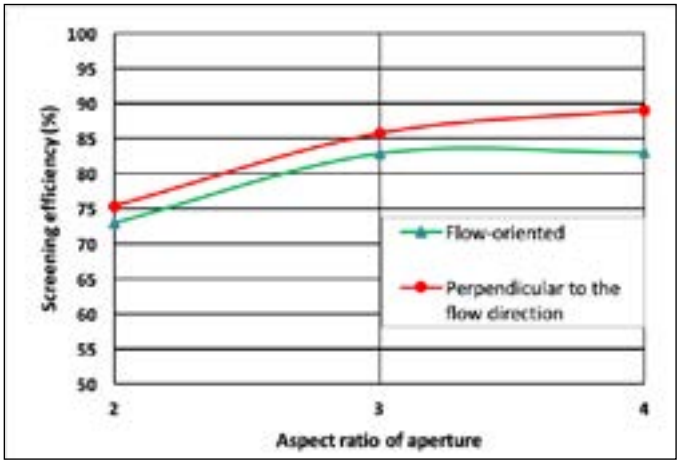

Fig. 9. Effects of aspect ratio and orientation of the screen aperture on the screening efficiency

Fig. 10, shows the respective partition curves for the simulations performed at various aperture aspect ratios and orientations and Table 4 shows the Imperfection values for performed simulations. According to Fig. 10 and Table 4, at constant aspect ratio, generally the partition curves of screening processes performed by screen

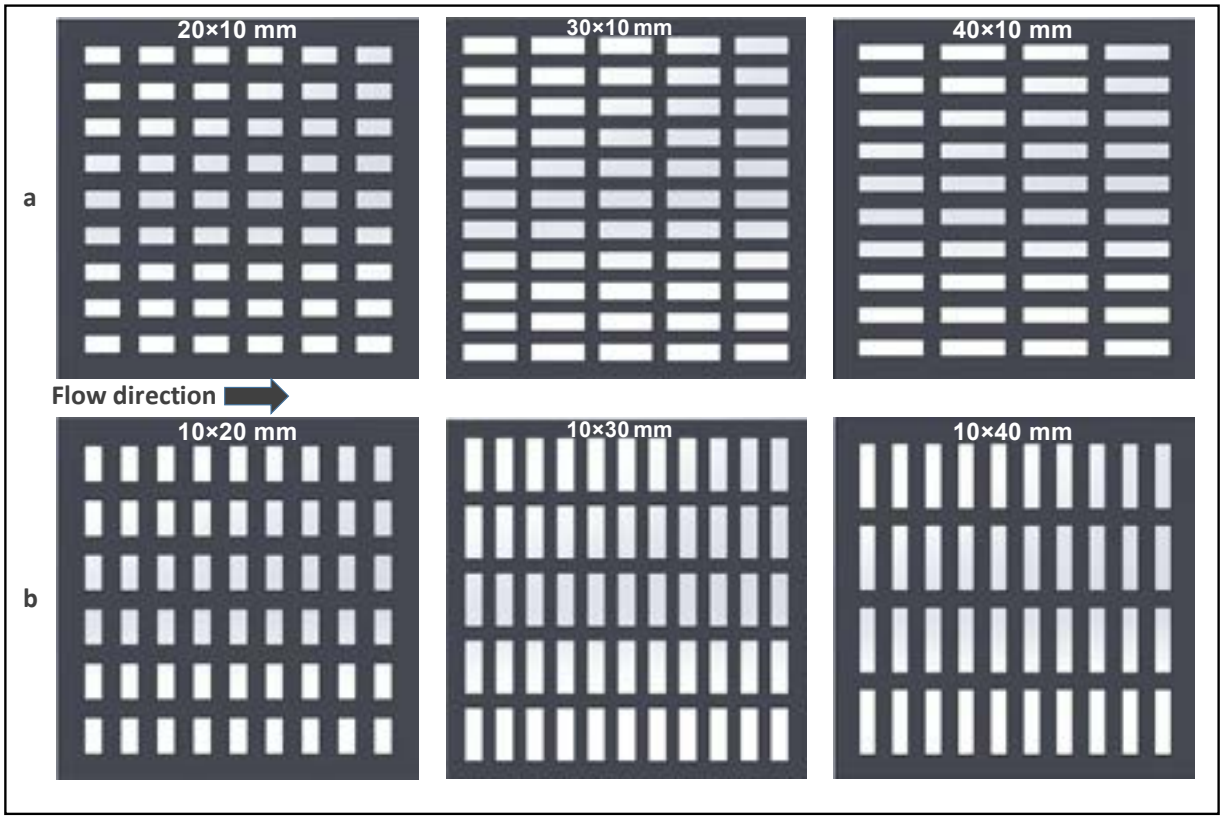

Fig. 8. Schematic view of designed screen surfaces with apertures at various aspect ratio and orientation (a: flow-oriented apertures, b: perpendicular to the flow direction apertures)

apertures perpendicular to the flow direction are a bit sharper (smaller Imperfection values) and the partition coefficient of near mesh particles (9.7mm) are smaller which shows that the screening is much more efficient. The results show that, regardless of the orientation of apertures, the sharpness of partition curves increases with increasing aspect ratio of screen aperture which means that an increase in aspect ratio of rectangular apertures increases the efficiency of the screening process.

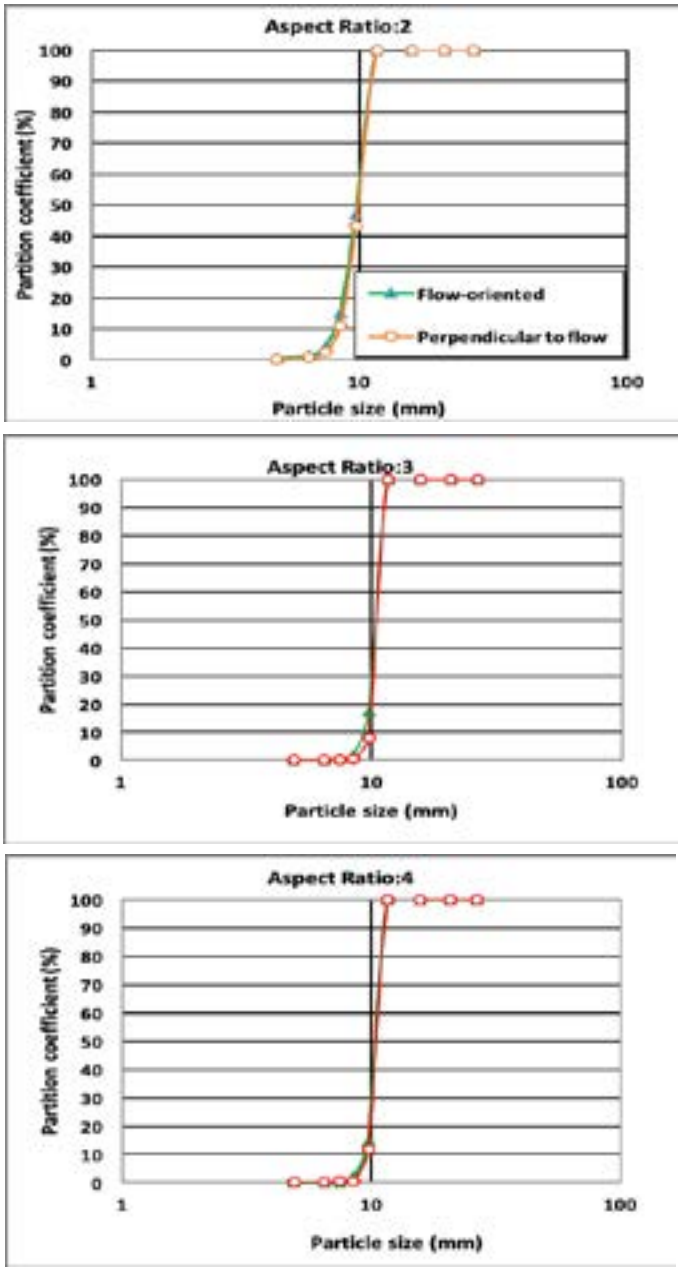

Fig. 10. Partition curves at various aperture aspect ratios and orientations

The investigation of mean residence time (MRT) for particles reporting to undersize and oversize streams with various aperture shapes (Fig. 11) reveals that MRT is higher for both particle types (oversize and undersize) across all particle sizes when using screens with apertures perpendicular to the flow direction. Although perpendicular orientation provides particles more time on screen surface and increases the probability of passing through apertures resulting in higher efficiency, higher residence time causes the accumulation of more particles on the screen surface and eventually resulting in lower screening capacity. Table 4. Imperfection values for different aspect ratios and orientations of screen apertures

Table 4. Imperfection values for different aspect ratios and orientations of screen apertures

Aspect Ratio	Direction	d_{25}	d_{50}	d_{75}	Imperfection
2	flow-oriented	8.90	9.85	10.50	0.081
	perpendicular to the flow	9.10	9.90	10.60	0.076
3	flow-oriented	9.90	10.40	10.90	0.048
	perpendicular to the flow	10.03	10.43	10.95	0.044
4	flow-oriented	10.00	10.45	10.90	0.043
	perpendicular to the flow	10.05	10.50	10.90	0.040

Fig. 12, shows the displays of screens and particles at 20th second of the performed simulations. The relative increase in bed depth and particle accumulation at the screen surface is observable in simulations performed by screens with perpendicular to the flow-oriented apertures (right column).

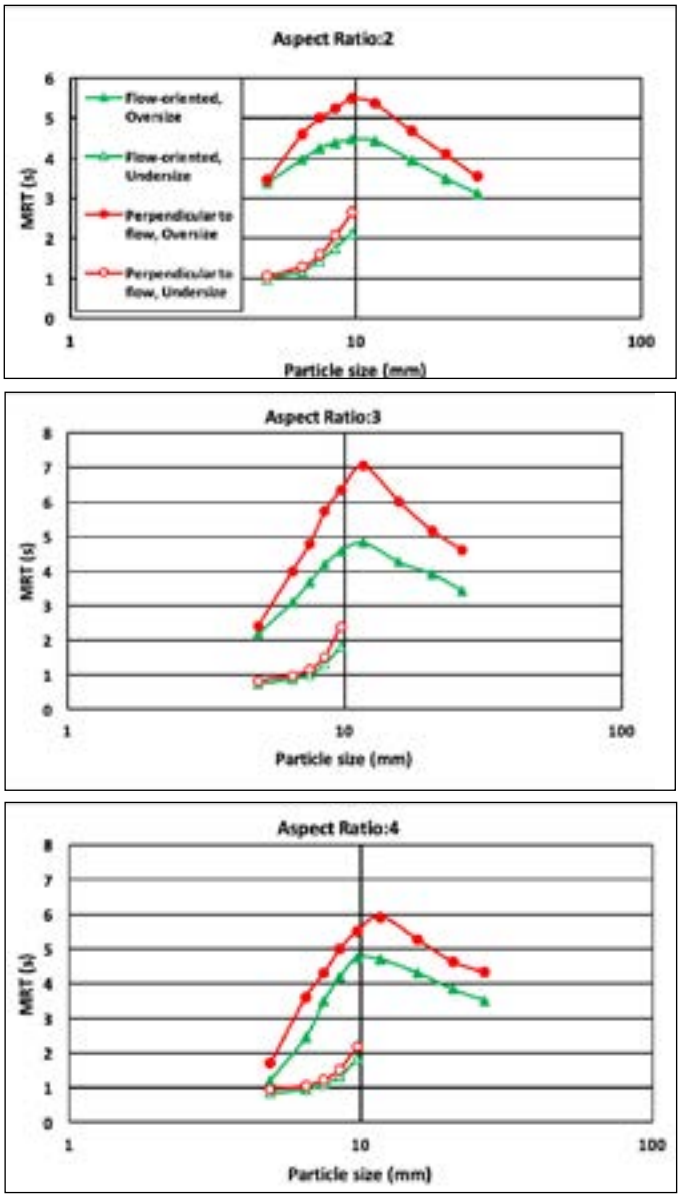

Fig. 11. The mean residence time of the particles reported to undersize and oversize streams at various aperture aspect ratios and orientations

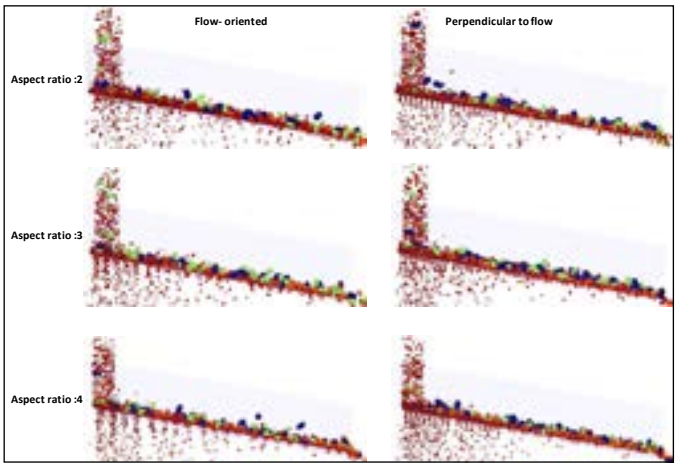

Fig. 12. The steady-state views of screens and particles obtained from the simulations performed at various aperture types

2.3 Effects of screen surface open area

The ratio of the total area of the openings in the screen surface to the total area of the screen surface is expressed as open area. It is well known that increasing the open area improves the screening efficiency by increasing the number of apertures. To examine the effects of open area on screening performance and particle behaviors, three different screen surfaces were designed. The surface dimensions (900×300mm) and aperture sizes (10×10mm) were kept constant in 3D models but the spaces between apertures were considered as 10, 14 and 20mm (Fig. 13). The open areas of these 3D models were calculated as 21.78, 16.00 and 11.11% respectively. The screen surface was constructed as 2x6 panels.

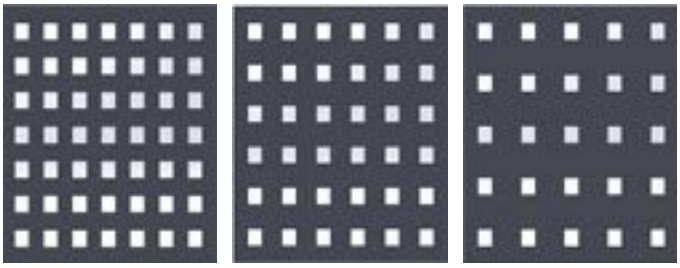

Fig. 13. Schematic view of screen surface 3D models with different screen surface open areas (single panel)

For isolating the effects of surface open area, other design and operating parameters like feed flowrate (25t/h), size distribution of the feed, vibration properties, surface inclination and etc. were kept constant in simulations (Table 1).

According to the results of the simulations, as expected, screening efficiency and mass of undersize increases by increasing surface open area (Fig. 14). The study of respective partition curves (Fig.table 15) together with d_{25}, d_{50}, d_{75} and the imperfection values (Table 5) exposes significant differences in both separation sharpness and cut-point-size as higher open areas offer steeper sharpness and higher cut-point-size. Calculated cut-point-sizes for screening at open area values of 21.78, 16.00 and 11.11% are 6.62, 5.93 and 5.18 mm respectively. it is apparent from partition curves that, despite the small difference between partition coefficients at near mesh particles (8.4mm), this gap is more pronounced for finer particles (2.8, 4.9, 6.4 and 7.4mm) which means that increasing the open area of the screen surface improves the screening efficiency mostly by increasing the recovery of the finer particles to undersize stream.

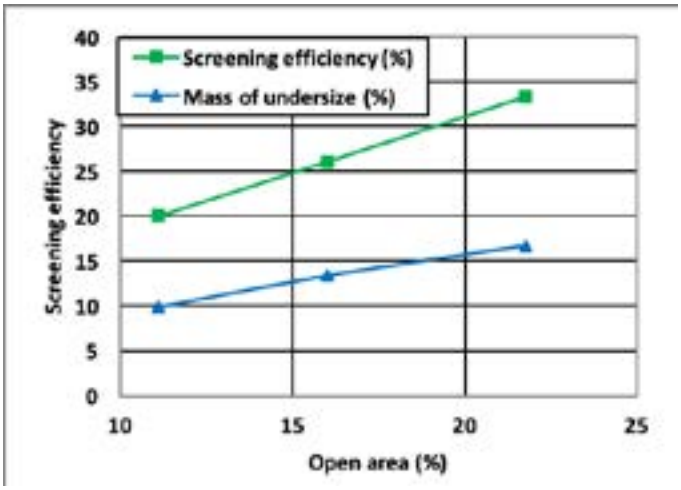

Fig. 14. Effects of the surface open area on screening efficiency and mass of undersize stream.

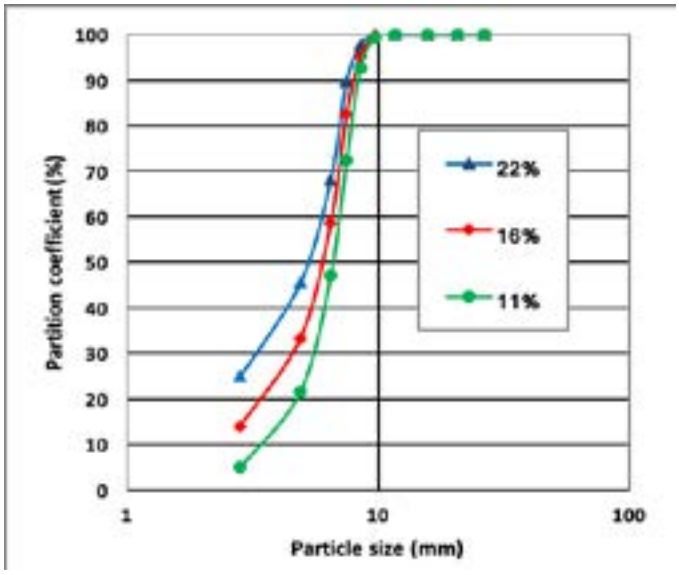

Fig. 15. Partition curves at various levels of surface open area

Table 5. Imperfection values for different screen surface open areas based on partition curves

Open Area (%)	d_{25}	d_{50}	d_{75}	Imperfection
11.11	2.83	5.18	6.83	0.39
16.00	4.00	5.93	7.15	0.27
21.78	5.20	6.62	7.60	0.18

Fig. 16, shows the mean residence time of the particles reporting to undersize and oversize streams at various surface open area values. Apparently, the mean residence time of both undersize and oversize particles on screen surface is higher in screen surfaces with larger open area. Larger open area means higher number of apertures on the surface causing more interaction between particles and screen surface which increase the MRT and particle accumulation on the screen surface. Although accumulation of particles looks like a negative effect on screening, under the influence of vibration and formation of a dynamic bed material on screen surface usually results in superior screening performance by segregation and placing fine and near mesh particles closer to the screen surface.

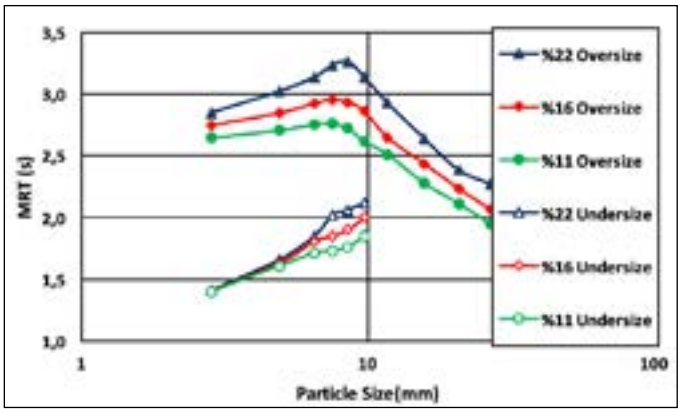

Fig. 16. The mean residence time of particles reporting to undersize and oversize streams at various surface open areas

3. conclusions

n this study, a three-dimensional DEM model was employed to numerically simulate the particle flow in a typical pilot-scale vibrating screen. The simulations utilized non-spherical particles, allowing for a more accurate representation of the real-world screening behavior. The effects of parameters related to the screen surface, such as surface dimensions, aperture shape and surface open area, on screening performance were investigated. The performance of the screening was evaluated in terms of screening efficiency, mass flow of the undersize stream, partition curves, imperfection values, cut-size, and mean residence time of the particles.

Key findings include:

- Longer screen surfaces increased screening efficiency and mass recovery in the undersize stream.
- Screens with perpendicular apertures to the flow direction achieved higher screening efficiency compared to those with flow-oriented apertures.
- Increased surface open area improved screening efficiency by enhancing the recovery of finer particles.

Acknowledgement

The authors express their sincere gratitude for the financial support provided by The Scientific and Technological Research Council of Turkey (TUBITAK) for the project titled "Numerical Modelling of Industrial Screening" (215M368).

References

Aghlmandi Harzanagh, A., Orhan, E.C., Ergun, S.L., 2018. Discrete element modelling of vibrating screens. Miner. Eng. 121, 107–121. doi:10.1016/j.mineng.2018.03.010

Beas, I.N., & Nongwe, I. (2021). An Overview of Plastic Waste Generation and Management in Food Packaging Industries. Recycling, 6(1), 12. https://doi.org/10.3390/recycling6010012

Chen, Y., Tong, X., 2010. Modeling screening efficiency with vibrational parameters based on DEM 3D simulation. Min. Sci. Technol. 20, 615–620. doi:10.1016/S1674-5264(09)60254-4

Cleary, P.W., Sinnott, M.D., Morrison, R.D., 2009a. Separation performance of double deck banana screens – Part 1: Flow and separation for different accelerations. Miner. Eng. 22, 1218–1229. doi:10.1016/j.mineng.2009.07.002

Cleary, P.W., Sinnott, M.D., Morrison, R.D., 2009b. Separation performance of double deck banana screens – Part 2: Quantitative predictions. Miner. Eng. 22, 1230–1244. doi:10.1016/j.mineng.2009.07.001

Cundall, P.A., 1971. A computer model for simulating progressive large-scale movements in blocky rock systems. Nancy, p. Symp. Int. Soc. Rock Mech.

Cundall, P.A., Strack, O.D.L., 1979. A discrete numerical model for granular assemblies. Géotechnique 29, 47–65. doi:10.1680/geot.1979.29.1.47

Delaney, G.W., Cleary, P.W., Hilden, M., Morrison, R.D., 2012. Testing the validity of the spherical DEM model in simulating real granular screening processes. Chem. Eng. Sci. 68, 215–226. doi:10.1016/j.ces.2011.09.029

Dong, K., Esfandiary, A.H., Yu, A.B., 2016. Discrete particle simulation of particle flow and separation on a vibrating screen: Effect of aperture shape. doi:10.1016/j.powtec.2016.11.004

Dong, K.J., Brake, I., 2009. DEM simulation of particle flow on a multi-deck banana screen. Miner. Eng. 22, 910–920. doi:10.1016/j.mineng.2009.03.021

Elskamp, F., Kruggel-Emden, H., 2015. Review and benchmarking of process models for batch screening based on discrete element simulations. Adv. Powder Technol. 26, 679–697. doi:10.1016/j.apt.2014.11.001

Elskamp, F., Kruggel-Emden, H., Hennig, M., Teipel, U., 2017. A strategy to determine DEM parameters for spherical and non-spherical particles. Granul. Matter 19, 46. doi:10.1007/s10035-017-0710-0

Extrica. (2023). Performance optimization of banana vibrating screens based on PSO-SVR under DEM simulations. Retrieved from https://www.extrica.com

Hilden, M.M., 2007. Dimensional analysis approach to the scale-up and modelling of industrial screens. PhD-thesis, University of Queensland.

Jahani, M., Farzanegan, A., Noaparast, M., 2015. Investigation of screening performance of banana screens using LIGGGHTS DEM solver. Powder Technol. 283, 32–47. doi:10.1016/j.powtec.2015.05.016

Jeanger, P.J., Labayen, I.V., & Yuan, Q. (2022). A Review on Textile Recycling Practices and Challenges. Textiles, 2(1), 174-188. https://doi.org/10.3390/textiles2010010

Jiang, Z., Zhang, C., & Zhao, Y. (2021). Quantification of the contribution ratio of relevant input parameters in DEM-based granular flow simulation. Powder Technology, 383, 313-322. https://doi.org/10.1016/j.powtec.2021.01.075

Kloss, C., Goniva, C., Hger, A., Amberger, S., Pirker, S., 2012. Models, algorithms and validation for open-source DEM and CFD-DEM. Prog. Comput. Fluid Dyn. 12, 140–152.

Li, J., Webb, C., Pandiella, S.S., Campbell, G.M., 2002. A Numerical Simulation of Separation of Crop Seeds by Screening—Effect of Particle Bed Depth. Food Bioprod. Process. 80, 109–117. doi:10.1205/09603080252938744

Liu, Q., Tang, S., & Zhang, X. (2023). A coupled FEM-DEM study on mechanical behaviors of granular soils considering particle breakage. Computers and Geotechnics, 143, 104551. https://doi.org/10.1016/j.compgeo.2021.104551

Polanía, A.F., Awich, J.V., & McCarthy, J.J. (2023). DEM study on the role of fines in the mobility of dry granular flows. Powder Technology, 391, 482-492. https://doi.org/10.1016/j.powtec.2021.01.076

Shimosaka, A., Higashihara, S., Hidaka, J., 2000. Estimation of the sieving rate of powders using computer simulation. Adv. Powder Technol. 11, 487–502. doi:10.1163/156855200750172088

Wang, Z., Li, Y., & Liu, G. (2023). DEM-based parameter optimization and tests of digging green onions. International Journal of Agricultural and Biological Engineering, 16(2), 140-148. https://doi.org/10.25165/j.ijabe.20231602.6842

Wills, B.A., Napier-Munn, T.J., 2006. Mineral Processing Technology. Elsevier Science & Technology Books.

Zhao, L., Zhao, Y., Bao, C., Hou, Q., Yu, A., 2017. Optimisation of a circularly vibrating screen based on DEM simulation and Taguchi orthogonal experimental design. Powder Technol. 310, 307–317. doi:10.1016/j.powtec.2017.01.049

Zhao, L., Zhao, Y., Bao, C., Hou, Q., Yu, A., 2016. Laboratory-scale validation of a DEM model of screening processes with circular vibration. Powder Technol. 303, 269–277. doi:10.1016/j.powtec.2016.09.034

Zhao, L., Zhao, Y., Liu, C., Li, J., Dong, H., 2011. Simulation of the screening process on a circularly vibrating screen using 3D-DEM. Min. Sci. Technol. 21, 677–680. doi:10.1016/j.mstc.2011.03.010

Madencilik - Mining, 2024, 63(2), 95-100

BİLİMSEL MADENCİLİK DERGİSİ
SCIENTIFIC MINING JOURNAL

TMMOB Maden Mühendisleri Odası Yayını / The Publication of the Chamber of Mining Engineers of Turkey

www.mining.org.tr

Original Research

Investigation of wet ground limestones on porous ceramic body properties

Yaş öğütülmüş kireçtaşlarının gözenekli seramik bünye özelliklerine etkisinin araştırılması

Emrah Durgut[a,*]

a Çanakkale Onsekiz Mart University, Çan Vocational School, Mining and Extraction Department, Çanakkale, TÜRKİYE

Received: 17 December 2024 • Accepted: 27 March 2025

A B S T R A C T

Wall tiles must have a 10-20% water absorption depending on the EN 14411 standard. In order to meet this water absorption criterion, calcite and dolomite minerals, which are in carbonated structure, are used in wall tile body composition. Manufacturers supply these minerals from limestone sources close to the enterprises, which are abundant in nature. The size of raw materials must be reduced to finer sizes (-45 µm) in aqueous medium in order to produce qualified wall tile body composition. In this context, this study aimed to investigate the effects of ground limestone samples obtained from the Derenti, Nevruz, and Terzialan regions of Çanakkale province (Türkiye), on ceramic wall tiles based on laboratory and industry-scale experiments/analyses. The limestone samples were firstly ground in a batch mill, and the grinding performances were compared in terms of time-dependent particle size, energy consumption, and capacity. Then, wall tile bodies were analyzed in terms of sintering properties and TS EN 14411 standards. The results from this study showed that Bond Work Indexes of Derenti, Nevruz, and Terzialan limestone samples were determined as 12.8, 11.7, and 13.0 kWh/t, respectively. As a result of industrial-based batch grinding studies, the energy consumption increased from 67.4 to 73.4 kW/t and the capacity decreased from 1.34 t/h to 1.23 t/h with quartz content increment of limestone samples from 0.8% to 2.1% and a ground limestone sample was gained with d90: 16.97 µm, d50: 1.85 µm, and d10: 0.37 µm values. Additionally, sintering studies showed that the shrinkage value decreased from 0.43% to 0.31% with CaO increment from 53.9% to 54.6% and wall tile with TS EN 14411 water absorption standard was obtained by using 13% limestone. In conclusion, the mineral content in limestone showed significant effects on particle size distribution, energy consumption, and capacity in the fine grinding process as well as on sintering properties of ceramic wall tile body.

Keywords: *Limestone, Wet grinding, Sintering, Wall tile ceramic properties.*

Introduction

Ceramic tiles are produced by sintering plastic and non-plastic raw materials such as clay, quartz, calcite, and feldspar minerals at high temperatures (1150-1200°C). These coating materials are widely used on interior and exterior spaces such as walls, floors, kitchens, bathrooms, etc. The usage areas of ceramic tiles are determined by abrasion, scratch/break resistance, water resistance, easy cleaning, frost resistance, hygiene, and aesthetics properties. And, ceramic tiles are divided into different classes according to measurable properties, and, the raw materials used in the structures differ depending on the ceramic tile classes.

Wall tiles consist of three layers; body, engobe, and glaze from bottom to top. The body is at the bottom of the wall tile where the physical properties are given. Nowadays, the producers want to use local resources due to economic reasons, so the color of the body of ceramic tile becomes darker. Therefore, engobe is applied as a lining between the body and the glaze to provide decorative effects on the top surface more visible. At the top of the wall tile, the glaze is applied and the product is presented to the customer aesthetically. The water absorption value is considerably high (10-20%) compared to the floor tile due to the porous structure (TS EN 14411). Because of this feature, it adheres well to the wall and creates less vertical load due to its low density. They are not paved on the floor because they do not have as much load-bearing capacity as floor tiles.

Ceramic tile production consists of different processes from the preparation of raw materials to the packaging of the final product (Sacmi, 2002). The process starts with the preparation of the raw materials that make up the ceramic tile body, engobe, and glaze compositions. Raw materials taken from nature in line with the criteria determined by the producers are first brought to very fine sizes by size reduction and classification processes. At this stage jaw, cone, and impact crushers are used to subject the

* Corresponding author: emrahdurgut@comu.edu.tr • https://orcid.org/0000-0002-4637-7087

https://DOI: 10.30797/madencilik.1600367

raw materials individually to primary size reduction and sieved to the size to be fed to the grinding or clay mixing system. Wall tile bodies generally consist of raw materials such as clay minerals, siliceous kaolin, and limestone (Niall and Evitt, 2000). Plastic clay group raw materials are fed into a clay mixer with high-speed agitators and dispersed to reach the size of natural clays from an agglomerated state. Non-plastic hard raw materials such as siliceous kaolin and limestone are ground in separate batches in mills. If the calcite mineral in the wall tile body has not reached a fine enough particle size, it will not form a crystalline or glassy phase and remain free in the sintering stage. This will lead to thermal shock resistance problems due to moisture expansion in the product and the limestone needs to be ground to very fine sizes, separate from the siliceous kaolin (Dvoáková et al., 2021). Raw material character, mill type (batch/continuous mill), lining material (alumina, silex, rubber), grinding media, mill rotation speed, and regime are affecting parameters in the grinding process (Bazin and Lavoie, 2000; Altun, 2014; Deniz, 2021).

Limestone is composed mostly of calcite that has a glassy luster, transparent, easily breakable, coarse crystalline properties, and is chemically composed of calcium carbonate. Besides, its hardness is 3 in terms of the Mohs scale and has a specific gravity of 2.6-2.8 g/cm^3. Calcite is also used in glass, paint, paper, and plastic industries as well as the ceramic industry and needs to be ground into fine particle size in order to be used effectively (El-Sherbiny, 2015; Çayırlı et al., 2023).

In ceramic wall tile production, firstly, the particle size reduction process is applied to raw materials. Then, clay, siliceous kaolin, and limestone groups brought to fine particle size are sieved and dosed in a wet medium. Afterward, wall tile granules are obtained from the body slip, which is mixed according to the recipe ratios determined in the laboratory and sent to spray dryers. The granules are shaped in press to form green tiles and the green tiles are then dried for gaining strength. The dried tile is sintered in the kiln after decorative effects are applied on the surface and the final product is obtained. The final product is first visually inspected for quality control purposes and then subjected to tests for compliance with quality control standards to be sent to the customer. For this reason, the compliance of each process step with the production conditions is very important (Framinan et al., 2014; TS EN 14411).

In this study, the structural properties of three different limestone samples from the Çanakkale region were first characterized by chemical, mineralogical, and physical methods. Then, the grinding characteristics of limestones were identified by laboratory-scale grinding tests, and, the effects of the grinding process in separate industrial-based mills on particle size, energy consumption, and capacity were investigated. Finally, the ground limestones were mixed with clay and siliceous kaolin/fired ceramic waste to produce porous wall tile ceramic bodies, and their sintering properties were determined. The effects of limestone grinding on particle size, energy consumption, capacity, and the use of ground limestone on ceramic wall tile bodies were novel aspects of the research.

1. Materials and Methods

In this study, the effects of wet grinding performances of several limestone samples obtained from different regions (Derenti, Terzialan, and Nevruz) in Çanakkale province (Türkiye) on wall tile sintering properties were investigated with the combination of laboratory scale and industrial approach. In this context, firstly, chemical and mineralogical analyses of the limestone samples along with local siliceous kaolin+fired waste (SK+FW) and İstanbul clay samples were performed, within the scope of characterization studies. The chemical analyses of the samples were carried out with PANALYTICAL Brand AXIOS MAX model X-Ray Spectrophotometer (XRF) device and the mineralogical analyses (XRD) were carried out with PANALYTICAL Brand X'PERT PRO MPD diffractometer with an angular range of 3-70° between 2θ, step size 0.02, deviation slit ¼, anti-reflection slit ½. The results of the chemical and mineralogical analyses of the samples used in the experimental studies are presented in Table 1.

Table 1. Results for chemical and mineralogical analysis of the samples used in this study

Raw materials	Chemical composition									Mineralogical composition
	SiO_2	Al_2O_3	TiO_2	Fe_2O_3	CaO	MgO	Na_2O	K_2O	LOI	
Derenti	1.4	0.3	0.0	0.1	54.3	0.8	0.0	0.0	43.1	
Nevruz	0.8	0.3	0.0	0.1	54.6	0.8	0.0	0.0	43.4	Calcite, quartz
Terzialan	2.1	0.3	0.0	0.1	53.9	0.6	0.0	0.0	42.9	
Siliceous kaolin + Fired waste	64.7	18.8	0.7	2.4	1.6	1.8	1.2	2.8	5.8	Kaolin, quartz, gehlenite, anorthite
Clay	63.2	21.6	1.2	2.8	0.6	0.6	0.5	2.1	7.2	Illite, quartz, kaolinite

LOI: Loss on ignition As seen in Table 1, the presence of calcite and quartz minerals in the mineralogical analyses of all limestone samples are the main sources of CaO and SiO_2 contents in the chemical analyses. Theoretically, calcite mineral consists of 56.0% CaO and 44.0% CO_2, which gives an idea about the CaO differences in the content of limestone samples (Rodriguez-Navarro et al., 2009). In this context, Derenti, Nevruz, and Terzialan limestones are composed of approximately 96.9%, 97.5%, and 96.3% calcite minerals, respectively. Such compounds were not seen in the mineralogical analyses due to the particularly strong calcite peak and trace amount of other minerals. SK+FW group minerals were mainly composed of kaolin+quartz and gehlenite+anorthite originating from raw materials and fired waste, respectively. The main mineral of clay was illite, and other minerals were quartz and kaolinite. The Al_2O_3, Fe_2O_3, and MgO contents are thought to be due to clay minerals, and alkaline and ferrous compounds in raw materials. The loss on ignition (LOI) value was due to the chemically bounded water of clay minerals in SK+FW and clay group raw materials (Kagonbe et al., 2021). In order to determine the sintering characteristics, the limestone, and SK+FW samples were ground to reach 2% for +63 µm, and the clay sample was mixed and sieved to -90 µm in a wet medium. Then, the ground slurries were dried in an oven at 105°C. Next, the dried raw materials were ground with agate and mortar and sieved to -250 µm and 6% humidified by spraying water to reach granules which were shaped to 5×5 cm by a laboratory press with 325 kg/cm^2 specific pressure and sintered in the wall tiles conditions. The application conditions and sintering properties as shrinkage, water adsorption, and color values of the sintered raw material groups are given in Table 2.

Table 2. Sintering properties of raw materials used in the study

Raw material group		Limestone Derenti	Nevruz	Terzialan	SK+FW	Clay
Specific pressure (kg/cm^2)		325				
Max. sintering temperature (˚C)		1150				
Sintering duration (min)		38				
Shrinkage (%)					5.0	5.4
Water absorption (%)					11.8	7.2
Color	L	88.0	88.8	87.2	62.7	74.9
	a	0.1	0.1	0.2	11.4	4.9
	b	4.2	3.8	4.9	17.1	23.5
Sintered specimen					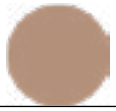	

*Shrinkage and water adsorption analysis could not be done due to the crumbled samples.

The wall tile body subject to the study currently consists of plastic clay minerals, SK+FW, and limestone raw materials. All of the raw material groups are prepared in aqueous media in the presence of dispersants in certain proportions. The clay minerals are dispersed in a mechanical mixer and then sieved into a clay stock pool. SK+FW sample was ground, sieved, and taken to the SK+FW stock pool. Fine-sized quartz as a silica source causes rheological problems in the ceramic slip as well as high shrinkage value in the sintering process (Dana and Das, 2002). On the other hand, quartz content in the ceramic body can remain as residual quartz without reacting with calcium and aluminum during the sintering process and cannot form crystal and glass phases (Tarhan and Tarhan, 2018). Therefore, the quartz amount and particle size are important parameters for ceramic wall tile recipes. Limestone was ground to a fine particle size compared to the other raw material groups and then sieved to the limestone stock pool. Afterward, 34% of clay, 53% of SK+FW, and 13% of limestone were mixed in the dosing pool by weight and sent to the spray dryer to obtain granules with 6% moisture content. The production process used in the wall tile body preparation is shown in Figure 1.

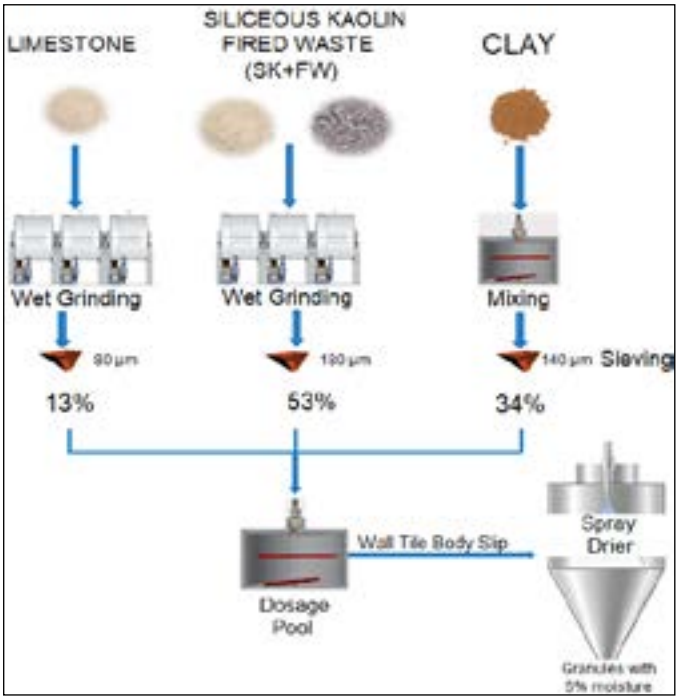

Figure 1. Wall tile body preparation process flowsheet

A laboratory-type jaw crusher was used for the primary particle size reduction of raw material. Within the scope of pre-grinding laboratory studies, 500 g of -5 mm crushed limestone samples were ground in a porcelain vibrating jet mill with a volume of 1100 mL until reaching 0.2% sieve residue for 45 µm in the presence of municipal water at 1800 g/L density and compared in terms of grinding duration. 300 g alumina grinding media were used with 50% of 15 mm, 35% of 20 mm, and 15% of 25 mm ball ratios in a porcelain vibrating jet mill. On the other hand, the grinding work indexes were also compared with a standard method, namely the Bond Work Index. The limestone samples were firstly crushed and then sieved to a size of -3.36 mm for feeding to the Bond Work Index experiments. A 30.5 cm diameter and 30.5 cm long stainless-steel standard Bond mill was used in the experiments. The mill was loaded with 22.648 kg of stainless steel balls with diameters of 38.1, 31.75, 25.40, 19.05, and 12.70 mm corresponding to 22% of the clearance volume, and operated at 70 rpm, 86% of the critical speed. In each experiment, 100% of the ball cavity volume (700 cm^3) was filled with -3.36 mm size feedstock. The experiments were performed according to TS 7700 for the standard bond work index determination.

-5 mm crushed limestone samples were fed to a batch mill with 310 cm diameter and 460 cm length and with an inside alumina liner to determine the industrial grinding characteristics. After 30% of the mill volume was filled with alumina balls, the effects of the grinding media on the yield were also investigated at a constant rotational speed of 16 rpm. The used batch mill and applied grinding parameters are given in Figure 2. The energy analysis was obtained by reading the electricity meter connected to the mill. The capacity was calculated by dividing the total grinding time by the amount of ground raw material. The particle size distribution analysis of the ground materials was performed using a Malvern Mastersizer Micro Plus laser scattering device with a measurement range of 0.03 to 555 µm.

Figure 2. Representative demonstration of batch mill and wet grinding parameters

Finally, the clay and SK+FW slips prepared according to the flow chart in Figure 1 were mixed with the limestone sample obtained from the grinding studies to obtain wall tile body granules. The granules were shaped in 5×5 cm size at 325 kg/cm^2 specific pressure and sintered in the conditions of maximum 1150ºC temperature and 38 min sintering duration and compared in terms of compliance with wall tile standards (EN 14411). Netzch brand DIL 402 CD model dilatometer was used to determine the thermal expansion coefficients. PCE XXM 30 color measuring device that had a 400-700 nm wavelength range was used for analyzing the color values (L, a, b) of sintered specimen by scanning the surface, and three analyses were applied for each specimen with 0.08 average color measurement accuracy (ΔE). Delta E (ΔE) is a calculation of the change in color as measured in three-dimensional axes L, a, and b color space. ΔE calculated from the color difference data of the colorimeter is the color difference between the product and the sample, where L_2: standard color, L_1: measuring color, a_2: standard color, a_1: measuring color, b_2: standard color, b_1: measuring color as given in Eq. 1:

$$\Delta E: \sqrt{[(L_2\text{-}L_1)^2 + (a_2\text{-}a_1)^2 + (b_2\text{-}b_1)^2]} \quad \sqrt{[(L_2\text{-}L_1)^2 + (a_2\text{-}a_1)^2 + (b_2\text{-}b_1)^2]} \qquad (1)$$

2. Results and discussion

The grinding times until reaching 0.2% sieve residue for +45 µm at a constant 1800 g/L density in the laboratory porcelain vibrating jet mill and Bond work index values of Derenti, Nevruz, and Terzialan limestone raw materials are shown in Figure 3.

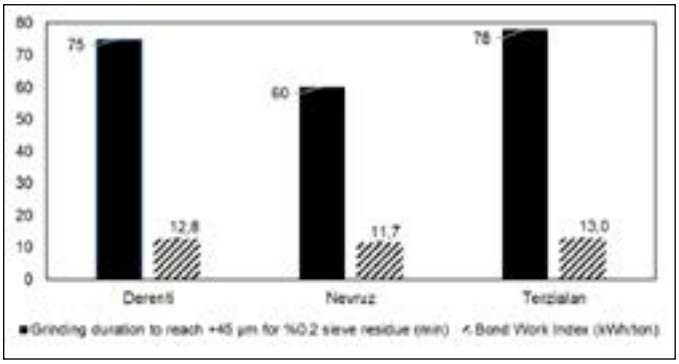

Figure 3. Results for Porcelain vibrating jet mill and Bond Work Index grinding experiments

As seen in Figure 3, there are grinding differences between Derenti, Nevruz, and Terzialan limestone samples in the laboratory-based vibrating jet porcelain mill and Bond mill. The grinding duration until reaching 0.2% sieve residue for +45 µm in the vibrating jet porcelain mill - Bond Work Index values were determined as 75.0 min - 12.8 kWh/ton, 60 min - 11.7 kWh/ton and 78 min - 13.0 kWh/ton for Derenti, Nevruz, and Terzialan samples, respectively. Limestones are composed of mainly calcite and small amounts of quartz minerals. The specific crushing energy values required for particle liberation were found to be considerably higher in quartz than in calcite (Ma et al., 2022). Quartz mineral is hard to grind compared to other raw materials in the particle size reduction of the ceramic body, so quartz behaves as a grinding medium and causes abrasion of other minerals (Haner, 2021). Besides, the Bond Work Index became higher with quartz mineral increment in the marl (Karakaş, 2006). It is also known that quartzite rock has higher specific fracture energy than limestone (Zhang and Ouchterlony, 2022). Therefore, the grinding duration in the vibrating jet mill and the Bond Work Index of the Terzialan sample are higher than the other samples due to the high quartz content and the structure due to the formed geological environment. Figure 4 shows the industrial-based grinding experiment results of Derenti, Nevruz, and Terzialan limestones in the alumina ball mill in terms of particle size change with grinding time.

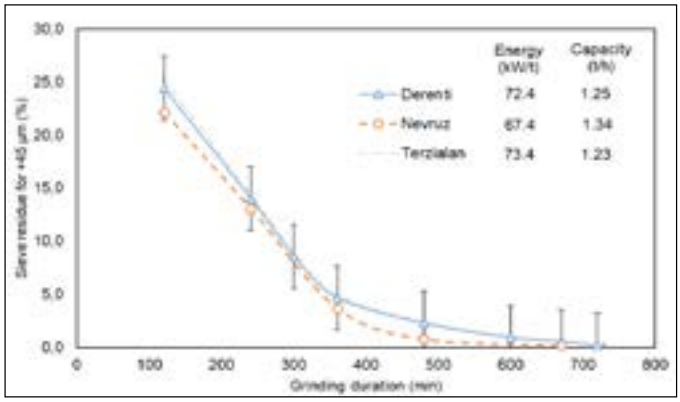

Figure 4. Results for industrial batch grinding experiments

As seen from Figure 4, 0.2% sieve residue for +45 µm was reached as a result of grinding Derenti, Nevruz, and Terzialan limestones at 720, 670, and 730 min, which resulted in 72.4, 67.4, 73.4 kW/t of energy consumption and 1.25, 1.34, 1.23 t/h of capacity, respectively.

Additionally, the ground limestone samples were conducted laser particle size distribution measurement. According to the results of laser particle size measurement performed after the grinding, the d_{90} values of Derenti, Nevruz, and Terzialan limestones were measured as 18.34 µm, 16.97 µm, and 18.79 µm, respectively (Figure 5). Laboratory results confirmed the industrial results and the Nevruz sample, which had a lower content of hard to grind quartz compared to the other samples, was ground in less time and obtained a finer size distribution.

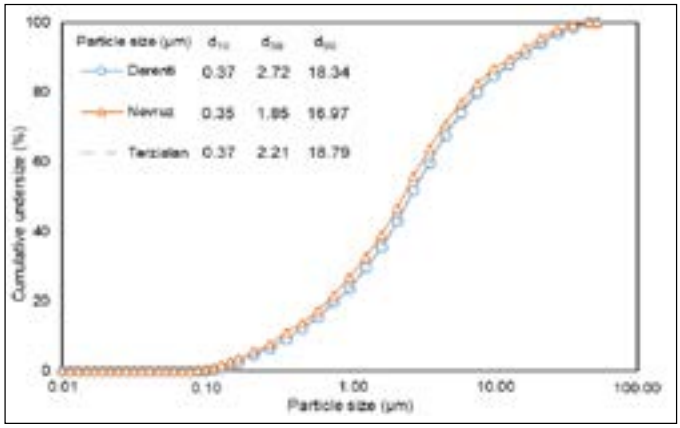

Figure 5. Particle size distribution of ground limestone samples to 0.2 sieve residue for +45 µm

Limestone samples ground to +45 µm with 0.2% sieve residue were mixed separately based on the ratios in Figure 1 and wall tile composition slurries were formed. The wall tile composition slurries were sent to a spray dryer to obtain granules with a 6% moisture content. The granules were firstly shaped in a laboratory-based press at a specific pressure of 325 kg/cm^2 in 5×5 cm size and sintered at a maximum temperature of 1150°C and 38 min (Table 3).

Table 3. Sintering conditions and results of wall tile body compositions obtained with different limestones

Wall tile composition with		Derenti	Nevruz	Terzialan
Specific pressure (kg/cm^2)		325		
Max. sintering temperature (˚C)		1150		
Sintering duration (min)		38		
Shrinkage (%)		0.36	0.31	0.43
Water absorption (%)		18.2	18.2	18.1
Color	L	75.6	76.1	75.7
	a	6.9	6.9	7.0
	b	18.2	17.7	18.3
Sintered specimen				

In the sintering studies carried out under wall tile conditions, the shrinkage-water absorption values were found to be 0.36-18.2%, 0.31-18.2%, and 0.43-18.1% for the bodies prepared with Derenti, Nevruz and Terzialan limestones, respectively. L-a-b values after sintering of Derenti, Nevruz, and Terzialan samples containing bodies were measured as 75.6-6.9-18.2, 76.1-6.9-17.7, and 75.7-7.0-18.3 (Table 3).

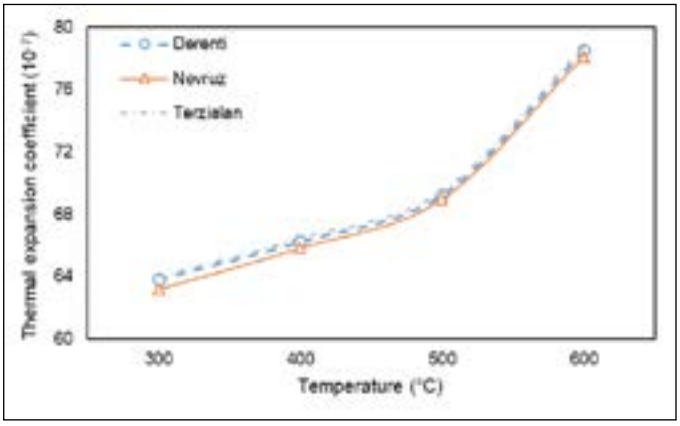

Figure 6. Thermal expansion coefficients of wall tile bodies

Thermal behavior of the wall tile body compositions prepared with Derenti, Nevruz, and Terzialan limestones are given in Figure 6 as dilatometric values. The volume change in ceramic bodies after α - β quartz transformation between 573°C significantly affects the coefficient of thermal expansion values (Johnson et al., 2020). Such change may cause crack formation during ceramic firing and is tried to be solved by passing the cooling phase slowly (Şan and Koç, 2011). While there is no important difference in the thermal expansion coefficient results of Derenti and Terzialan samples containing bodies, the thermal expansion coefficient was lower in the Nevruz sample containing body due to the low amount of quartz that was seen in chemical composition (Table 1).

3. Conclusion

In this study, the properties of different limestone samples were determined by mineralogical and chemical analysis. Then, the effects of their structural differences on grinding and porous wall tile composition were investigated by experimental studies.

As a result of mineralogical analysis, calcite and quartz minerals were observed in limestone samples. In chemical analyses, calcite components were reflected as CaO and loss on ignition, while quartz was reflected as SiO_2 value, and mineral quantity differences were observed accordingly.

The effects of mineral content in limestone on grinding were first investigated in a laboratory-based environment, and the results obtained from laboratory experiments were confirmed by industrial-based studies. It was determined that with an increase in the amount of quartz in limestone from 0.8% to 2.1%, the industrial grinding time will increase from 670 min to 730 min, the energy consumption will increase from 67.4 kW/t to 73.4 kW/t, and the capacity will decrease from 1.34 t/h to 1.23 t/h. As a result of industrial limestone grinding carried out in an alumina ball environment under the specified conditions, d_{10}; d_{50}; and d_{90} values were analyzed as 0.37; 2.72; 18.34 µm, 0.35; 1.85; 16.97 µm and 0.27; 2.21; 18.79 µm for ground Derenti, Nevruz and Terzialan samples, respectively.

As a result of the sintering studies, the increase in the CaO content in the limestone (from 53.9% to 54.6%) and the decrease in the SiO_2 content (from 2.1% to 0.8%) caused a decrease in the wall tile shrinkage value (from 0.43% to 0.31%) and thermal expansion coefficients. It has been determined that wall tile structures complying with EN 14411 water absorption standard could be obtained by using 13% ground limestone.

Quartz increment in limestone thought to be an increase in grinding time and energy consumption while capacity decreases. The increase in CaO content resulted in shrinkage decrement of the wall tile body after sintering. On the other hand, the increase in quartz in the wall tile body caused the thermal expansion coefficient increment, while the fine particle size of limestone was one of the reasons for to decrease. In conclusion, chemical and mineralogical differences in limestone structure have important effects on the grinding and sintering properties of wall tile composition.

Acknowledgments

This work was supported by Çanakkale Onsekiz Mart University The Scientific Research Coordination Unit, Project number: FBA-2024-4812. Besides, thanks to the Kaleseramik R&D Center for experimental support.

References

Altun, O., Benzer, H., & Enderle, U. 2014. The effects of chamber diameter and stirrer design on dry horizontal stirred mill performance. Minerals Engineering, 69, 24-28. https://doi.org/10.1016/j.mineng.2014.07.008.

Bazin, C., & Lavoie, G. 2000. Ball mill rotation speed and rate of particle breakage: application to a full scale unit. Trans Inst Min Metall Sect-C, 109,161-164.

Çayırlı, S., Gökçen, H.S., Yüce, N., Elchi, O. 2023. Utilization of wastes/by-products as a grinding additive. Scientific Mining Journal, 62(3), 123-130. https://doi.org/10.30797/madencilik.1342929.

Dana, K., & Das, S. 2002. Some Studies on Ceramic Body Compositions for Wall and Floor Tiles. Transactions of the Indian Ceramic Society, 61, 83 - 86. https://doi.org/10.1080/0371750X.2002.10800032.

Deniz, V. 2021. The effects on the grinding parameters of chemical, morphological and mineralogical properties of three different calcites in a Hardgrove mill. Minerals Engineering, 176, 107348. https://doi.org/10.1016/j.mineng.2021.107348.

Dvoáková, P., Kloužková, A., Kohoutková, M., & Kolářová, M. 2021. IOP Conf. Ser.: Mater. Sci. Eng. 1050 012004.

El-Sherbiny, S., El-Sheikh, S. & Barhoum, A. 2015. Preparation and modification of nano calcium carbonate filler from waste marble dust and commercial limestone for papermaking wet end application. Powder Technology, 279, 290–300. https://doi.org/10.1016/j.powtec.2015.04.006

Framinan, J.M., Leisten, R., & García, R.R. 2014. A case study: Ceramic tile production. In Springer eBooks (pp. 371-395). https://doi.org/10.1007/978-1-4471-6272-8_15.

Haner, S. (2021). Fine dry grinding with cylpebs of quartz sand in the Şile district of İstanbul Turkey. Archives of Mining Sciences, 66(4), 625-634. ttps://doi.org/10.24425/ams.2021.137457.

Johnson, S.E., Song, W.J., Cook, A.C., Vel, S.S., & Gerbi, C.C. 2020. The quartz α↔β phase transition: Does it drive damage and reaction in continental crust? Earth and Planetary Science Letters, 553, 116622. https://doi.org/10.1016/j.epsl.2020.116622.

Kagonbé, B.P., Tsozué, D., Nzeukou, A.N., & Ngos, S., III. 2021. Mineralogical, geochemical and physico-chemical characterization of clay raw materials from three clay deposits in northern Cameroon. Journal of Geoscience and Environment Protection, 09(06), 86–99. https://doi.org/10.4236/gep.2021.96005.

Karakaş, F. (2006). Energy optimization for grinding of cement raw materials [master's thesis]. [Istanbul]: Istanbul Technical University.

Ma, S., Li, H., Shuai, Z., Yang, J., Xu, W., & Deng, X. 2022. Research on grinding characteristics and comparison of particle-size-composition prediction of rich and poor ores. Minerals, 12(11), 1354. https://doi.org/10.3390/min12111354.

Niall, S. & Evitt, T.S. 2000. Compositions for ceramic tiles (Patent No. 6,127,298). United States Patent. https://patentimages.storage.googleapis.com/56/8b/a4/62bc90ddf24fbf/US6127298.pdf

Rodriguez-Navarro, C., Ruiz-Agudo, E., Luque, A., Rodriguez-Navarro, A. B., Ortega-Huertas, M. 2009. Thermal decomposition of calcite: Mechanisms of formation and textural evolution of CaO nanocrystals. American Mineralogist, 94(4), 578-593. https://doi.org/10.2138/am.2009.3021.

Sacmi 2002. Applied Ceramic Technology, Volume 1-2, Editrice La Mondragora S.R.L., Imola, Italy.

Şan, O. & Koç, M. 2011. Fabrication of microporous silica ceramics with varied polymorphic forms and investigation of their thermal shock behavior. DOAJ (DOAJ: Directory of Open Access Journals). https://doaj.org/article/f846712fe28b48d1847ebefb669428ab.

Tarhan, B & Tarhan, M. 2018. Effect of usage of perlite on technical properties of ceramic wall tile. International Journal of Research and Development, 10(1). https://doi.org/10.29137/umagd.364552.

TS EN 14411 2016. Ceramic tiles - Definition, classification, characteristics, assessment and verification of constancy of performance and marking, Turkish Standards Institution.

TS 7700 1989. Determination Method of Grinding Work Index, Turkish Standards Institution.

Zhang, ZX., Ouchterlony, F. 2022. Energy requirement for rock breakage in laboratory experiments and engineering operations: A Review. Rock Mech Rock Eng., 55, 629-667. https://doi.org/10.1007/s00603-021-02687-6.

Madencilik - Mining, 2024, 63(2), 101-110

BİLİMSEL MADENCİLİK DERGİSİ
SCIENTIFIC MINING JOURNAL

TMMOB Maden Mühendisleri Odası Yayını / The Publication of the Chamber of Mining Engineers of Turkey

www.mining.org.tr

Research Article

Reasonable width of coal pillar in fully mechanized caving mining face of extra-thick coal seam–A case study

Xueqi Zhang[1, 2, *], Hongbin Li[1,**], Yongwei Du[1,***], Zhongqiu Wang[1,****]

1 Inner Mongolia Yitai Coal Co., Ltd., Ordos, Inner Mongolia, 017000, China
2 State Key Laboratory of Coal Mine Disaster Dynamics and Control, Chongqing University, Chongqing, 400044, China

Received: 30 December 2024 • Accepted: 26 March 2025

A B S T R A C T

To address the issue of resource wastage caused by the extraction of thick coal seams with large coal pillars, this study is based on the first Panel of the 110 Working Face at the Suancigou Coal Mine. It employs methods such as on-site measurement, physical similarity model experiments, theoretical analysis, and numerical simulation to investigate the reasonable width of coal pillars under the disturbance of comprehensive mechanized mining in thick coal seams. The study reveals the damage and deformation evolution patterns of the coal pillars, calculates the critical width of the coal pillars based on limit equilibrium theory and strength theory, and simulates the distribution characteristics of stress and damage failure zones in the coal pillars. The results indicate that a 45 m coal pillar still possesses the substantial load-bearing capacity after multiple mining activities, suggesting the possibility of reducing its width to enhance coal recovery rates. The calculations show that the minimum width of the coal pillar should not be less than 26.18 m. Simulations demonstrate that when the width of the coal pillar is 30 m, the coal recovery rate is relatively high and meets safety production requirements. The findings of this research are significant for improving coal recovery rates in the Suancigou Coal Mine and similar mining conditions.

Keywords: *damage and deformation evolution; critical width; stress distribution; reasonable width; damage and failure zone.*

Introduction

Coal accounts for 60-70% of China's primary energy consumption structure and serves as the fundamental guarantee of energy security (Xie et al., 2021; Chen et al., 2021). Among them, the extra-thick coal seam is the main coal seam with high productivity and high efficiency, which is distributed in all major mining areas in China. Extra-thick coal seams are generally mined by longwall fully mechanized top coal caving, and a certain width of coal pillar is usually reserved between adjacent working faces to ensure the stability of the roadway. Therefore, the setting of the coal pillar width is crucial (Yuan et al., 2023). If the coal pillar is too narrow, it is prone to instability and failure, making it difficult to control the roadway; if it is too wide, it may lead to issues such as low coal recovery rates (Yang et al., 2022; He et al., 2023; Xue et al., 2024; Liu et al., 2023).

The most widely used method at present is A.H. Wilson's coal pillar design theory and formula, which overcomes the shortcomings of other methods, making it more practical and reliable (Gao et al., 2022). However, in actual applications, simplified empirical formulas are used, which only consider the coal pillar's ultimate strength and the width of the yielding zone (Yin et al., 2022; Song, 2016; Chen, 2005; Guo et al., 2014). With the introduction of long-term strength parameters of coal, the issue of insufficient consideration of coal pillar long-term strength in the theory has been addressed (Wang et al., 2002). Today, the application of advanced reasonable coal pillar design theories and methods, such as numerical simulation (Chang and Xu, 2021; Tian et al., 2021), internal and external stress field theories (Zheng et al., 2019; Li et al., 2012), and limit equilibrium theory coupled with elastoplastic theory (Kong et al., 2022; Wang and Dou, 2022; Zhu et al., 2021), has led to the continuous rationalization of coal pillar width design. However, in some long-operating mines, the coal pillar width design still relies on single or outdated theoretical methods. To ensure mining safety (Xing et al., 2024; Gu et al., 2024; Li et al., 2023), designs are overly conservative, leading to excessively large coal pillar widths, which result in significant coal resource wastage. Therefore, it is urgent to conduct relevant research, optimize coal pillar widths, and improve coal recovery rates.

To address the above-mentioned issues, this study took the 6_{upper}110 Working Face in the First Panel of Suancigou Coal Mine as the research background. Methods such as on-site monitoring, theoretical analysis, and numerical simulation were employed to study the reasonable width of the original 45-meter coal pillar.

* Corresponding author: qzhang1980@163.com • https://orcid.org/0009-0009-5491-9550
** lihb@mail.vinhelp.com • https://orcid.org/0009-0004-1668-5080
*** yidu195880698@163.com • https://orcid.org/0009-0001-4995-1515
**** zhongxunwang231@sina.com • https://orcid.org/0009-0000-0676-9652

https://DOI: 10.30797/madencilik.1609775

The study analyzed the damage and deformation evolution of the coal pillar, calculated the critical width of the coal pillar based on limit equilibrium theory and strength theory, and simulated the distribution characteristics of the coal pillar's stress and damage failure zones (Rong et al., 2024; Li et al., 2024; Liu et al., 2024; Yun et al., 2024). The research findings solved the problem of significant coal resource wastage caused by excessively large coal pillar widths at Suancigou Coal Mine. Additionally, the results provided a reference for optimizing coal pillar design in similar mining conditions.

1. Engineering background

1.1 Project Overview

The Suancigou Coal Mine is in the central region of the Jungar Coalfield in Inner Mongolia. It was completed and began trial production in August 2008. The mine covers an area of 49.82 km^2, with a reserve of 136,690,000 tons and an annual production capacity of 18 million tons. Currently, the mine primarily extracts from the 6_{upper} coal seam, which has a thickness ranging from 8 to 30 meters, with an average thickness of 20 meters. The immediate roof consists of medium sandstone with an average thickness of 22.2 meters, and the main roof is made up of sandy mudstone with an average thickness of 4.2 meters. The 110 Working Face is an active mining face, located in the northern wing of the First Panel in the northeastern part of the mine. The face has an approximately northeast-southwest orientation, with a strike length of 2,058 meters and a dip width of 244.6 meters. The area of the working face is 503,387 m^2, with a designed mining height of 3.8 meters and a maximum mining height of 24.2 meters, resulting in a mining ratio of 1:6. The layout of the roadways is shown in Figure 1.

1.2 Mine Pressure Manifestation Characteristics of Roadways and Stress Variation Patterns of Coal Pillars

(1) Deformation and Stress Characteristics of Roadways

Monitoring stations are set up in the 108 Transportation roadway, as shown in Figure 1, where the mine pressure manifestation characteristics are observed during the recovery of the 110 Working Face.

① Surface displacement analysis of the surrounding rock in the 108 Transportation Roadway (Figure 2)

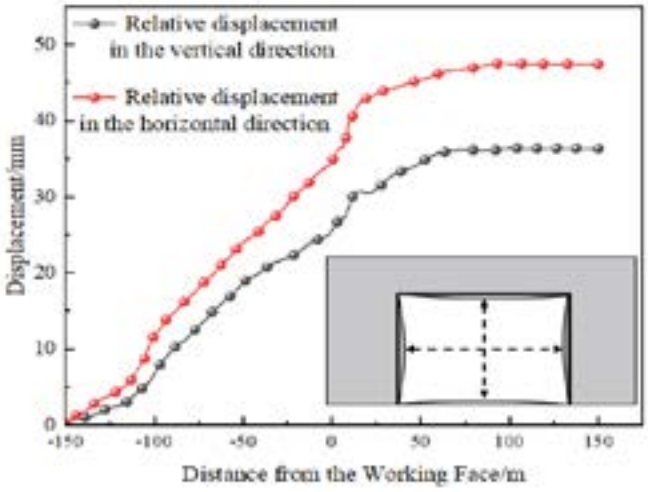

Fig.2 Evolutionary law of roadway surface displacement with advancement of working face

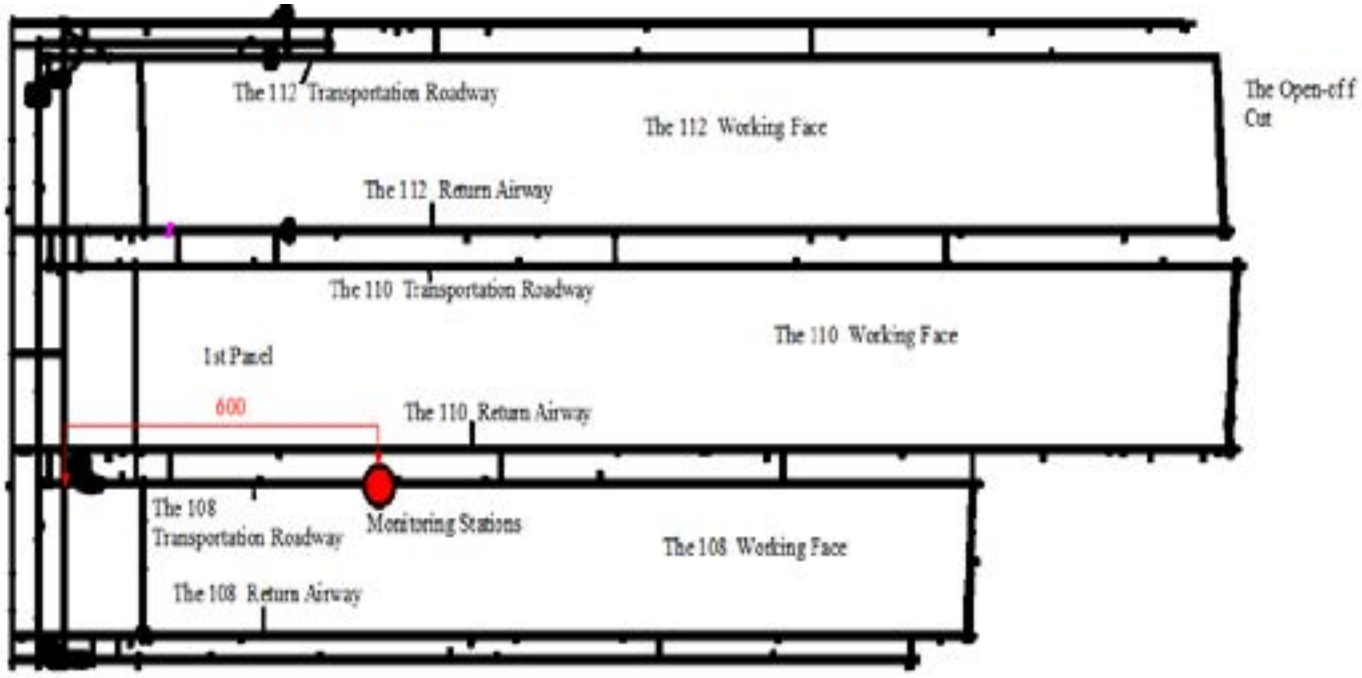

Fig.1 The layout of the roadways

During the observation period, the relative convergence of the surrounding rock in the 108 Transportation Roadway at the roof-floor and left-right sides is 48 mm and 37 mm, respectively. The surface deformation velocity of the surrounding rock in the range of -110 to 70 meters from the working face is relatively high, with the maximum relative displacement velocities of the roof-floor and left-right sides reaching 4 mm/s and 3 mm/s, respectively. As the working face advances, the surface deformation velocity of the surrounding rock in the 108 Transportation Roadway continuously decreases. After reaching 60 meters from the working face, the deformation velocity of the surrounding rock tends to stabilize, and the deformation of the roadway surrounding rock also becomes stable.

② Roof Stratum Separation Analysis of the 108 Transportation Roadway (Figure 3)

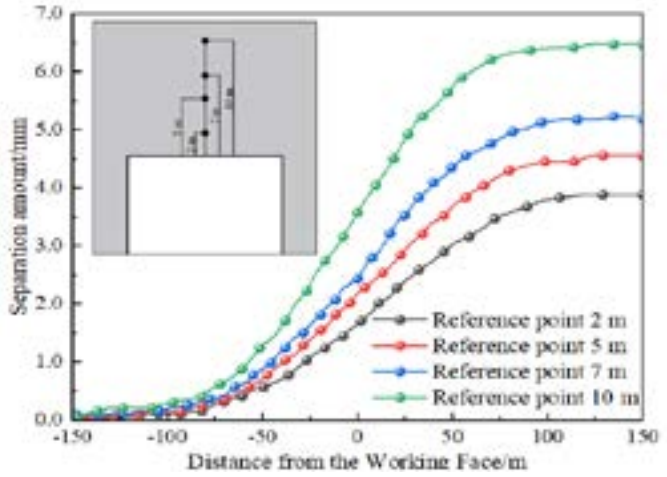

Fig.3 Variation law of roof stratum separation with the advancement of the working face

From Figure 3, the roof stratum separation in the 108 Transportation roadway mainly occurs between 80 meters ahead and 65 meters behind the 110 Working Face. Overall, as the reference point depth increases, the separation amount also increases. The maximum separation occurs at a depth of 10 meters in the roof, but the maximum separation is only 3.25 mm, indicating that roof separation is not significant. Based on the monitoring results of roof stratum separation in the 108 Transportation Roadway, it can be concluded that the recovery of the 110 Working face has little impact on the roof separation in the 108 Transportation Roadway. It is analyzed that the 45-meter protective coal pillar effectively ensures the stability of the 108 Transportation Roadway and limits the occurrence of significant roof separation.

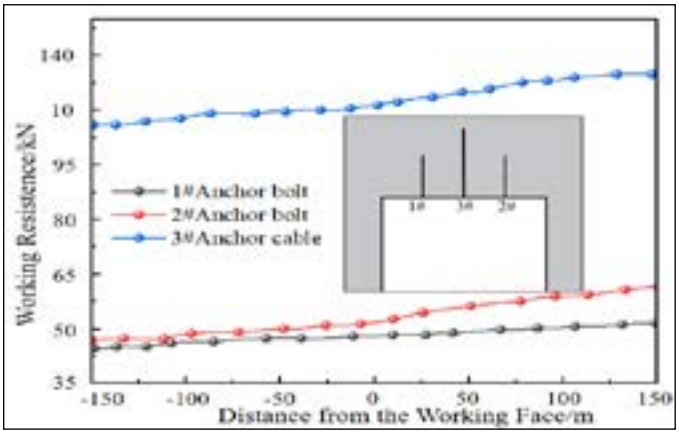

Fig.4 Variation law of anchor bolt(cable) working resistance with the advancement of the working face

From Figure 4, it can be observed that the working resistance of anchor bolts (cables) in the 108 Transportation Roadway shows minimal changes during the recovery of the 110 Working Face, generally tending towards a stable state. Within the monitoring range of 150 meters ahead and behind, the working resistance of anchor bolts (cables) in the 108 Transportation Roadway exhibits a slow increasing trend: the 1# anchor bolt increases by 6.9 kN, the 2# anchor cable increases by 14.4 kN, and the 3# anchor cable increases by 14 kN.

The roadway pressure monitoring results indicate that during the recovery of the 110 Working Face, the surface displacement and roof separation in the 108 Transportation Roadway are relatively small, and the working resistance of the anchor bolts (cables) shows minimal variation, reflecting good roadway system stability. The analysis suggests that the 45-meter coal pillar is the key factor ensuring the stability of the 108 Transportation Roadway system. The large width of the protective coal pillar minimizes the impact of mining activities on the exposed roadway, resulting in insignificant roadway pressure manifestation.

(2) Stress Variation Law of Coal Pillars

A group of borehole stress meters is installed at the same position as the roadway pressure monitoring station, as shown in Figure 2, to monitor the stress distribution law of the protective coal pillar within the range of 150 meters ahead to 150 meters behind the 110 Working Face. The monitoring results are shown in Figure 5. It should be noted that the results in the figure represent the stress increment caused by production activities at the working face, with the stress increment set to zero at 150 meters ahead of the working face (i.e., -150 m).

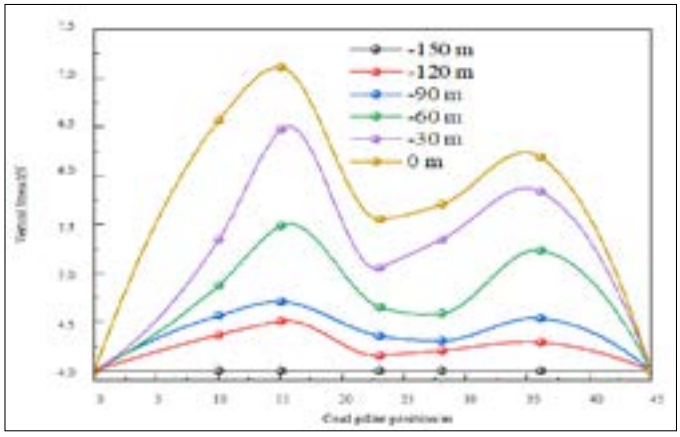

(a) From -150 m to 0 m relative to the working face

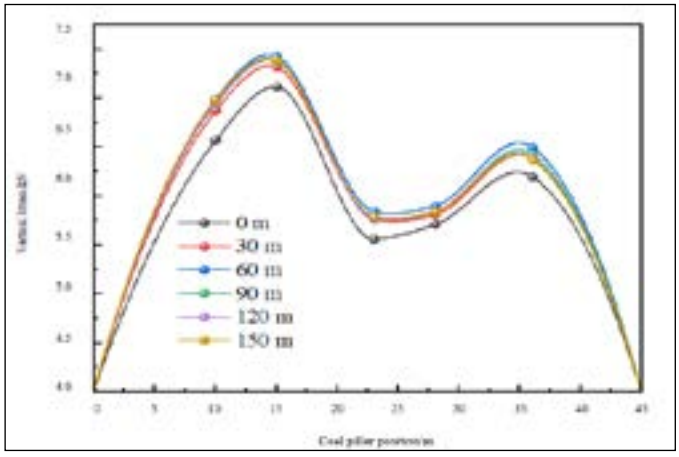

(b) From 0 m to 150 m relative to the working face

Fig.5 Variation law of coal pillar stress increment with the advancement of the working face

From Figure 5, it can be observed that under the influence of single-sided mining activity at the 110 Working Face, the stress increment of the coal pillar exhibits a double-peak asymmetric distribution pattern, with a greater increase in stress on the coal pillar near the goaf. As the 110 Working Face advances, the distance between the monitoring station and the working face gradually decreases, causing the load from the roof strata to transfer to the coal seam, which gradually increases the pressure on the coal pillar and leads to a continuous rise in the stress increment. The maximum stress increment occurs at 15 meters from the 110 Working Face, as shown in Figure 5(a). After the 110 Working Face advances a certain distance past the monitoring point, the stress increment of the coal pillar shows a negative growth trend, as illustrated in Figure 5(b). This is analyzed to be due to a slight release or transfer of coal pillar stress following periodic fracture of the roof strata. As the working face advances further, the stress increment of the coal pillar stabilizes, indicating that the stress distribution of the coal pillar gradually stabilizes.

Under the influence of mining activities at the 110 Working Face, the coal pillar near the goaf gradually fails, with the yielding failure region expanding inward and its load-bearing capacity gradually decreasing. However, due to the large width of the coal pillar, the coal pillar on the side of the 108 Working Face is less affected by mining activities over a larger area and still retains a high load-bearing capacity, maintaining a significant proportion of its elastic region. Therefore, based on the roadway pressure monitoring results of the 108 Transport Roadway, it is concluded that the original coal pillar width can be appropriately reduced to some extent to improve the coal resource recovery rate of the mine.

2. Characteristics of Coal Pillar Failure

The failure characteristics of the coal pillar are analyzed by combining a two-dimensional physical similarity model test with field measurements, based on the overburden distribution and its physical and mechanical characteristics in the Suancigou Coal Mine (Yang et al., 2023; Cao and Wei, 2024; Yang et al., 2024).

Table 1 Basic parameters of the physical similarity model

Item	Parameter	Item	Parameter
Model Length	2.6 m	Excavation Distance	2.2 m
Model Thickness	0.3 m	Model Boundary	10 cm
Model Height	1.54 m	Excavation Steps	44
Coal Seam Thickness	10 cm	Excavation Distance per Step	5 cm
Geometric Ratio	200:1	Excavation Time Interval	0.5 h
Density Ratio	1:1	Excavation Time	22 h
Stress Ratio	200:1	Upper Load	0.0355 MPa

The experiment is conducted using a similar simulation test platform at the State Key Laboratory of Coal Mine Disaster Dynamics and Control of Chongqing University. The geometric similarity ratio C_1 of the model is 1:200. The basic parameters of the model are shown in Table 1, and the physical model is shown in Figure 6.

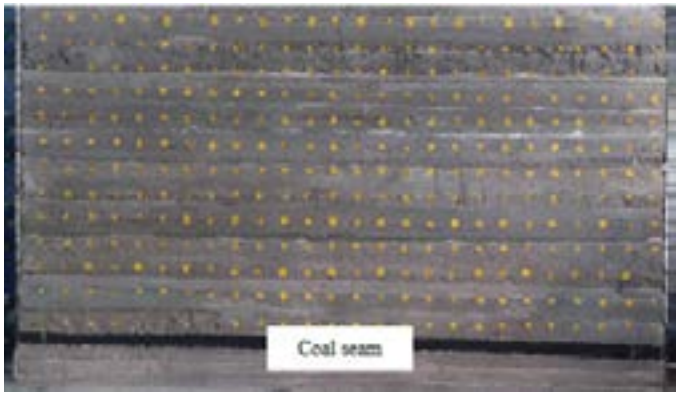

Fig.6 Physical similarity model

2.1 Analysis of Experimental Results

Figure 7 shows the deformation and damage characteristics of the coal pillar after excavation on both sides of the working face.

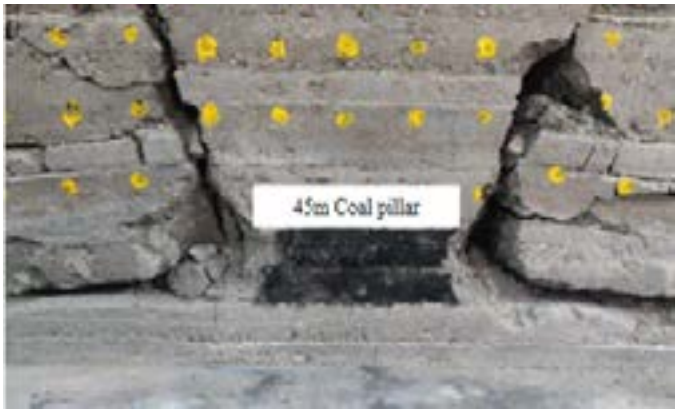

Fig.7 The deformation characteristics of the coal pillar

From Figure 7, it can be concluded that the influence of mining-induced stress from the left-side working face causes a certain amount of block collapse on the coal pillar near the goaf, accompanied by the formation of fractures. As the right-side working face is mined, the damage degree of the coal pillar on the goaf side of the left-side working face further intensifies, with an increased amount of block collapse and more extensive fracture development. Similar phenomena also occur in the coal pillar near the goaf of the right-side working face.

Overall, the damage caused by mining-induced stress to the coal pillar occurs only on both sides of the coal pillar, with minimal impact on its elastic core zone. After mining on both the left and right working faces, a relatively wide elastic zone still exists within the coal pillar, maintaining a high load-bearing capacity.

Therefore, to improve the coal recovery rate of the 6th Upper coal seam at Suancigou Coal Mine, the width of the coal pillar between working faces can be appropriately reduced, which will effectively enhance the coal resource recovery rate.

2.2 Evolution Characteristics of Coal Pillar Damage and Deformation

Based on the results of field monitoring and physical similarity simulation tests, the evolution characteristics of damage and deformation in the protective coal pillars of the First Panel working face at Suancigou Coal Mine are obtained, as shown in Figure 8.

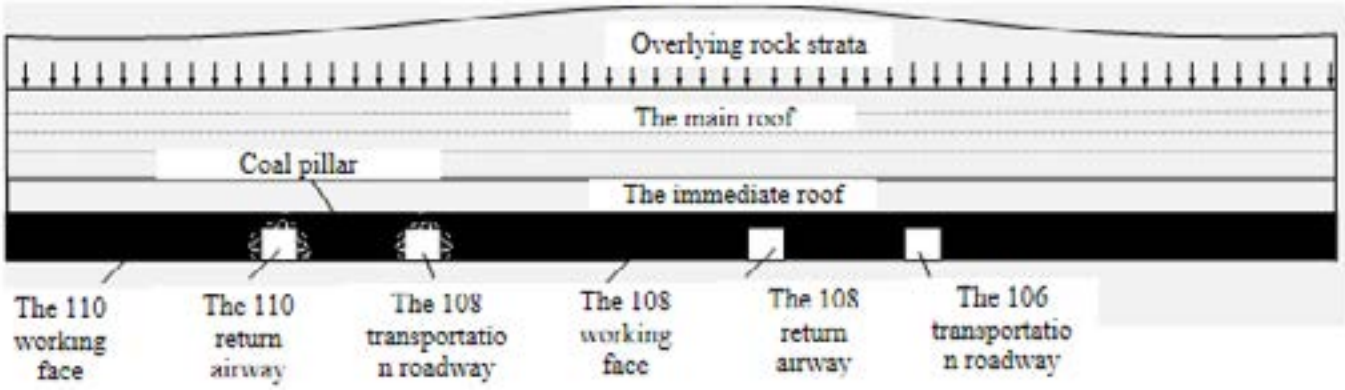

(a) Phase 1: Roadway Excavation

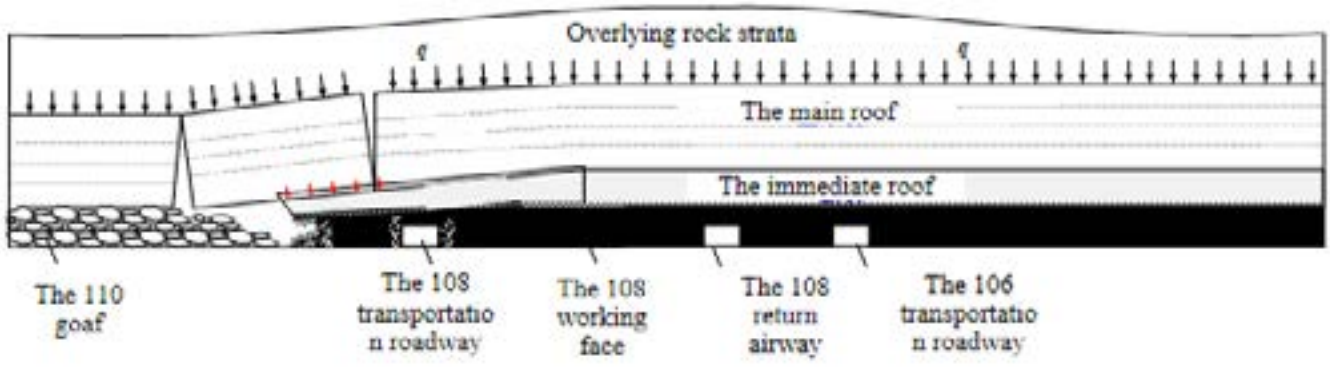

(b) Phase 2: Recovery of the 6th 110 Working Face

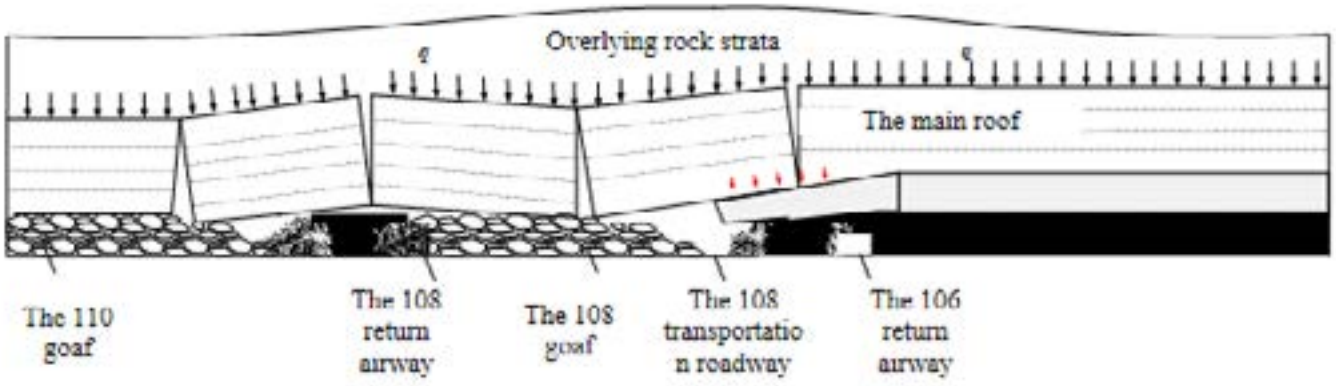

(c) Phase 3: Recovery of the 6_{upper} 108 Working Face

Fig.8 Coal pillar deformation characteristics

From Figure 8, it can be seen that the deformation and damage of the coal pillar can be divided into three stages:

① Phase 1: This is the stage where the coal pillar is influenced by roadway excavation for the recovery of the 110 Working Face and the 108 Working Face. During this phase, a loosened zone of approximately 1-2 meters is formed in the coal pillar, as shown in Figure 8(a).

② Phase 2: This is the stage where the coal pillar is influenced by the first mining activity at the 110 Working Face. During this phase, slight separations occur on the side of the coal pillar near the 108 Working Face within the 45-meter pillar between the 110 Return Airway and the 108 Transport Roadway. The elastic zone in the middle of the coal pillar decreases, forming stress concentration areas. The stress peak and the plastic zone gradually expand toward the deeper regions of the coal pillar, reducing its load-bearing capacity. A larger plastic zone is formed on the side of the coal pillar near the 110 Working Face, as shown in Figure 8(b).

③ Phase 3: This is the stage where the coal pillar is influenced by the second mining activity at the 108 Working Face. During this phase, separations occur on both sides of the 45-meter coal pillar. The fractured zone and the plastic zone expand toward the center of the coal pillar, reducing the proportion of the elastic zone and redistributing the stress within the coal pillar. The stress peak and the plastic zone further expand toward the deeper regions of the coal pillar, significantly reducing its load-bearing capacity. However, due to the large width of the coal pillar, the effective load-bearing area of the coal pillar remains substantial, as shown in Figure 8(c).

3. Theoretical Analysis of Critical Coal Pillar Width

3.1 Critical Coal Pillar Width under Limit Equilibrium Theory

According to the limit equilibrium theory (Zhang et al., 2015), the stress at the boundary interface of the ultimate equilibrium zone in the coal seam is:

$$\sigma_y = \left(\frac{C_0}{\tan\varphi_0} + \frac{P_x}{l}\right) e^{\frac{2\tan\varphi_0}{Ml}} - \frac{C_0}{\tan\varphi_0} \tag{1}$$

$$\tau_{xy} = -\left(C_0 + \frac{P_x \tan\varphi_0}{l}\right) e^{\frac{2\tan\varphi_0}{Ml}x} \tag{2}$$

Width of Plastic Zone (Stress Limit Equilibrium Width):

$$R = \frac{Ml}{2\tan\varphi_0} \ln \frac{\frac{kgH}{1000} + \frac{C_0}{\tan\varphi_0}}{\frac{C_0}{\tan\varphi_0} + \frac{P_x}{l}} = \tag{3}$$

The parameters corresponding to Equation (3) are presented in Figure 2.

Table 2 Basic parameters of stress limit balance width calculation formula

Symbol	Parameter Description	Value/Unit
H	Mining depth	350 m
λ	Lateral pressure coefficient	1.05
k	Stress concentration factor	1.25
γ	Average unit weight of overlying strata	25 kN/m^3
p_x	Supporting strength of roadway support on coal rib	0.2 MPa
M	Mining thickness of coal seam	20 m
C_0	Cohesion of coal-rock interfaces (e.g., bedding planes)	2.45 MPa
φ_0	Internal friction angle of coal-rock interfaces	32.6°
-	Theoretical calculation result	Coal pillar width ≥ 21.34 m

In summary according to the limit equilibrium theory, the coal pillar width should not be less than 21.34 meters.

3.2 Critical Coal Pillar Width under Strength Theory

For strip coal pillars, where the length L is much greater than the width a, they are regarded as a plane problem, ignoring the edge effects at the front and rear ends of the strip coal pillar. Under this condition, the ultimate load that the coal pillar can bear is given a (Wang et al., 2002):

$$\sigma_s = \left(\frac{2C\cos\varphi}{1-\sin\varphi} + \frac{1+\sin\varphi}{1-\sin\varphi} k\gamma H\right) \times \left(a - 0.00492\lambda MH\right) L \tag{4}$$

Actual load bearing of the coal pillar:

$$\sigma_p = \gamma H \left[a + \frac{b}{2}\left(2 - \frac{b}{0.6H}\right)\right] L \tag{5}$$

The parameters corresponding to Equation (5) are presented in Figure 3.

Table 3 The basic parameters of the actual bearing formula of coal pillar

Symbol	Parameter Description	Value/Unit
b	Mining width (dip width of the working face)	244.6 m
C	Cohesion of the coal body	2.45 MPa
φ	Internal friction angle of the coal body	32.6°
k	Stress concentration factor	1.25
L	Length of the coal pillar	1500 m

The necessary condition to ensure the coal pillar remained stable is:

$$\sigma_p \le \sigma_s \tag{6}$$

By combining Equations (4), (5), and (6), the coal pillar width is determined to satisfy the following condition (Wang et al., 2002):

$$a \ge \frac{\frac{\gamma H\left(1.2bH - b^2\right)}{4.8H} + 0.00123\lambda MH \frac{2C\cos\varphi + k\gamma H\left(1+\sin\varphi\right)}{1-\sin\varphi}}{\frac{2C\cos\varphi}{1-\sin\varphi} + \frac{1+\sin\varphi}{1-\sin\varphi} k\gamma H - \gamma H} \tag{7}$$

From Equation (7), it is determined that when the coal pillar width exceeds 26.18 m, the actual load borne by the coal pillar does not exceed the ultimate load, and the coal pillar remains stable. Therefore, under the strength theory, the coal pillar width should not be less than 26.18 m.

Combining the theoretical analysis results from Sections 3.1 and 3.2, the critical width of the protective coal pillar for the recovery roadway in the First Panel at the Suancigou Coal Mine is determined as max(21.34, 26.18) = 24.45 m. Thus, the minimum coal pillar width should not be less than 26.18 m.

4. Analysis of Governance Effectiveness

4.1 Model Construction and Simulation Scheme

Based on the engineering geological parameters of the Suancigou Coal Mine, a two-dimensional calculation model is established using Phase 2. The model dimensions are 644 m × 200 m, as shown in Figure 9. The bottom boundary of the model is fixed, the top boundary is free, and horizontal displacement constraints are applied to all other boundaries. The weight of the overlying strata above the model is applied to the upper boundary in the form of a uniformly distributed load, with a magnitude of 6.88 MPa. The Mohr-Coulomb constitutive model is selected for the material of the model elements.

Due to the large thickness of the coal seam, local large deformations of the mesh might cause errors during the calculation. To address this issue, flexible material parameters are assigned to the caving zone of the mined-out working face to ensure accuracy and convergence during the model calculation (Wang et al., 2025; Sebacher and Hanea, 2024; Shi et al., 2024).

Based on the theoretical calculation results in Chapter 3, the simulation scheme is designed to perform calculations for coal pillar widths of 35 m, 30 m, and 25 m. According to actual working conditions, the roadway dimensions are set to 5.4 m (width) × 3.8 m (height). The simulation calculations are divided into three steps: roadway excavation, recovery of Working Face 1, and recovery of Working Face 2.

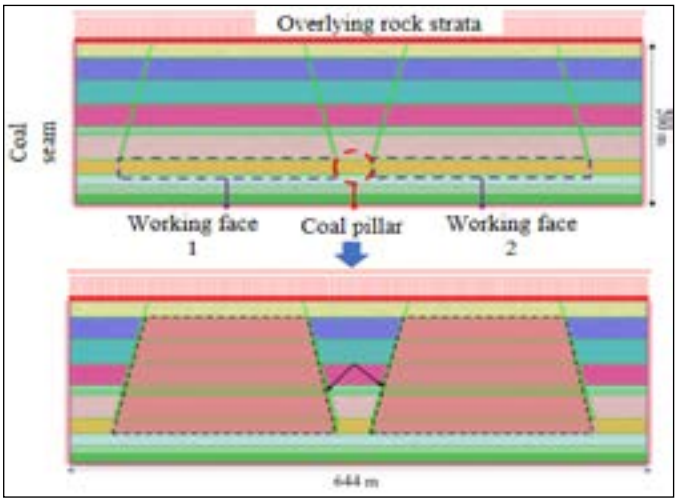

Fig.9 Model meshing diagram

4.2 Simulation Results

(1) Coal pillar width of 35 m

Figure 10 shows the stress and damage distribution characteristics of the 35 m coal pillar under the influence of mining and excavation.

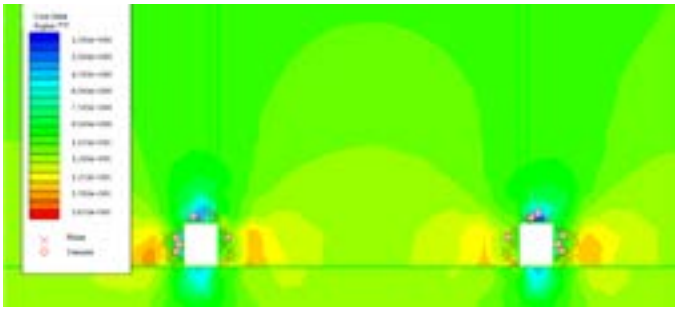

(a) Roadway Excavation

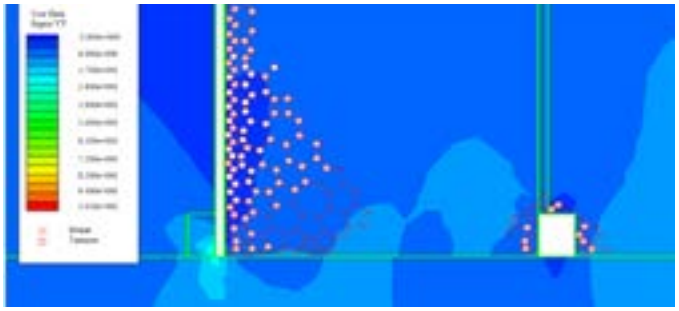

(b) Recovery of Working Face 1

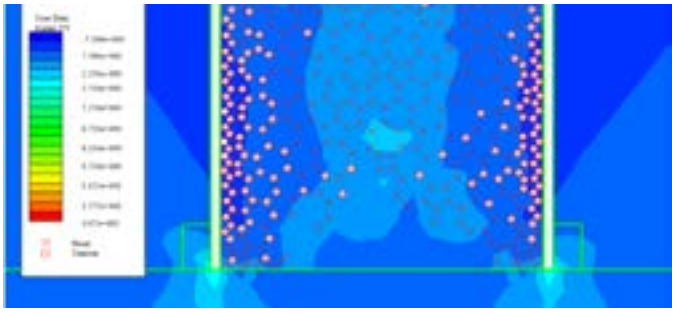

(c) Recovery of Working Face 2

Fig.10 The stress and damage distribution characteristics of the 35 m coal pillar

From Figure 10, it can be observed that during roadway excavation, the vertical stress field of the surrounding rock is symmetrically distributed around the central axis of the coal pillar. Slight stress concentration occurs near both sides of the roadway, and there is some damage and failure in the shallow regions. However, due to the large width of the coal pillar, the distribution of the elastic-plastic zone within the coal pillar is not significantly affected by roadway excavation, and no notable damage is observed in the interior, as shown in Figure 10(a).

During the recovery of Working Face 1, the damaged area on the side of the coal pillar near the goaf gradually expands toward the interior of the coal pillar, and the plastic zone begins to develop. A slight stress concentration phenomenon forms on the goaf side of the coal pillar. Additionally, the recovery of Working Face 1 exacerbates the shallow damage and failure of the surrounding rock in the roadway near the goaf, as shown in Figure 10(b).

During the recovery of Working Face 2, the damaged area within the coal pillar further develops toward the deeper regions of the coal pillar, forming a distinct "three-zone" distribution consisting of a fractured zone, a plastic zone, and an elastic zone, with the elastic zone accounting for the largest proportion. Furthermore, the vertical stress exhibits a symmetrical distribution along the central axis of the coal pillar, as shown in Figure 10(c).

(2) Coal pillar width of 30 m

Figure 11 shows the stress and damage distribution characteristics of the 30 m coal pillar under the influence of mining and excavation.

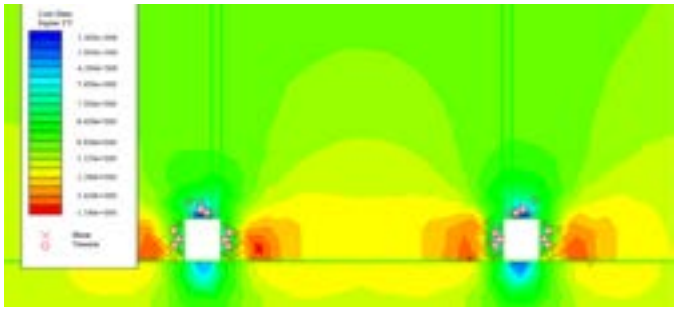

(a) Roadway Excavation

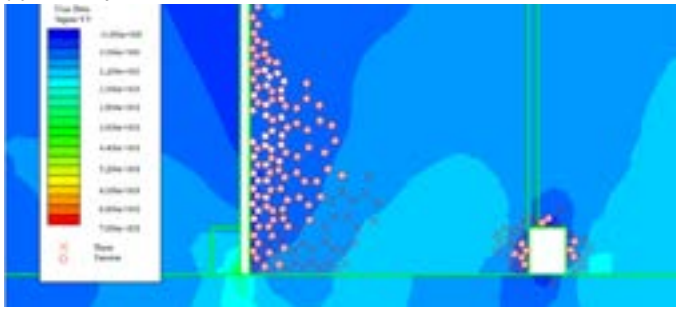

(b) Recovery of Working Face 1

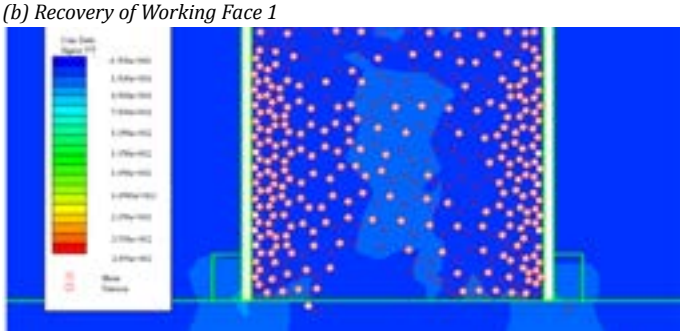

(c) Recovery of Working Face 2

Fig.11 The stress and damage distribution characteristics of the 30 m coal pillar

From Figure 11, it can be observed that during roadway excavation, the vertical stress field within the coal pillar exhibits an approximately "saddle-shaped" pattern, symmetrically distributed along the central axis of the coal pillar. The maximum vertical stress is 16.2 MPa, as shown in Figure 11(a).

During the recovery of Working Face 1, similar to the 30 m coal pillar, the plastic zone of the coal pillar continuously expands toward its interior, and the fractured zone gradually begins to develop and expand. The vertical stress exhibits an asymmetric distribution pattern. Likewise, the recovery of Working Face 1 exacerbates the damage and failure of the surrounding rock in the roadway near the goaf, as shown in Figure 11(b).

During the recovery of Working Face 2, the damaged and fractured zones within the coal pillar gradually connect, causing large-scale failure of the coal pillar and a significant reduction in its load-bearing capacity, as shown in Figure 11(c).

(3) Coal pillar width of 25 m

Figure 12 shows the stress and damage distribution characteristics of the 25 m coal pillar under the influence of mining and excavation.

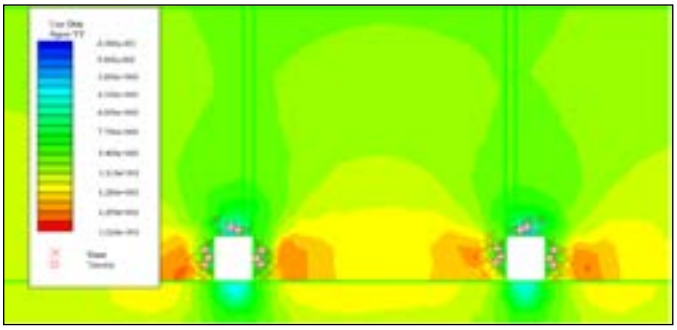

(a) Roadway Excavation

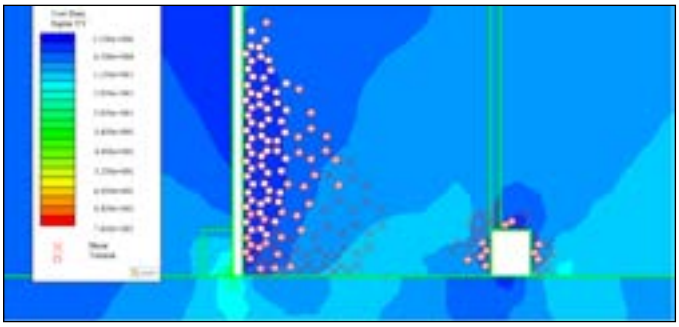

(b) Recovery of Working Face 1

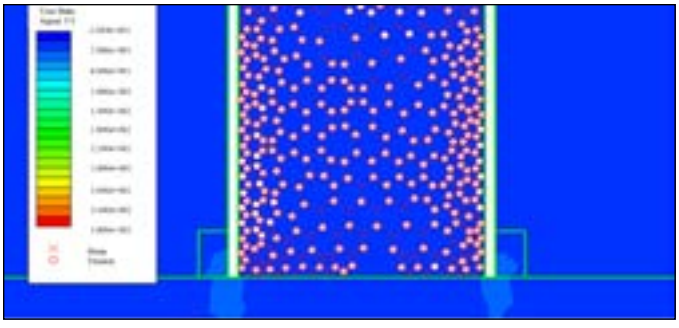

(c) Recovery of Working Face 2

Fig.12 The stress and damage distribution characteristics of the 25 m coal pillar

From Figure 12, it can be observed that during roadway excavation, the vertical stress field is symmetrically distributed along the central axis of the coal pillar. The maximum vertical stress is 15.6 MPa, and the overlapping stress region increases, resulting in a higher degree of stress concentration, as shown in Figure 12(a).

During the recovery of Working Face 1, a plastic zone penetration phenomenon appears at the base of the coal pillar, and the fractured zone on the goaf side of the coal pillar expands and develops. Overall, the coal pillar suffers severe damage and failure. Additionally, the recovery of Working Face 1 causes the failure of the surrounding rock in the exposed roadway to extend deeper, significantly reducing its stability, as shown in Figure 12(b).

During the recovery of Working Face 2, the fractured zone of the coal pillar becomes completely penetrated, leading to the overall failure of the coal pillar, which loses its load-bearing capacity.

The numerical calculation results indicate that the coal pillar width should not be less than 25 m and not exceed 30 m. Multiple mining and excavation activities have a severe impact on the stress distribution, the degree of fracturing, and the load-bearing capacity of coal pillars with widths between 25 m and 30 m. However, after the recovery of Working Face 1, the coal pillar still retains a significant load-bearing capacity, and certain technical measures can be applied to control the stability of the exposed roadway to ensure the safe recovery of Working Face 2.

Therefore, it is concluded that the coal pillar width for the 6_{upper} coal seam in the Suancigou Coal Mine should not be less than 25 m and not exceed 30 m. This range ensures a high coal recovery rate while guaranteeing the safe recovery of the working face. However, due to the significant variations in coal seam thickness, it is necessary to adopt roadway reinforcement support measures in areas with greater coal seam thickness.

5. Conclusions

(1) Under the influence of multiple mining and excavation activities, the 45-meter-wide protective coal pillar still retains a significant elastic zone and maintains a high load-bearing capacity. Therefore, the original coal pillar width can be reduced to a certain extent to improve the coal recovery rate of the mine.

(2) Theoretical calculations determined that the minimum critical width of the protective coal pillar is 26.18 m, meaning the coal pillar width should not be less than 26.18 m.

(3) When the coal pillar width is no less than 25 m and no more than 30 m, it achieves a high coal recovery rate, ensures the economic benefits of the mine, and guarantees safe mining operations. However, due to significant variations in coal seam thickness, roadway reinforcement support measures must be adopted in areas with greater coal seam thickness.

Acknowledgements

This work was supported by the National Natural Science Foundation of China (52204127) and the Chongqing Scientist Responsibility System Project (Grant No. CSTC2022YCJH-BGZXM0005). The authors gratefully acknowledge the financial support from the organizations.

Author Contributions

Yongwei Du developed the computational model and performed the simulations. Zhongqiu Wang analyzed the data and interpreted the results. Xueqi Zhang and Hongbin Li prepared the manuscript with contributions from all co-authors.

Conflict of Interest

The authors declare no conflicts of interest.

Informed Consent

Informed consent was obtained from all participants involved in the study.

Reference

Cao, J., & Wei, X. 2024. Research on mining-induced surface soil cracking mechanism and development depth of downward fracture. *Engineering Failure Analysis*, 160, 108180. https://doi.org/10.1016/j.engfailanal.2024.108180

Chang, H.W., Xu, Q.Y. 2021. Determination of Coal Pillar Width of Gob-side Entry Driving with Fully Mechanized in Medium-thick Coal Seam. *Coal Technology*, 40(10), 27-31. DOI: 10.13301/j.cnki.ct.2021.10.007

Chen, F., Yu, H., Bian, Z., & Yin, D. 2021. How to handle the crisis of coal industry in China under the vision of carbon neutrality. *Journal of China Coal Society*, 46(06), 1808-1820.

Chen, S.J. 2005. Test Study of Coal's Strength & Deformation Characterestic and Application in Strip Pillar Design (in Chinese). Shandong University of Science and Technology.

Gao, L., Liu, P.Z., Zhang, P.D., Wu, G.Y., Kang, X.T. 2022. Influence of fracture types of main roof on the stability of surrounding rock of the gob-side coal-rock roadway in inclined coal seams and its engineering application. *Coal Geology & Exploration*, 50(06), 73-80. DOI: 10.12363/issn.1001-1986.21.10.0588

Gu, W., Xu, D., Wang, Y., Miao, K., Yao, S., Zhang, H., & Han, Z. 2024. Research on the stability and water isolation of waterproof coal pillars between adjacent working faces under the influence of water ponding goaf—a case study. *Applied Sciences*, 14(2), 884. https://doi.org/10.3390/app14020884

Guo, L.Q., Cai, Q.P., Peng, X.Q. 2014. Effect of strength criterion on design of strip coal pillar. *Rock and Soil Mechanics*, 35(03), 777-782. DOI: 10.16285/j.rsm.2014.03.024

He, F., Zhai, W., Song, J., Xu, X., Wang, D., & Wu, Y. 2023. Reasonable coal pillar width and surrounding rock control of gob-side entry driving in inclined short-distance coal seams. *Applied Sciences*, 13(11), 6578. https://doi.org/10.3390/app13116578

Kong, F.L., Liu, J.D., Tian, L.T., Zhang, Z.Q., Wang, D.D., Zheng, Z.Q., Xu, Q. 2022. Study on reasonable width of coal pillar under water-rock interaction. *Journal of Mine Automation*, 48(12), 144-150. DOI: 10.13272/j.issn.1671-251x.2022060062

Li, L., Bo, J.B., Wang, X.Y. 2012. Rational position and control technique of roadway driving along next goaf in fully mechanized top coal caving face. *Journal of China Coal Society*, 37(09), 1564-1569. DOI: 10.13225/j.cnki.jccs.2012.09.029

Li, X., Li, H., Zhang, X., Yuan, H., Li, X., Shi, C., Lei, G. 2024. Damage evolution of coal with a strong bursting liability and 3d measurement method for elastic deformation energy distribution. *Theoretical and Applied Fracture Mechanics*, 133(Part A), 104534. https://doi.org/10.1016/j.tafmec.2024.104534

Li, Z., Fan, J., Feng, G., Qi, C., & Zhang, J. 2023. A new method for identifying coal pillar instability based on energy and stress correlation characteristics and its engineering application. *Minerals*, 13(12), 1507. https://doi.org/10.3390/min13121507

Liu, B., Zhu, L., Liu, X., Liu, Q., Fan, Y., Yao, W., & Deng, W. 2024. Energy evolution and damage deformation behavior of cemented broken coal specimen under triaxial compression condition. *Energy*, 310, 133203. https://doi.org/10.1016/j.energy.2024.133203

Liu, Q., Xue, Y., Ma, D., & Li, Q. 2023. Failure characteristics of the water-resisting coal pillar under stress-seepage coupling and determination of reasonable coal pillar width. *Water*, 15(5), 1002. https://doi.org/10.3390/w15051002

Rong, Y., Sun, Y., Chen, X., Ding, H., & Xu, C. 2024. Analysis of damage and permeability evolution of sandstone under compression deformation. *Applied Sciences*, 14(16), 7368. https://doi.org/10.3390/app14167368

Sebacher, B., & Hanea, R. 2024. Bridging element-free galerkin and pluri-gaussian simulation for geological uncertainty estimation in an ensemble smoother data assimilation framework. *Petroleum Science*, 21(3), 1683-1698. https://doi.org/10.1016/j.petsci.2023.12.020

Shi, H., Li, J., Shen, H., Li, X., Wei, N., Wang, Y., Pan, H. 2024. Quantitative analysis of the numerical simulation uncertainties from geological models in CO_2 geological storage: a case study of shenhua CCS project. *International Journal of Greenhouse Gas Control*, 135, 104142. https://doi.org/10.1016/j.ijggc.2024.104142

Song, H. 2016. The Current Status and Development Trends of Strip Mining Research in China (in Chinese). *Technology and Market*, 23(08), 197-198.

Tian, J.S., Jia, J.D., Zhu, H.Y., Lian, K.Y. 2021. Reasonable coal pillar width in deep high-stress working face with double lane. *Coal Engineering*, 53(04), 6-10.

Wang, J., Liu, Y., & Zhang, N. 2025. Advancing practical geological co_2 sequestration simulations through transfer learning integration and physics-informed networks. *Gas Science and Engineering*, 134, 205523. https://doi.org/10.1016/j.jgsce.2024.205523

Wang, X.C., Huang, F.C., Zhang, H.X., Zhang, L.G. 2002. Discussion and improvement for A.H.Wilsons coal pillar design. *Journal of China Coal Society*, (06), 604-608.

Wang, X.Y., Dou, S.Y. 2022. Determination of small coal pillar parameters in goaf excavation of fully-mechanized caving face in Tongxin Coal Mine. *Coal Science - Technology Magazine*, 43(06), 44-48+52. DOI: 10.19896/j.cnki.mtkj.2022.06.011

Xie, H., Ren, S., Xie, Y., & Jiao, X. 2021. Development opportunities of the coal industry towards the goal of carbon neutrality. *Journal of China Coal Society*, 46(07), 2197-2211.

Xing, K., Cheng, J., Zhen, Z., Wan, Z., Han, Z., Yan, W., Yang, Y. 2024. Effect of super-high water materials backfilling on stress decrease and energy release during strip coal pillar mining: a case study. *Heliyon*, 10(18), e37441. DOI: 10.1016/j.heliyon.2024.e37441

Xue, Y.P. 2024. Optimization of small coal pillar width and control measures in gob-side entry excavation of thick coal seams. *Scientific Reports*, 14(1), 23304. https://doi.org/10.1038/s41598-024-74793-8

Yang, T., Zhang, Y., Zhang, J., Lin, H., Bao, R., He, Y., Pang, H. 2024. Study on the stability and reasonable width of coal pillars in "three soft" coal seams based on a physical similarity simulation experiment. *Applied Sciences*, 14(14), 6127. https://doi.org/10.3390/app14146127

Yang, Y., Li, Y., Wang, L., & Wu, Y. 2023. On strata damage and stress disturbance induced by coal mining based on physical similarity simulation experiments. *Scientific Reports*, 13(1), 15458. https://doi.org/10.1038/s41598-023-42148-4

Yang, Y., Sun, J., Wang, W., & Zhang, R. 2022. Research on coal pillar width and support design of gob-side entry. *Geotechnical and Geological Engineering*, 41(2), 847-860. https://doi.org/10.1007/s10706-022-02309-0

Yin, S.F., Zuo, A.J., Ma, L.J., Ren, Y.X., Shi, S.H. 2022. Surrounding rock stability during gob-side entry driving with narrow coal pillar in medium-thick coal seam. *Coal Engineering*, 54(05), 90-96.

Yuan, L., Wang, E., Ma, Y., Liu, Y., & Li, X. 2023. Research progress of coal and rock dynamic disasters and scientific and technological problems in China. *Journal of China Coal Society*, 48(05), 1825-1845. DOI: 10.13225/j.cnki.jccs.2023.0264

Yun, Q.L., Wang, X.H., Jing, W., Zhang, W.B., Wei, X.X., & Wang, J.H. 2024. Characteristics of deformation and damage of surrounding rock along the top roadway in the working face of an isolated island and its evolution law. *Scientific Reports*, 14(1), 15092. https://doi.org/10.1038/s41598-024-63246-x

Zhang, K.X., Zhang, Y.J., Ma, Z.Q., Bi, W.G., Yang, Y.M., Li, Y. 2015. Determination of the narrow pillar width of gob-side entry driving. *Journal of Mining and Safety Engineering*, 32(03), 446-452. DOI: 10.13545/j.cnki.jmse.2015.03.016

Zheng, Z., Yang, Z.Q., Zhu, H.Z., He, F.L., Du, C.Y., Liu, B.Q. 2019. Study on reasonable coal-pillar width and surrounding-rock control of gob-side irregular roadway in inclined seam. *Journal of Mining and Safety Engineering*, 36(02), 223-231. DOI: 10.13545/j.cnki.jmse.2019.02.002

Zhu, S.T., Wang, B., Jiang, F.X., Zhang, X.F., Sun, X.K., Sun, X., Liu, J.H., Zhang, A.M. 2021. Study on reasonable width of isolated coal pillar based on rock burst-mine earthquake coordinated control. *Coal Science and Technology*, 49(06), 102-110. DOI: 10.13199/j.cnki.cst.2021.06.012

ISSN 2544-7024